Master Thesis

Joining kirigami sheets consisting of a single continuous and smooth cut by constraining discretized strips with origami

S.P.P. Allard

Delft University of Technology

TU Delft

Master Thesis

Joining kirigami sheets consisting of a single continuous and smooth cut by constraining discretized strips with origami

by

S.P.P. Allard

To create a solid knowledge base for constraining with origami,
Delft University of Technology.

Student number:	4330846	
Project duration:	July 1, 2020 – May 20, 2021	
Thesis committee:	Prof. dr. ir. J.L. Herder,	TU Delft, Daily supervisor, supervisor PME
	F.G.J. Broeren Msc. ,	TU Delft, Daily supervisor, supervisor PME
	dr. ir. T. Horeman,	TU Delft, supervisor BMD
Previous supervisor:	Ph.D. A. Yellowhorse,	NTU

This thesis is confidential and cannot be made public until May 20, 2021.

An electronic version of the thesis is available at `http://repository.tudelft.nl/`.

TU Delft

Abstract

Kirigami can be used to create objects with a nonzero Gaussian curvature. A mathematical method is presented that can be applied to join a single continuous and smooth cut of a kirigami sheet. This is realized by constraining additional discretized strips with origami. The mathematical model evaluates how the strips from both sides of the cut can be constrained. The mathematical model is validated with an experiment, which confirmed the direction of the constraints. However, due to physical elements which are not part of the presented mathematical model, the relative proportion between the constraints did not fully represent reality. Finally, this treatise shows the optimization of a crease pattern, by using this model, resulting in a joined kirigami object.

Preface

Thursday, the fourth of April of 2019 brought my first acquaintance with origami. That day I followed the compliant mechanism course (ME46115) by Dr. N. Tolou. He had something special in mind: there was a guest lecture on origami given by Ph.D. A. Yellowhorse. It sparked my interest. Although origami is still in its infancy, it did seem to have huge potential. Difficult but interesting shapes could be made on demaned from a plane, reducing manufacturing costs and easing transportation. Possible applications were emerging in various fields, from biomedical sciences, to aerospace and robotics. Origami was clearly state of the art.

Many conversations followed with Alden Yellowhorse. We had brainstorm sessions on possible topics for the master thesis. Ultimately, we found an agreement that was inspired by our common interest for origami. We were going to join kirigami sheets in order to realize the assembly of an antenna for outer space. Ambiguous plans for folding towards possible zipper designs were discussed. Ph.D. A. Yellowhorse was my mentor for the literature review on origami but also my responsible supervisor for the research assignment I did with the faculty of Aerospace Engineering, won the topic: "Removing vibrations from the Delfly Nimble for camera applications".

I would like to congratulate Ph.D. A. Yellowhorse on his promotion to Assistant Professor at Navajo Technical University. Unfortunately, it turned out to be the end of our collaboration on the topic of origami. Luckily though, I found myself two new inspiring supervisors: Prof. dr. ir. J.L. Herder and Ph.D. F. Broeren, by the end of the early stages of the project.

With their help I went through the more difficult stages of the master thesis, the optimization of the mathematical model. The process was hampered by an accumulation of software problems, with the corona virus just around the corner. The unfailing constructive input, out of the box ideas and fast thinking of Prof. dr. ir. J.L. Herder and Ph.D. F. Broeren definitely helped me to present to you my report.
The report consists of three parts: the "General Introduction", the "Article" and the "Recommendations & applications". Each part can be read independently.

My thesis could not have been realized without the support and effort of friends and family. I would like to thank some of them: Paulien, Youp, Suzanne, Daan, Nol, Paul, Michelle, Tim and Luke. I would also like to offer my sincere gratitude to the thesis committee: Prof. dr. ir. J.L. Herder, Ph.D. F. Broeren and dr. ir. T. Horeman

To those who read this thesis, I wish reading pleasure and the chance to be fascinated by origami, as I have been from that first acquaintance in 2019.

S.P.P. Allard
Delft, April 2021

List of Figures

List of Plots

*

Contents

1

General introduction

The general introduction of the master thesis precedes the article which represents the master thesis. The article can be read independently with respect to the general introduction and the accompanied appendices. The article includes an introduction, method, result, discussion and conclusion of the entire master thesis. However, the general introduction will provide a more elaborated insight in why kirigami sheets are joined. The potential joining method comes from the literature review which is summarized within this chapter.

1.1. Situation

The entire project is based on the desire to create an object which has in unfolded state a large area, but in folded state a compact volume. This may be wanted for several reasons such as easy transportation or low costs manufacturing processes [1]. Most often this goal is reached with the use of origami, see for example biomedical applications: a stent graft [19], aerospace applications: a foldable solar array [20] or robotics: self-folding robot [21]. All these examples have in common that in unfolded state they have a large area but in folded state compact/desired shape or vice versa. The folding operation occurs without stretching, cutting or deforming the sheet. Therefore origami is perfectly suitable to create Euclidean shaped designs [22].

Nonetheless, origami is not suitable for non-Euclidean shapes, for instance a sphere and a paraboloid. These objects can not be made from a flat sheet without violating the principles of origami. This issue is shown by Fig. 1.1 from S.J. Callens and A.A. Zadpoor [1]. First, a sphere is approximated with origami, crease lines are alligned with respect to the longitudinal direction and are clear from the eye. Next there is an attempt to create an accurate sphere. Deformations can be seen halfway the sphere which are unpredictable and therefore undesired. To solve this problem, cuts can be made within the sheet preventing deformations leading to a predictable design. The combination of a cut and origami is called kirigami [1].

The master thesis involves only uncomplicated kirigami objects. For instance a sphere (Fig. 1.2), a sphere is not necessarily a kirigami object but can be created with kirigami. The most obvious way to design a sphere is to use not one single sheet but several sheets. These sheets represents individual gores (Fig. 1.3) of the sphere as is often done for globes. All flattened out gores of Fig. 1.3 will form together a sphere of Fig. 1.2 if assembled.

In stead of making several incisions, it is often also possible to make one single cut, see Fig. 1.4. The flattened sphere has the shape which is known as an Euler spiral or the Cornu spiral [23] consisting of one single sheet. One flat sheet is easier to store in a compact volume and should be easier to reassemble to the desired object compared to a sphere with several gores.

During this thesis only large kirigami structures will be considered, large in the order of room-sized kirigami structures. These structures will also consist of one single cut. This has big implication for the dimensions. The intersection of these objects are very large (in order of meters) compared with the thickness of the sheets (in order of 0.01 mm to 1 mm like paper sheets).
This type of kirigami objects could be useful for deployable antenna's up in space, inflatable habitats or free-form architecture.
A closed 3D kirigami object can be based on a D-form. An example D-form is shown in Fig. 1.5 [3] which consist of two sheets and therefore of one single cut. Other examples can be found in [24] and [25]. However, the question remains how to assemble room-sized kirigami objects with one single cut.

For the joining method it doesn't matter if the surfaces, which are going to be connected, are complex, e.g. having a single or multiple curvatures or holes.
The aligned surfaces must have an equal shape on the adjacent edge in such a way that they can be joined together. Figure 1.8 and 1.9 shows schematically how

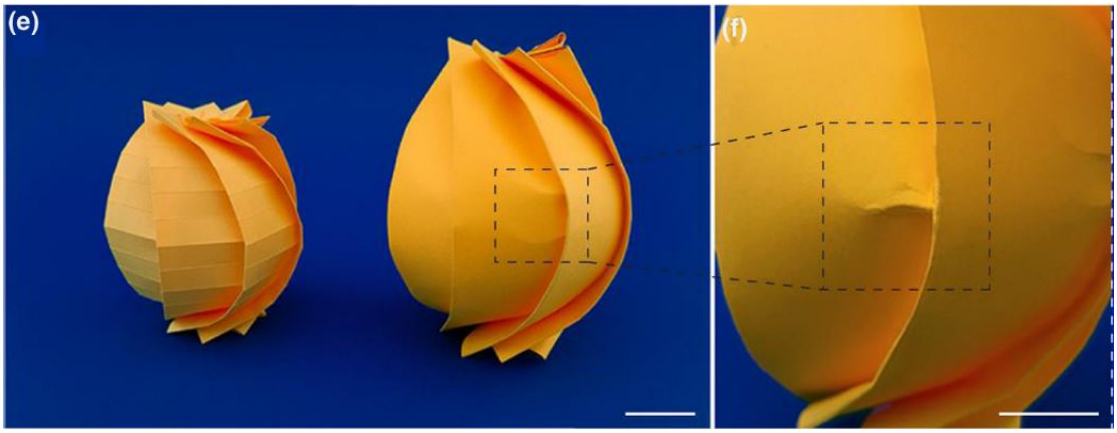

Figure 1.1: The first sphere is approximated with origami with folds in the longitudinal direction. The second sphere is an attempt to create a perfect sphere with origami, induced deformations are shown on right. Source: [1].

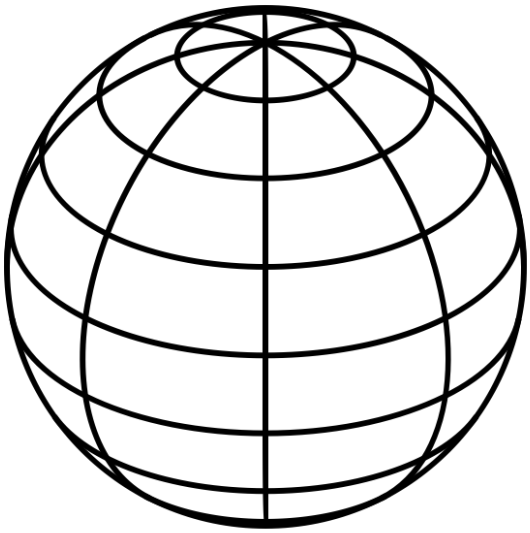

Figure 1.2: A sketch of a sphere is shown. Source: Noun-project.

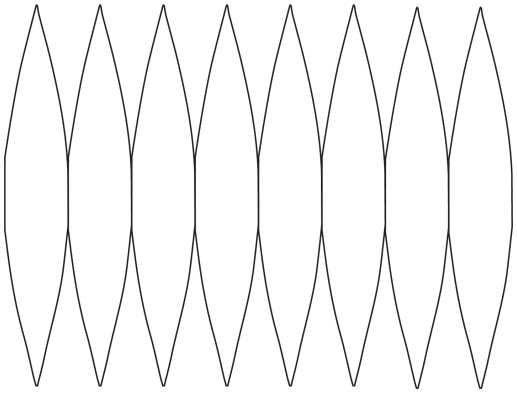

Figure 1.3: A sketch of a flattened sphere with several cuts, also called gores. Source: Noun-project

surfaces are aligned for an arbitrary kirigami structure.

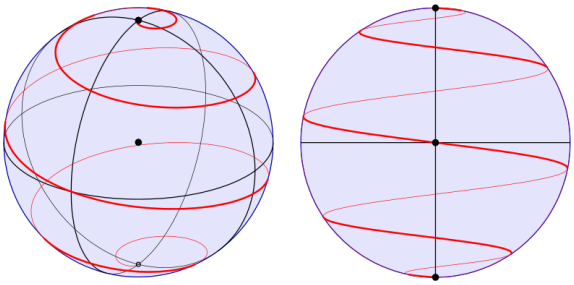

Figure 1.4: A sphere with one single cut, created with the use of parametric equations. Source:[2]

1.2. The intended solution

The original question; *How to assemble relative large continuous surfaces with an equal shape for kirigami purposes?* The intended solution to this problem will be discussed in detail inside the article. The solution is a direct result from the literature study. Hereinafter the alternatives will be discussed. Lifting off with the zipper design, followed with an overview of the already available joining techniques, finishing with the proposed solution.

1.2.1. Zipper design

Products as "the Zippermast" from the company Geo Systems, Fig. 1.7, and "the Spirallift" from the company Gala Systems, Fig. 1.6, are existing examples of automatic assembly of relatively thick sheets into one particular shape. These systems are intriguing due to their static zipper. Sheets move through a static zipper creating a 3D object from a 2D-sheets. The Spirallift will obtain a cylinder and the Zipermast will result in a prism. Both the Spirallift and the Zipermast make use of a snap fit assemble technique. According to the database CES Edupack snap fits are used from a sheet thickness of 1 mm upwards [6]. Reasonably,

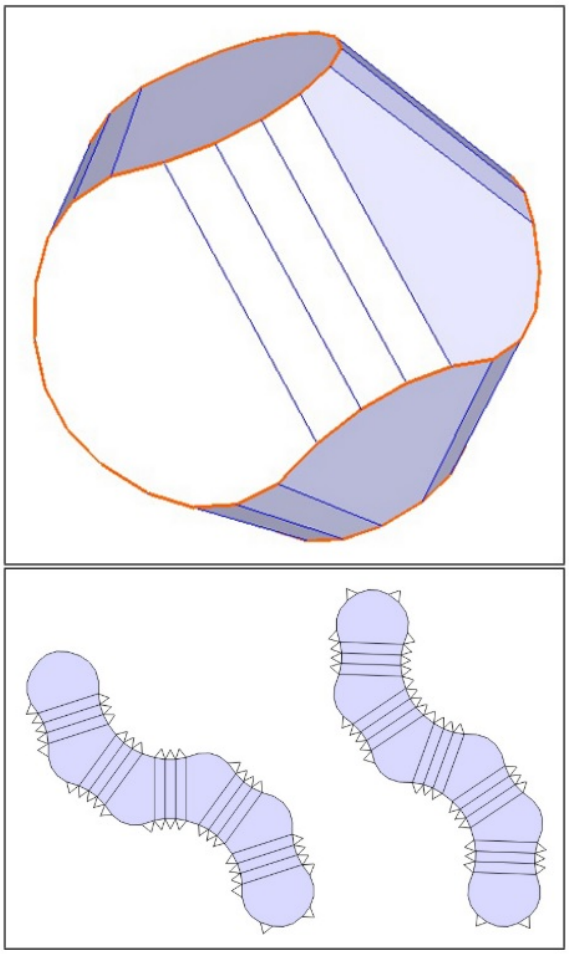

Figure 1.5: "The top row shows computer generated D-forms. The second row shows unfolded versions of the same D-forms". The D-form consist of two pieces. Source:[3].

the systems do not use paper but other materials.
The Spirallift and the Zipermast are used for the applications as movable theater seats or a robot-arm, see Fig. 1.7.
[26]

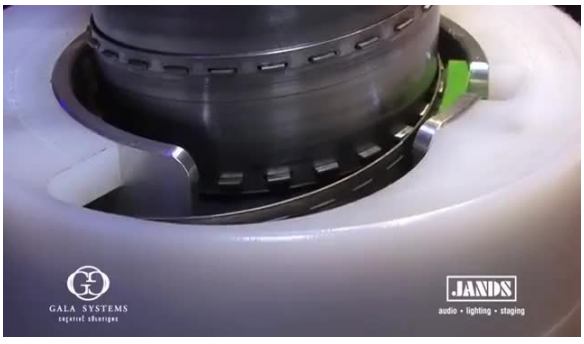

Figure 1.6: Close up of a zipper of the Spirallift of the company Gala Systems. Source: [4].

The zipper strategy of "the Zippermast" and "the Spirallift" could perhaps be applied to kirigami

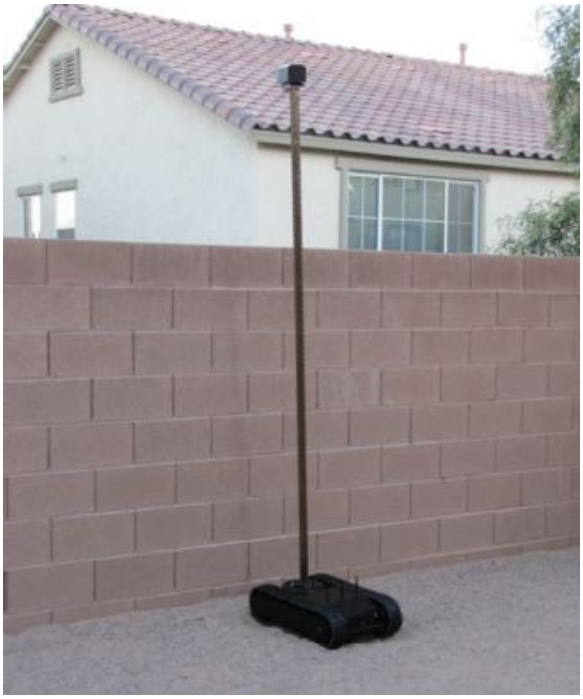

Figure 1.7: The zippermast of the company Geo Systems in action. It is composed of three sheets. On the top of the arm a robot camera is mounted. Source: [5].

structures in general instead of one single predefined shape. The zipper would move along the edge of the cut and connect the two sheets with a certain joining technique, as can be seen in figure 1.8. A zipper design creates new opportunity's for applications due the realization of arbitrary kirigami designs.

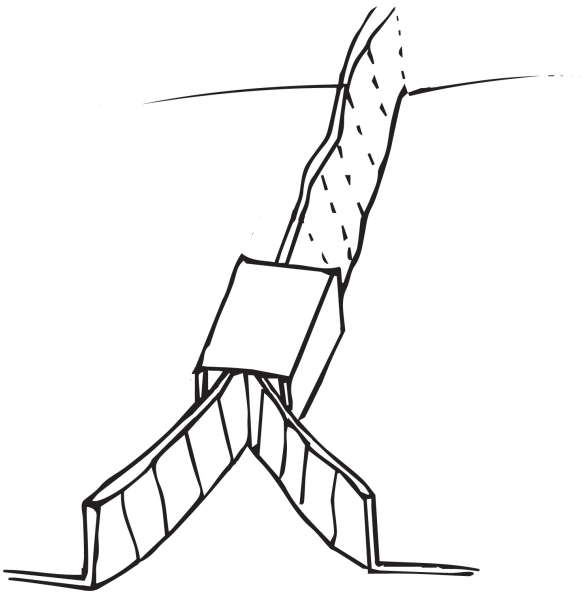

Figure 1.8: The zipper moves along the flaps of two arbitrary surfaces and connects them with a certain joining technique

.

1.2.2. Available joining techniques

Arbitrary surfaces (Fig. 1.8) can be joined with the two flaps. Nowadays, several joining techniques exists and are shown in Fig. 1.10 and 1.11. These two figures only shows assembly methods of the CES Edupack database[6] which can be used for 1 mm or less. As mentioned in section 1.1, the thickness of the kirigami sheets are in order of 0.01 mm to 1 mm. Well known assembly methods such as threaded fasteners, snap fit or some types of welding are not included, because they can only be used from a thickness of 1 mm and upwards [6].
Also tolerances and the time before handling are important factors for consideration to select an assembly technique in combination with a zipper design.

From Fig. 1.10 it is clear that in general fasteners have a high tolerance, so they are less accurate in comparison with other joining techniques.
Adhesives are precise and suitable for sheets with very thin section thickness, while for mechanical and thermal welding the tolerance depends on the type of weld. Although the precision of the adhesives is an asset, a disadvantage can be seen in Fig. 1.11. Figure 1.11 shows the time the "joint" needs to rest after a treatment. For example the adhesives must harden before they can be used, this can take 100 s up to 100 000 s. Depending on the situation this can be an advantage or a disadvantage. In contrary, fasteners like staples are not as accurate as adhesives, but they require substantially lower time before handling. In case of the staple the "time before handling" is literally the time needed to place a staple.

An ideal assembly method should be able to handle sheets with a thin thickness in combination with a low tolerance and little time before handling. These objectives are indicated with an arrow in Fig. 1.10 and 1.11.

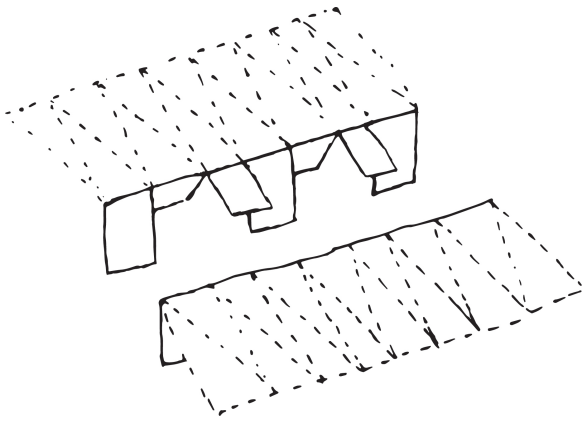

Figure 1.9: Discretized flaps which are created with virtual monohedral tiles with isosceles triangles which are dashed.

1.2.3. The proposed solution

The desire to have an accurate assembly method combined with little time before handling, motivates to come up with a new solution. The sheets to be joined are used for origami and kirigami purposes. Therefore origami and kirigami can also be considered as a joining technique. For the assembly of large kirigami structures the literature is thin, perhaps due the lack of applications for large structures. Alternatively, the field of modular origami could be used. Modular origami connects objects with pockets and flaps, see for example M. Kawamura [27] or R.J. Lang and B. Hayes [28]. The use of flaps and pockets are useful when an object consists of many small sheets. However, the intended kirigami object of this paper consists of two sheets having a large and single cut. Therefore, the proposed solution takes advantage of the more extensive area of origami, making it useful for a zipper design.

Figure 1.8 shows a zipper which moves along the flaps of two arbitrary surfaces. In order to use origami, the flaps are discretized, see figure 1.9. The discretized flaps are created with virtual monohedral tiles with isosceles triangles. Also different types of tiles are optional as spiral tiles [29] which can be used to make curved paths. The discretized flaps will be folded into each other making origami suitable for a joint.

1.3. Towards the article

The first section of the general article described the possible applications and environment for a certain joining technique. The second section introduces the origami itself as a joining technique.

Kirigami is an art of folding (creases) including cuts. But when considered as a joining technique the question can be raised were to place those folds? How does a possible crease pattern look like? Is there an optimal crease pattern for every situation?

These are valuable questions, designs for engineering purposes are often made under the influence of different combinations of stresses. For example a large thin walled cylinder laying on its side needs to carry its own weight, resulting in tensile stresses in the top of the cylinder while having compressive stresses in the bottom part of the cylinder. The combination of several creases (folds) are needed to make the joint suitable for a particular situation. Therefore a crease pattern needs to be optimized in order to find an optimal combination of creases.

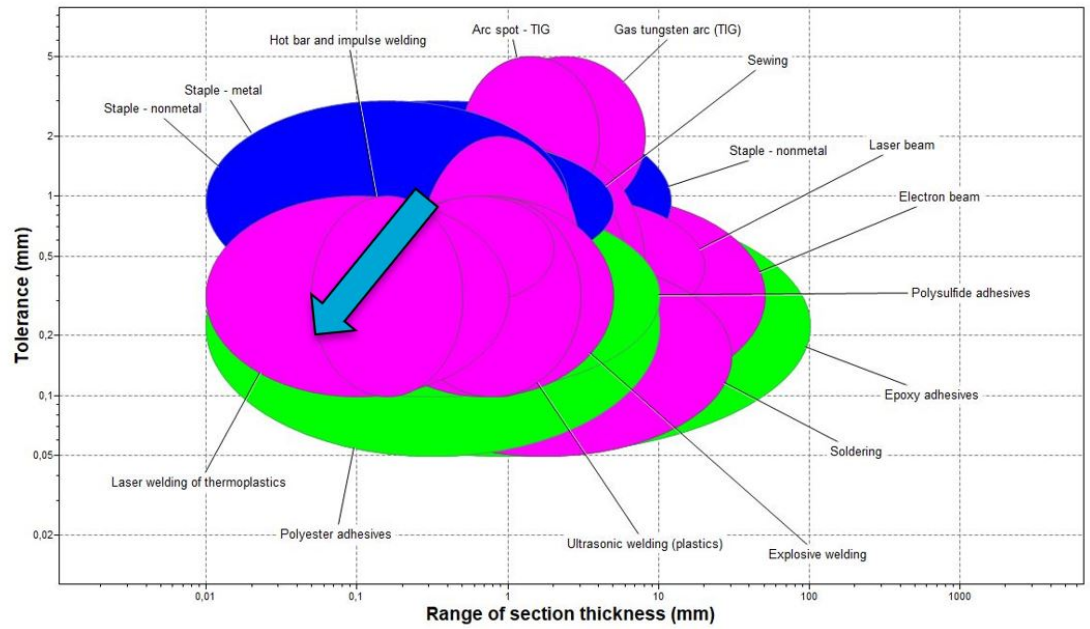

Figure 1.10: The Range of section thickness in mm is plotted against the tolerance of the joining technique. This plot is created with "level 3" of the CES Edupack database. Level 3 includes an overview of more than 200 material processes. This graph shows only the joining techniques that are suitable for plates with a section thickness of 1 mm or less. The green bars represent adhesives, the blue bars represent fasteners, and the purple bars represent mechanical and thermal welding. Source:[6]

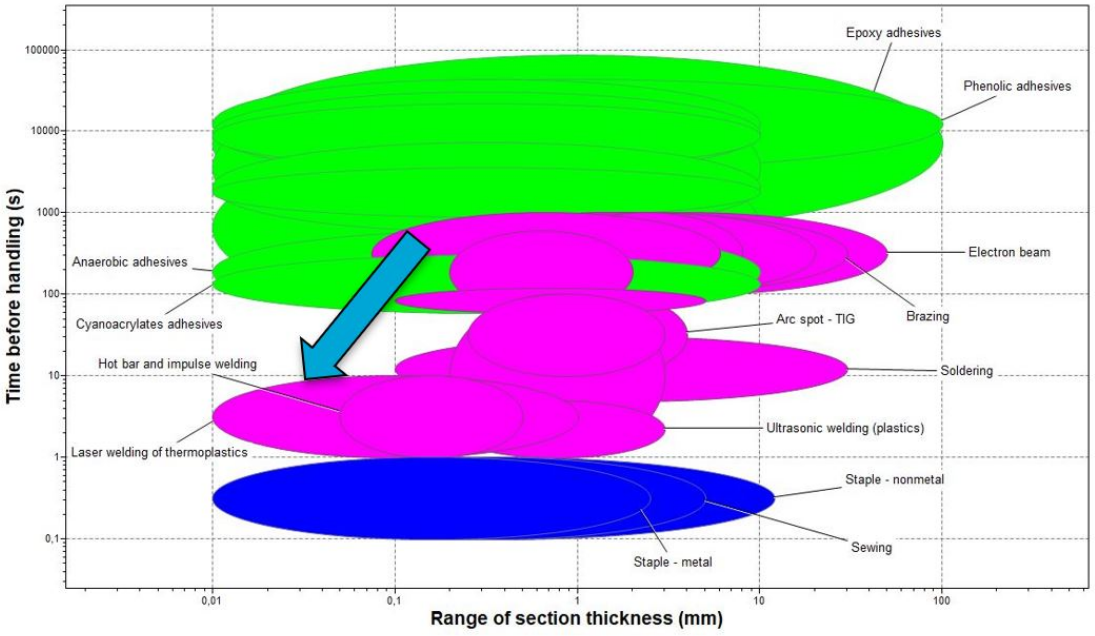

Figure 1.11: 4: The Range of section thickness in mm is plotted against the time before handling. Time before handling means the time an object needs to rest after the treatment before it can be handled. This plot is created with "level 3" of the CES Edupack database. Level 3 includes an overview of more than 200 material processes. This graph shows only the joining techniques that are suitable for plates with a section thickness of 1 mm or less. The green bars represent adhesives, the blue bars represent fasteners, and the purple bars represent mechanical and thermal welding. Source:[6]

The article discusses how to join kirigami sheets consisting a single continuous and smooth cut by constraining discretized strips with origami. The crease patterns are applied on top of the strips and will be optimized.

Bibliography

[1] S. J. Callens and A. A. Zadpoor, "From flat sheets to curved geometries: Origami and kirigami approaches," *Materials Today*, vol. 21, no. 3, pp. 241–264, apr 2018. [Online]. Available: https://doi.org/10.1016/j.mattod.2017.10.004https://linkinghub.elsevier.com/retrieve/pii/S1369702117306399

[2] Ag2gaeh, "File:Kugel-spirale-1-2.svg." [Online]. Available: https://commons.wikimedia.org/wiki/File:Kugel-spirale-1-2.svg

[3] Ö. Gönen, E. Akleman, and V. Srinivasan, "Modeling D-Forms," *Bridges: Mathematical Connections between Art, Music and Science*, pp. 209—-216, 2007.

[4] G. Systems, "GALA SYSTEMS (@GalaSystems)," 2014. [Online]. Available: https://twitter.com/galasystems

[5] G. Woodruff, P. Muench, and G. Witus, "Zipper mast for enhanced communications and surveillance," in *SPIE 8045, Unmanned Systems Technology XIII*, D. W. Gage, C. M. Shoemaker, R. E. Karlsen, and G. R. Gerhart, Eds., vol. 8045, no. May 2011, may 2011, pp. 1–6. [Online]. Available: http://proceedings.spiedigitallibrary.org/proceeding.aspx?doi=10.1117/12.885525

[6] GRANTA DESIGN, "CES EduPack software," Cambridge, UK, pp. 1–2, 2019. [Online]. Available: www.grantadesign.com

[7] A. W. Rudge and N. A. Adatia, "Offset-Parabolic-Reflector Antennas: A Review," in *Proceedings of the IEEE*, vol. 66, no. 12. IEEE, 1978, pp. 1592–1618.

[8] K. J. Kennedy, "Horizontal inflatable habitat for SEI," *NASA*, no. February 1992, pp. 135–146, 1992.

[9] A. F. Brinsmade, "US6216984B1 - Gravity Habitat Module for Space Vehicle," p. 10, 2001. [Online]. Available: https://patents.google.com/patent/US6216984B1/en

[10] Leonel, "Bilbao's Guggenheim Museum in Spain," p. 1, 2016. [Online]. Available: https://magazine.world-pass.com/en/bilbaos-guggenheim-museum-in-spain/

[11] A. Freason, "Department of Islamic Arts at Musée du Louvre by Mario Bellini and Rudy Ricciotti," 2012. [Online]. Available: https://www.dezeen.com/2012/09/24/department-of-islamic-arts-at-louvre-by-mario-bellini-and-rudy-ricciotti/

[12] H. Pottmann, A. Schiftner, P. Bo, H. Schmiedhofer, W. Wang, N. Baldassini, and J. Wallner, "Freeform surfaces from single curved panels," *ACM Transactions on Graphics*, vol. 27, no. 3, 2008.

[13] T. Hull, "Counting mountain-valley assignments for flat folds," *Ars Combinatoria*, vol. 67, no. August, pp. 175–187, 2003.

[14] J. Schneider, "Flat-Foldability of Origami Crease Patterns," pp. 1–18, 2004. [Online]. Available: https://organicorigami.com/

[15] E. D. Demaine and J. O'Rourke, *Geometric Folding*. Cambridge, UK: Cambridge University Press, 2007.

[16] D. J. Balkcom and M. T. Mason, "Robotic origami folding," *International Journal of Robotics Research*, vol. 27, no. 5, pp. 613–627, may 2008. [Online]. Available: http://journals.sagepub.com/doi/10.1177/0278364908090235

[17] "Genetic Algorithm and Direct Search Toolbox ™ 2 User ' s Guide," Natrick, 2008.

[18] J. Stewart, *Calculus Early transcendentals International Metric Version*, 7, Ed. Athenaeum Uitgeverij, 2008.

[19] K. Kuribayashi, K. Tsuchiya, Z. You, D. Tomus, M. Umemoto, T. Ito, and M. Sasaki, "Self-deployable origami stent grafts as a biomedical application of Ni-rich TiNi shape memory alloy foil," *Materials Science and Engineering A*, vol. 419, no. 1-2, pp. 131–137, 2006.

[20] S. A. Zirbel, B. P. Trease, S. P. Magleby, and L. L. Howell, "Deployment methods for an origami-inspired rigid-foldable array," in *Proceedings of the 40th Aerospace Mechanisms Symposium*. Greenbelt: NASA Goddard Space Flight Center, 2014, pp. 189–194. [Online]. Available: http://www.esmats.eu/amspapers/pastpapers/pdfs/2014/zirbel.pdf

[21] S. Felton, M. Tolley, E. Demaine, D. Rus, and R. Wood, "A method for building self-folding machines," *Science*, vol. 345, no. 6197, pp. 644–646, aug 2014. [Online]. Available: http://www.sciencemag.org/cgi/doi/10.1126/science.1252610

[22] J. C. Lucero, "Folding a 3D Euclidean Space," in *Origami7 Volume 2: Mathematics*. Tarquin, 2018, pp. 331–346.

[23] L. Bartholdi and A. Henriques, "Orange Peels and Fresnel Integrals," *The Mathematical Intelligencer*, vol. 34, no. 3, pp. 1–3, sep 2012. [Online]. Available: http://link.springer.com/10.1007/s00283-012-9304-1

[24] R. R. Orduño, N. Winard, S. Bierwagen, D. Shell, N. Kalantar, A. Borhani, and E. Akleman, "A Mathematical Approach to Obtain Isoperimetric Shapes for D-Form Construction A Mathematical Approach to Obtain Isoperimetric Shapes for D-Form Construction Departments of Visualization & Computer Science and Engineering ,," *Proceedings of Bridges 2016: Mathematics, Music, Art, Architecture, Education, Culture*, no. August, pp. 277–284, 2016.

[25] J. Sharp, "D-forms and developable surfaces," *Renaissance Banff: Mathematics, Music, Art, Culture*, pp. 121–128, 2005.

[26] GALA Systems INC, "GALA Systems INC." [Online]. Available: https://www.galasystems.com/en/

[27] M. Kawamura, "The Celes Family of Modular Origami," in *Origami4: Fourth International Meeting of Origami Science, Mathematics, and Education*. Taylor & Francis Inc, 2009, pp. 21–30.

[28] R. J. Lang and B. Hayes, "Paper Pentasia: An Aperiodic Surface in Modular Origami," *The Mathematical Intelligencer*, vol. 35, no. 4, pp. 61–74, dec 2013. [Online]. Available: http://link.springer.com/10.1007/s00283-013-9405-5

[29] B. Grünbaum and G. C. Shephard, *Tilings and Patterns*. New York: Freeman, 1987.

[30] Y. Rahmat-Samii, V. Manohar, and J. M. Kovitz, "For Satellites, Think Small, Dream Big: A review of recent antenna developments for CubeSats." *IEEE Antennas and Propagation Magazine*, vol. 59, no. 2, pp. 22–30, apr 2017. [Online]. Available: http://ieeexplore.ieee.org/document/7862180/

[31] C. Granet, "Designing axially symmetric Cassegrain or Gregorian dual-reflector antennas from combinations of prescribed geometric parameters," *IEEE Antennas and Propagation Magazine*, vol. 40, no. 2, pp. 76–82, apr 1998. [Online]. Available: https://www.cambridge.org/core/product/identifier/CBO9781107415324A009/type/book{_}parthttp://ieeexplore.ieee.org/document/683545/

[32] E. Sharon and E. Efrati, "The mechanics of non-Euclidean plates," *Soft Matter*, vol. 6, no. 22, p. 5693, 2010. [Online]. Available: http://xlink.rsc.org/?DOI=c0sm00479k

[33] B. Dunbar, "Apollo 50th Anniversary." [Online]. Available: https://www.nasa.gov/specials/apollo50th/back.html

[34] M. Majowiecki and I. Venice, "Architecture & Structures: Ethics in free-form design," in *Proceedings of the International Association of Shell and Spatial Structures (IASS)*, Venice, 2007, p. 24.

[35] R. Hibbeler, *Engineering Mechanics: Statics*, 13th ed. Singapore: Pearson Prentice Hall Pearson Education inc., 2013.

[36] F. Collins and M. Yim, "Design of a spherical robot arm with the Spiral Zipper prismatic joint," *Proceedings - IEEE International Conference on Robotics and Automation*, vol. 2016-June, pp. 2137–2143, 2016.

[37] Mathworks, "MATLAB R2018a," Nathick, 2018.

[38] J. B. Hopkins and M. L. Culpepper, "Synthesis of multi-degree of freedom, parallel flexure system concepts via Freedom and Constraint Topology (FACT) – Part I: Principles," *Precision Engineering*, vol. 34, no. 2, pp. 259–270, apr 2010. [Online]. Available: http://dx.doi.org/10.1016/j.precisioneng.2009.06.008https://linkinghub.elsevier.com/retrieve/pii/S0141635909000920

[39] R. Narain, T. Pfaff, and J. F. O'Brien, "Folding and crumpling adaptive sheets," *ACM Transactions on Graphics*, vol. 32, no. 4, 2013.

[40] FUTEK Advanced Sensor Technology, "LSB200 JR S-Beam Load Cell – FSH00104." [Online]. Available: https://datasheets.globalspec.com/ds/10/FutekAdvancedSensorTechnology/DD15764B-56A5-4AFC-8558-83E69B817F3A

[41] F. M. Dekking, C. Kraaikamp, H. P. Lopuhaä, and L. E. Meester, *A Modern Introduction to Probability and Statistics*, 1st ed., ser. Springer Texts in Statistics. London: Springer London, 2005. [Online]. Available: http://link.springer.com/10.1007/1-84628-168-7

[42] T. van den Boom and B. De Schutter, "Optimization in Systems ans Control, dictation for the course SC42055, article nr:

06917680006," Delft, p. 198, 2018. [Online]. Available: www.dcsc.tudelft.nl

[43] A. Gupta and A. Siakumar, "Simulation based multiobjective schedule optimization in semiconductor manufacturing," in *2002 Winter Simulation Conference*, 2002, pp. 1862–1870. [Online]. Available: https://brill.com/view/journals/njz/46/3-4/article-p163{_}1.xml

[44] P. Cortez, "Multi-Objective Optimization," 2014, pp. 99–117. [Online]. Available: http://link.springer.com/10.1007/978-3-319-08263-9{_}6

[45] M. S. Team, "Is it possible to solve a mixed-integer multi-objective optimization problem using Global Optimization Toolbox?" [Online]. Available: https://nl.mathworks.com/matlabcentral/answers/103369-is-it-possible-to-solve-a-mixed-integer-multi-objective-optimization-problem-using-global-optimizati{#}comment{_}840970

[46] "Mathworks Help Center." [Online]. Available: https://nl.mathworks.com/help/

2

Article

Joining Kirigami sheets consisting of a single continuous and smooth cut by constraining discretized strips with origami
20-05-2021

S.P.P. Allard
Mechanical Engineering
Delft University of Technology

Prof.dr.ir. J.L. Herder
Precision and Microsystems Engineering
Delft University of Technology

F.G.J. Broeren Msc.
Precision and Microsystems Engineering
Delft University of Technology

Kirigami can be used to create objects with a nonzero Gaussian curvature. A mathematical method is presented that can be applied to join a single continuous and smooth cut of a kirigami sheet. This is realized by constraining additional discretized strips with origami. The mathematical model evaluates how the strips from both sides of the cut can be constrained. The mathematical model is validated with an experiment, which confirmed the direction of the constraints. However, due to physical elements which are not part of the presented mathematical model, the relative proportion between the constraints did not fully represent reality. Finally, this treatise shows the optimization of a crease pattern, by using this model, resulting in a joined kirigami object.

1 Introduction

Origami is used in a broad range of mechanical engineering from biomedical applications [1], aerospace applications [2] to robotics [3]. The origami sculptures commonly share that they are flat having a large area in unfolded state and compact/desired shape in a folded state. This happens without stretching, cutting or deforming the sheet, while preserving the distances and angles, also known as isometric deformation [4]. This makes origami only suitable for the creation of objects with a zero Gaussian curvature [5]. Origami objects are desired for several reasons, such as easy transportation or low costs for manufacturing processes [4].
Origami is not suitable for objects with a non-zero Gaussian curvature, for example spheres and paraboloids. Non-zero Gaussian objects created with origami will have undesired distortions in folded state [4]. To avoid deformations, cuts can be made within the sheet [5]. The combination of origami and cuts is called kirigami [4]. For certain applications a single cut needs to be joined.
Often thin sheets are joined with adhesives, fasteners or mechanical and thermal welding [6]. An origami approach of joining can be seen in the field of modular origami. Snapology is an origami technique invented by Heinz Stroble [7], the foundation for example for the origami Menger Sponge [8] [9], the creation of meta materials [10] or a simple ”witch ladder” or ”Jacobs ladder” [11]. Closely related is a connection with flaps and pockets, for instance the Celes family by M. Kawamura [12] or the paper Pentasia of R.J. Lang and B. Hayes [13]. However, modular origami is mostly used for small objects [14], with the ZEBRA method for constructing architectural 3D from paper [14] merely an exception. This paper extends the field of modular origami towards the assembly of large kirigami objects. Only kirigami objects with large and single cuts are considered for the presented joining technique of this paper.

This treatise presents a mathematical methodology to join a continuous and smooth edge of two flat kirigami sheets with the use of origami. Accomplished with additional discretized flaps located on the edge (Fig. 1) that are folded into each other.

The paper has the following layout. Firstly, a possible cut is derived to define the position of the additional strips relative to the sheets. Secondly, a mathematical methodology will be defined on how the strips can constrain each other. Thirdly, the mathematical methodology will be validated. Fourthly, a crease pattern will be optimized. Finally, a kirigami object is joined with the established crease pattern.

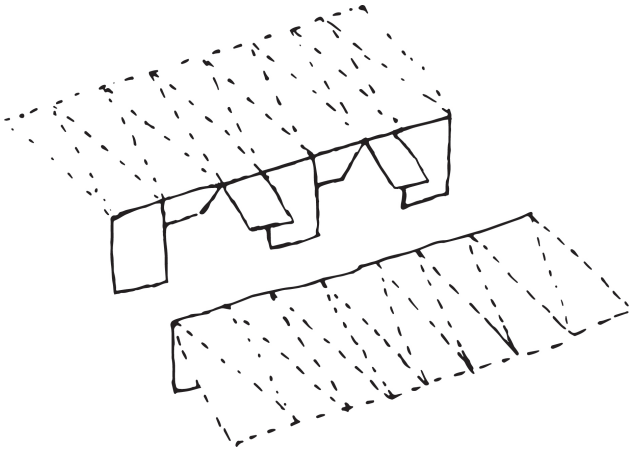

Fig. 1. Discretized flaps which are created with virtual monohedral tiles with isosceles triangles which are dashed.

2 Problem definition

A potential cut can be described as a line (C) on a certain surface. A space curve C can be defined by a continuous vector function $\mathbf{r}(t) = \begin{bmatrix} f(t) & g(t) & h(t) \end{bmatrix}^T$ [15] with $f(t)$, $g(t)$ and $h(t)$ real valued. The cut of the kirigami object needs to be smooth, that is the case if $\mathbf{r}'(t) \neq 0$ on interval I.
The strips (flaps) are aligned with $\mathbf{r}(t)$ and have their own coordinate system, $\hat{x}$ and $\hat{y}$. The y-axis is aligned with the binomial vector and the x-axis is aligned with the tangent vector of $\mathbf{r}(t)$.

The discretized strips will be folded into each other in such a way that the strips constrain each other. Resulting in a joined kirigami object along the cut. The question remains where to place the folds. And how does a crease ensure that there is no relative movement between the sheets?

3 Method: Mathematical description of constraining.

The basic principle is that two strips (flaps), each from a different sheet, are paired together and are "sticky" with each other. Sticky in the sense that no misalignment gadget is allowed (lemma 3.2). Hence, every crease placed on one of the strips is also placed on the other with an identical orientation and mountain-valley assignment. In such a way that the sheets are able to constrain each other.
Hereinafter a mathematical description can be found of why which crease should be placed where. starting with the introduction of subsets, sheet orientation and on how to constrain free movement.

3.1 Map folding applied to strip folding

The methodology of map folding is closely related to the intended model for strips. Both models include intersecting creases. For map folding the creases are either parallel or perpendicular, while for folding with strips the creases do not have to be so. Following Demaine and Rourke [16] map folding needs to have at least one continuous crease which is labeled valley or mountain throughout the sheet. In map folding creases are either assigned to subset $\mathcal{H}_i$ (horizontal) or subset $\mathcal{V}_i$ (vertical) with an accompanied indexation number for the ordering (i). A subset can be assigned with multiple creases which are independent of each other. In case of map folding for each subset can be said that "all creases must be parallel; otherwise the vertex of intersections between crossing crease lines violate Maekawa's Theorem" [16]. Note that creases from the same subset can be folded independently from each other.

The strip model will exclude the condition of perpendicular and parallel creases while including the requirement of independent creases within a subset, with 'independently' defined only within a strip. Reformulated, by definition the creases may not intersect inside the strip. The completely independent creases will be placed in subset $\mathcal{H}$. Afterwards the creases of subset $\mathcal{V}_1$ will be folded and so on till $\mathcal{V}_n$.
The first set of creases are labeled differently with $\mathcal{H}$ because it has a distinctive number of variables per crease compared to subset $\mathcal{V}$. At first sight subset $\mathcal{V}_1$, $\mathcal{V}_2$ etc. do not differ in constraints nor the number of variables. They are therefore characterized with the same label $\mathcal{V}$ accompanied with a unique index number.

The letters $\mathcal{H}$ and $\mathcal{V}$ are inherited from map folding but for the presented model the creases are not necessarily aligned with the horizontal or vertical. For conventional reasons we will stick to the labels $\mathcal{H}$ and $\mathcal{V}$.

3.2 Dimensions of origami

Flat origami models are in reality in $\mathbb{R}^3$ and satisfy the five origami axioms [17]. For mathematical reasons the sheet thickness is assumed to be zero. Therefore the origami model will be mapped to the folding space $\mathbb{R}^2 \times \mathbb{Z}$ [17]. Note that the origami objects throughout this paper are part of flat origami. The folded and unfolded state are related by the "*semifolding map* $\mu : C \to \mathbb{R}^2$ that determines only the final position of the sheet in a plane and *superposition ordering* $\sigma : C \to \mathbb{Z}$ determines only the overlap order of the layers"[17] of folded sheets.

3.3 Free movement of the strips

The $\mathbb{R}^2$-space is spanned by x-axis and y-axis from the point of view of the strip and not the kirigami object. The strips can only be constrained inside this plane (3 degree of freedom), resulting into possible constraint space of x, y, R_z and a freedom space of z, R_x, R_y.
However, keeping in mind how the origami object will act in the physical world the freedom space can be reduced even further. By stacking faces on top of each other, translation in the z-direction can be constrained [18]. Therefore the constraint of z-direction relates to the size of the $\mathbb{Z}$-space.
Assuming that the origami object is constrained and therefore static, the rotations (R_x, R_y and R_z) are within this paper left out of consideration. Concluding, the strips can be constrained into the x, y, z-direction.

3.4 Stacking of the faces

To preserve/enforce the "stickiness" of the two strips (sheets), the translation into the z-direction needs to be reduced. As mentioned earlier the constraint of the z-direction is related to the stacked number of faces (F). The numbering of stacked faces, L, gives an indication of the total constraints. Only faces which are enclosed by a crease (opposite folding) attribute to the constrain.

Definition 3.1. *A set of faces, F_i, composes a crease pattern C. After a mapping, μ, into folded state the number of layers, L, can be determined by counting, n, the number of intersections of the faces. The faces needs to be enclosed by a crease (opposite folding, see) in order to attribute to the constrain. Mathematically:*

$$\bigcap_{i=0}^{n} F_i \quad for \quad F_i \cap F_{i+1} \neq 0 \quad \rightarrow \quad L = max(n) \qquad (1)$$

3.5 Sheet orientation

Demain et al. (2007) describes the "function λ which specifies the above/below relations of every two regions of paper that are collocated according to f" [16]. The most important notes are summarized below which have implications on constraining with origami.

"A folded state of a 2D piece of paper is a pair (f,λ) consisting of an isometric function $f : P \rightarrow \mathbb{R}^3$ (the geometry) and a partial function λ from $P \times P$ to $\{-1,+1\}$ defined on pairs (p,q) of distinct noncrease points $p,q \in P$ for which $f(p) = f(q)$ (the order). ... A value +1 or -1 is assigned to $\lambda(p,q)$, with the intent that λ disambiguates whether p is stacked "above" q ($\lambda(p,q) = +1$) or p is stacked "below" q ($\lambda(p,q) = -1$)" [16]. For the constraining of two sheets two conditions are important to mention; antisymmetry condition and the transitivity condition.

Antisymmetry condition, "for any two points $p,q \in P$ at which $\lambda(p,q)$ is defined, that $\lambda(q,p)\mathbf{n}_f(p) = -\lambda(p,q)\mathbf{n}_f(q)$, that is, p and q must be on opposite sides of each other" [16]. With $\mathbf{n}_f(p)$ as the normal vector on point p, see Fig. 2.

Transitivity condition, "for any three points $p,q,r \in P$ at which λ is defined pairwise, if $\lambda(p,q) = -\lambda(r,q)$, then $\lambda(r,p) = \lambda(q,p)$; that is, if p and r are on opposite sides of q, then r and q are on the same side of p" [16]. See also Fig. 6.

3.6 Primary constraint: imposed by one single crease

Two sheets (S_I & S_{II}) are placed on top of each other, both sheets have the same orientation in unfolded state ($\mathbf{n}_I^{\mathcal{F}^{-1}} = \mathbf{n}_{II}^{\mathcal{F}^{-1}}$). A crease pattern G is embedded on top of these two sheets. G consist of vertices (V), edges (E), and faces (F) [17]. During a folding operation the two sheets will remain sticky, no misalignment gadget will be allowed (lemma 3.2). As a consequence, the creases that are placed into sheet I will also be placed into sheet II. The two sheets, represented by a blue and a pink line from Fig. 2, are sticky and remain therefore parallel to each other regardless of any folding operations.

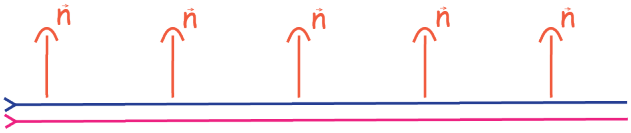

Fig. 2. Two flat sheets which are "sticky" shown in pink and blue. The corresponding normal vectors of the blue sheet are shown. The sheets remain sticky also in the folding operations.

A crease can be defined by $E_{ij} = \overline{V_i V_j}$ within the $\mathbb{R}^2$-space of a sheet including the raw edges [17]. The creases $E_{ij,I}$ and $E_{ij,II}$ are the duplicate of crease E_{ij} but projected on sheet S_I or S_{II}.

Depending on the point of view either S_I or S_{II} is fixed at the bottom raw edge of the strip. Sheet S_I and S_{II} can constrain each other with a crease E_{ij}. In reality the creases $E_{ij,I}$ and $E_{ij,II}$ will be near each other in folded state ($\mathcal{F}$) at an almost negligible distance. Therefore sheet I will be folded into sheet II or vice versa. If $det(E_{ij,II}, E_{ij,I}) < 0$, so $E_{ij,II}$ is on the left of $E_{ij,I}$, then the sheets are constrained by $\vec{E}_{ij,II} \preceq \vec{E}_{ij,I}$. Or if $det(E_{ij,II}, E_{ij,I}) > 0$, so $E_{ij,II}$ is on the right of $E_{ij,I}$ then the sheets are constrained by $\vec{E}_{ij,II} \succeq \vec{E}_{ij,I}$. Satisfying the origami axiom that paper can not self intersect [17] or intersect a different paper, sheet S_I and S_{II} have a previously mentioned constrain imposed by E_{ij}. This leads to lemma 3.1

Lemma 3.1. *If the crease $E_{ij,I}$ of sheet I and $E_{ij,II}$ of sheet II lay both inside $\mathbb{R}^2$ and are folded into each other. And if $det(E_{ij,II}, E_{ij,I}) < 0$ then the sheets are constrained by $\vec{E}_{ij,II} \preceq \vec{E}_{ij,I}$. Or if $det(E_{ij,II}, E_{ij,I}) > 0$ then the sheets are constrained by $\vec{E}_{ij,II} \succeq \vec{E}_{ij,I}$. Independent of which sheet is fixed or which orientation the creases have:*

If $E_{ij,II} \neq E_{ij,I}$ then sheet I or II is somewhere in the freedom-space

If $E_I = E_{ij,II}$ and $E_{ij,I} \parallel E_{ij,II}$ then the creases are on the constraint

If $E_I = E_{ij,II}$ and $E_{ij,I} \nparallel E_{ij,II}$ then the creases have a collision

Proof. Lets say E_{II} lies left of E_I for $E_I \parallel E_{II}$. Then E_I can be rewritten as $E_I = \vec{d} + \hat{E}_{II}|E_I|$ with $\vec{d} \geq 0$ as the distance between E_I and E_{II}. In that case $det(E_{II}, \vec{d} + \hat{E}_{II}|E_I|) \leq 0$. If $det(\ldots) < 0$ then E_I is located to the right of E_{II} and if $det(\ldots) = 0$ then E_I and E_{II} lay into each other. So $E_{II} \leq \vec{d} + \hat{E}_{II}|E_I|$ results in $E_{II} - \hat{E}_{II}|E_I| \leq \vec{d}$. Indeed, if $d = 0$ then E_I and E_{II} are equal to each other and are therefore laying on the same location and if $d > 0$ then E_I lies indeed on the right hand side of E_{II}.

This article excludes the use of a misalignment gadget, which is defined in lemma 3.2

Lemma 3.2. *Misalignment gadget; If the crease E_I of sheet I and E_{II} of sheet II lay both inside $\mathbb{R}^2$ and are **not** folded into each other. Independent of the location and orientation of the creases, the sheets are not constrained. Mathematically: Freedom space of both creases $< -\infty, -\infty > \preceq E_I \preceq < \infty, \infty >$ and $< -\infty, -\infty > \preceq E_{II} \preceq < \infty, \infty >$.*

3.7 Freedom and Constraint space

One single crease has one directional constraint (lemma 3.1) also called a unilateral constraint. Sheet II can impose a constraint on sheet I with the use of a crease. If the directional constraint, for example, is aligned with the x-axis the constraint can either be into the positive or negative direction. A unilateral constraint can be seen as an half degree of freedom (DOF). Hence, it will be sufficient to split the $\mathbb{R}^2$-space into four subspaces, namely: x^+, x^-, y^+, y^- in such a way we can track constraints for individual directions. Resulting in a freedom space of $\mathbf{F} : \{x^+, x^-, y^+, y^-\}$ and a constraint space of
$\mathbf{C} : \{x^+, x^-, y^+, y^-\}$.

3.8 Constraining with a single crease

Figure 3 shows a projected view of a cross-section. Within the figure the orientation of the sheet ($\vec{n}$, orange vectors) and the resulting constraints ($\vec{C}$, black vectors) are shown. The folding direction ($\vec{N}$) does not match the direction of the constraint. Rather, the constraints ($\vec{C}$) are coupled to the orientation of the sheet ($\vec{n}$). This is described in lemma 3.3. This implies that with one single fold the sheet is able to move into three directions, tangent to the crease and into the the orientation of the sheet.

Lemma 3.3. *Each individual crease has a freedom space: $\mathbf{F} = \{-\vec{T}, \vec{T}, \vec{n}\}$ and a constraint space: $\mathbf{C} = \{-||\vec{N}||\hat{n}\}$ in $\mathbb{R}^2$ with $\vec{T}$ as the tangent vector of the crease. The $\mathbb{R}^2$-space is the union of the subsets $\{x^-, x^+, y^-, y^+\} = \mathbf{F} \cup \mathbf{C}$ for which $\mathbf{F} \not\parallel \mathbf{C}$.*

3.9 Constraint imposed by multiple creases

To avoid ambiguity, we assume that there are only two types of folding, see Fig. 4; 1) folding around the entire (flat) origami object, folding with opposite creases. Or 2) **not** folding around the entire origami object, resulting in a Jacobs ladder. The choice between these two options has consequences for the resulting constraint.
Note that throughout this paper the creases are placed from the bottom raw edge to the top raw edge. As a result, all creases within a subset are placed in chronological order.

The origami objects of Fig. 4 appear to pop up in $\mathbb{R}^3$ but mathematically they do not, due to the fact of sharp fold angles and infinitely thin sheets. Opposite folding and the Jacobs ladder will be discussed separately thenceforth.

3.9.1 Folding around the object, Opposite folding

The origami object in the middle of Fig. 4 is part of opposite folding. It includes two folds from lemma 3.1. Sheet I is enclosed by sheet II with the creases E_A and E_B. The resulting constraints of the creases are stated as $\vec{E}_{A,II} \preceq \vec{E}_{A,I}$ and $\vec{E}_{B,II} \succeq \vec{E}_{B,I}$. Note that the constraints are in the opposite direction, if $E_A || E_B$. Therefore sheet I is locked for one direction (y-axis) by sheet II, removing an entire degree of freedom (DOF) from the freedom space (**F**) which is added to the constraint space (**C**).

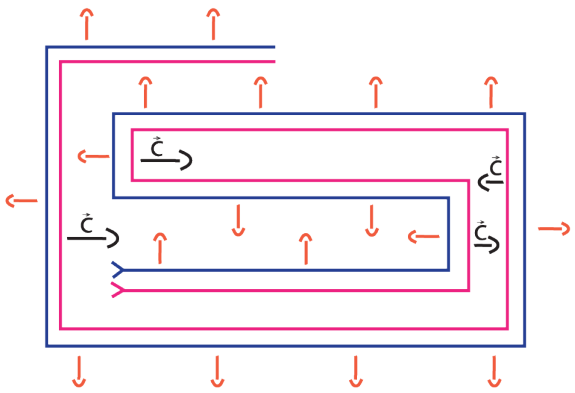

Fig. 3. A combination of the Jacobs ladder and opposite folding from a cross-section projected on a 2D plane. The normal vector and constrain vectors cross-section are shown. Note that the figure represents a folded crease pattern in the 1D-space. So, mathematically, the sheets remain in the same plane, although the figure suggests otherwise.

3.9.2 Not folding around the object, Jacobs ladder

The origami object on the right of Fig. 4 is part of a Jacobs ladder. It includes twice a fold from lemma 3.1. The constraints of the creases are stated as $\vec{E}_{A,II} \preceq \vec{E}_{A,I}$ and $\vec{E}_{B,II} \preceq \vec{E}_{B,I}$. Therefore, the constraints have the same direction. As a result, this is a one-directional constraint, removing a half DOF from the freedom space (**F**) which is added to the constraint space (**C**).

A crease E_n is part of opposite folding if the partial function λ_n is equal to λ_{n-1} from the previous laid crease E_{n-1}, when it is not then it is part of a Jacobs ladder. This can be formulated in the following way:

Lemma 3.4. *There are two creases next to each other, namely: E_{n-1} and E_n. With $\lambda(p,q) = \lambda(q,p)$ for two points with one intermediate crease E_j will be reformulated as λ_j. The crease E_{n-1} has a corresponding λ_{n-1} and E_n has a corresponding λ_n. Note; that λ_n is located on the crease E_n and is therefore aligned with the folding direction, positive or negative.*

if $\lambda_{n-1} = \lambda_n$ then E_n is part of opposite folding
if $\lambda_{n-1} \neq \lambda_n$ then E_n is part of a Jacobs ladder

A combination of multiple creases with a unilateral constraint can result in a bilateral constraint, although this is not necessarily the case with a Jacobs ladder.

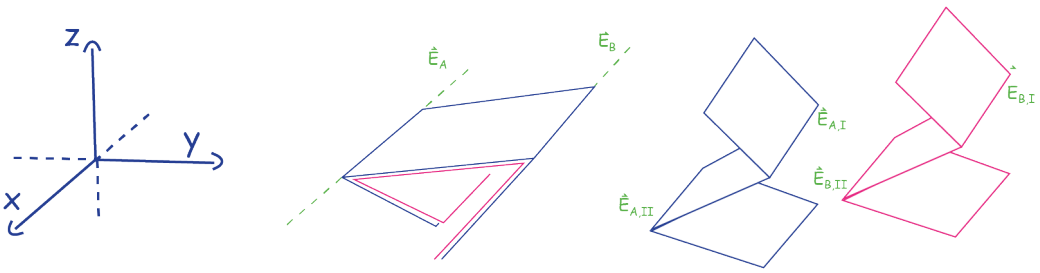

Fig. 4. The creases A and B are located in the same location. The figure in the middle shows an origami object with opposite folding while the object on the right is part of a Jacobs ladder.

3.10 Relation of the constraint and the folding direction

A crease pattern in unfolded state is a roadmap to the folded state. It consist of vertices (V), edges (E), and faces (F) [17], but it lacks a representation of the orientation of the sheet ($\vec{n}$) in folded ($\mathcal{F}$) and unfolded state ($\mathcal{F}^{-1}$). It becomes even more complex with the introduction of multiple creases. In order to keep track of the orientation of the sheet, the set of variables (Λ) is introduced. The variable Λ will help to relate the type of folding with the orientation of the sheet.
The variable Λ will indicate if a crease is part of opposite folding or part of a Jacobs ladder. If a crease is part of a Jacobs ladder then it will be represented with a 1, if not then the crease will be represented with a 2. The folding direction $\vec{N}$ and the orientation of the sheet ($\vec{n}$) can be related to each other on crease m as is shown in Eqn. (2).

$$\vec{n}_m = \vec{N}_m(-1)^{\sum_{i=1}^{m}\Lambda} \tag{2}$$

The resulting constraint can be formulated as $C_m = -||\vec{N}_m||\hat{n}_m = -\vec{N}_m(-1)^{\sum_{i=1}^{m}\Lambda}$ for crease m.

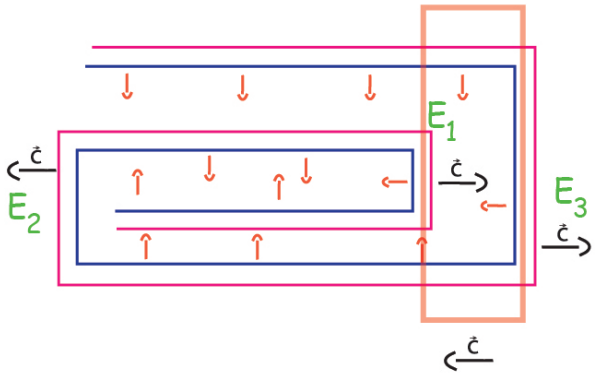

Fig. 5. A combination of the Jacobs ladder and opposite folding from a cross-section projected on a 2D plane. The normal vectors and constrain vectors are shown. Note that the figure represents a folded crease pattern in the 1D-space. So, mathematically, the sheets remain in the same plane, although the figure suggests otherwise.

3.11 Secondary constraint

The strips can be constrained by a creases. However, if there are multiple creases, the creases can interact with each other, resulting in a secondary constraint. See for example Fig. 5, where crease E_1, E_2 and E_3 each have their own constraint, defined as $C_i = -||\vec{N}_i||\hat{n}_i$. But the interaction between the creases E_1 and E_3 will also result in a constraint, which will be mentioned as a secondary constraint. The pink sheet of E_1 is constrained twice by the blue sheet of E_1 and E_3. While the blue sheet of E_3 is also constrained twice by the pink sheet of E_1 and E_3.

The transitivity condition [16] of λ is used to determine the direction of the secondary constraint. Figure 6 represents the transitivity condition. The transitivity condition relates λ from p to r. So if p is pointing towards r then $\lambda(r,p) = +1$ else $\lambda(r,p) = -1$. Note that the sheets q and r are sticky, they are paired with each other.
The orientation of the the secondary orientation is determined to be $\vec{n}_s = \lambda(r,p)\vec{n}_r$ with n_r as the orientation of the outer crease which enclose a crease. If crease i is enclosed by crease j the secondary constraint can be formulated as $C_j = -\vec{n}_s = -\lambda(r,p)\vec{n}_r$. The size of $\vec{n}_r$ is equal to the smallest overlap between E_i and E_j, mathematically $min(proj_{E_i}\hat{E}_j, proj_{E_j}\hat{E}_i)$. The direction of $\vec{n}_r$ is equal to the orientation of the sheet in crease j.

3.12 Add a constraint to the constraint space

There are two types of constraints: primary and secondary constraints. These constraints (C_i) need to be added to the constraint space ($\mathbf{C}$) in order to have a complete overview of the resulting constraint of a crease pattern. Recall that the constraint space is defined as $\mathbf{C}$: $\{x^+, x^-, y^+, y^-\}$. The constraint space can be filled with the projection as is shown in Eqn. (3, 4).

$$proj_{C_i}\hat{x} = \frac{\hat{x}\cdot C_i}{||\hat{x}||^2} \quad \begin{cases} \text{if: } proj_{C_i}\hat{x} < 0 \Rightarrow x^- = \{|proj_{C_i}\hat{x}|\} \\ \text{if: } proj_{C_i}\hat{x} > 0 \Rightarrow x^+ = \{|proj_{C_i}\hat{x}|\} \end{cases} \tag{3}$$

$$proj_{C_i}\hat{y} = \frac{\hat{y}\cdot C_i}{||\hat{y}||^2} \quad \begin{cases} \text{if: } proj_{C_i}\hat{y} < 0 \Rightarrow y^- = \{|proj_{C_i}\hat{y}|\} \\ \text{if: } proj_{C_i}\hat{y} > 0 \Rightarrow y^+ = \{|proj_{C_i}\hat{y}|\} \end{cases} \tag{4}$$

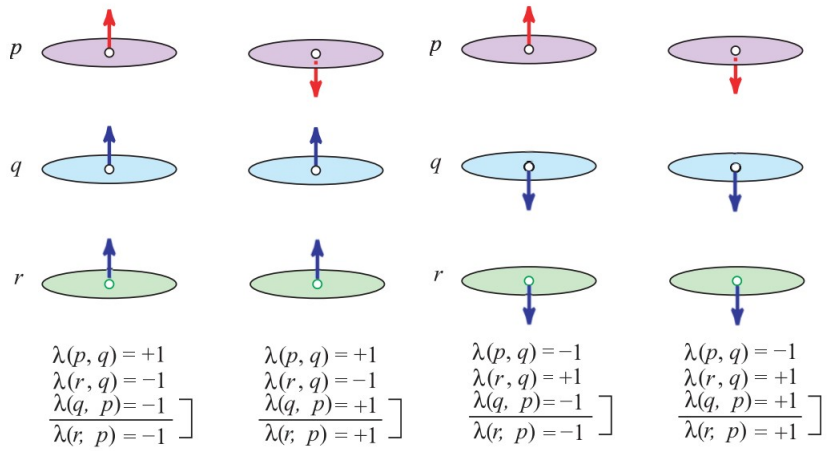

Fig. 6. The transitivity condition of of λ. Adapting from [16], the final two columns are added.

3.13 Constraining with several subsets ($\mathcal{H}$, $\mathcal{V}$)

The creases of subset $\mathcal{H}$ are completely independent, but the creases of subset $\mathcal{V}$ are not, resulting in a mountain-valley assignment when intersecting creases from a lower subset. The mountain-valley assignment alters the direction of the sheet orientation $\vec{n}$. A schematic overview is shown in Fig. 7. The folding operation from the figure has one crease from subset $\mathcal{V}$ which intersects two creases of subset $\mathcal{H}$. The first partial crease from subset $\mathcal{V}$ has a sheet orientation pointing inwards, the second partial crease is pointing outwards and the third partial crease is pointing inwards again. Just as before the sheet orientations are accompanied by a constraint. The directions of the constraints are alternating with the mountain valley assignment.
The first partial crease ($E_{m,1}$) of crease (m) determines the direction of all other partial creases due to the mountain valley sequence. The direction ($n_{m,i}$) of the partial crease ($E_{m,i}$) is mathematically shown in Eqn. (5). Note that i corresponds with the indexation number.

$$\vec{n}_{m,i} = (-1)^{1+i} ||E_{m,i}|| \vec{n}_{m,1} \tag{5}$$

Although it is not validated yet, it is expected that also the secondary creases play a role in constraining subsets of $\mathcal{V}$. Further research should determine a correct formulation.

4 Validation of the mathematics with an experiment

The previously mentioned projection method to determine the constraint of the creases is verified with an experiment. The verification is divided into two separate research questions. Firstly, is the crease pattern constraint as expected? Secondly, is the crease pattern constraint in proportion?
This section will briefly discuss the result of the experiment. Extensive reporting on the experiment can be found in the appendix.
Both objectives are achieved within the same experiment. A top view of the experimental set up is shown in Fig. 8. The experiment has the following layout; two sheets are folded into each other. One sheet is fixed to the ground. The second sheet is moved.

This relates to the research questions (objectives) in the following way. The first objective: if the second sheet can not move into a certain direction, then it is constrained in that particular direction.
The second objective: the relative proportion between the constraints is related by the needed force to deform a crease pattern into a certain direction.
The objectives are validated with an elementary sets of creases. Seven creases of subset $\mathcal{H}$ are sufficient for the validation. The crease patterns differ in number of creases and whether they are part of opposite folding or not. All crease patterns are shown in Fig. 9.

The measurements are taken with a ”PI Stage” which is able to measure the displacement. An additional force sensor FSH00104 is used, which has a full scale accuracy of -0.1 to $0.1 \pm \%$ [19]. The measurements are taken in Newtons (N) and the displacements in μm.

For some measurements deformation did not occur on the crease but on a different location, often at the base of the strip. If deformation did occur in the wrong location, the strip could even tear instead of unfold. In order to prevent this issue a second template has been used if necessary.

The hypothesis of objective one is shown in Tab. 1. The creases are labeled from A to G and are shown in Fig. 9. If the resulting constraint of a crease pattern constrains a particular direction the table will display ”yes”. If the sheets can move relative to each other, the table displays ”no”.

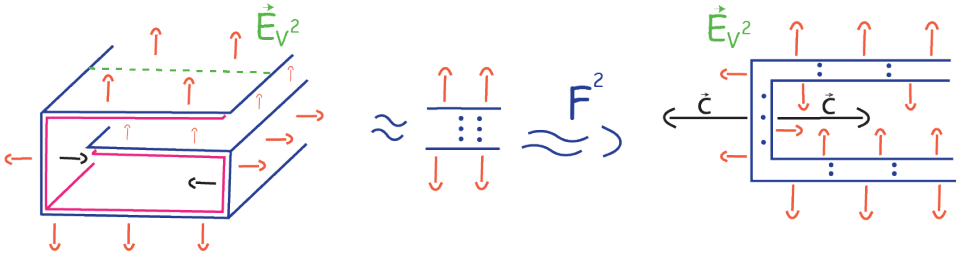

Fig. 7. Folding operation of subset $\mathcal{V}$. Note that the figure represents a folded crease pattern in the 1D-space. So, mathematically, the sheets remain in the same plane, although the figure suggests otherwise. The vertical dots represent are the inner layers and are omitted for clarification.

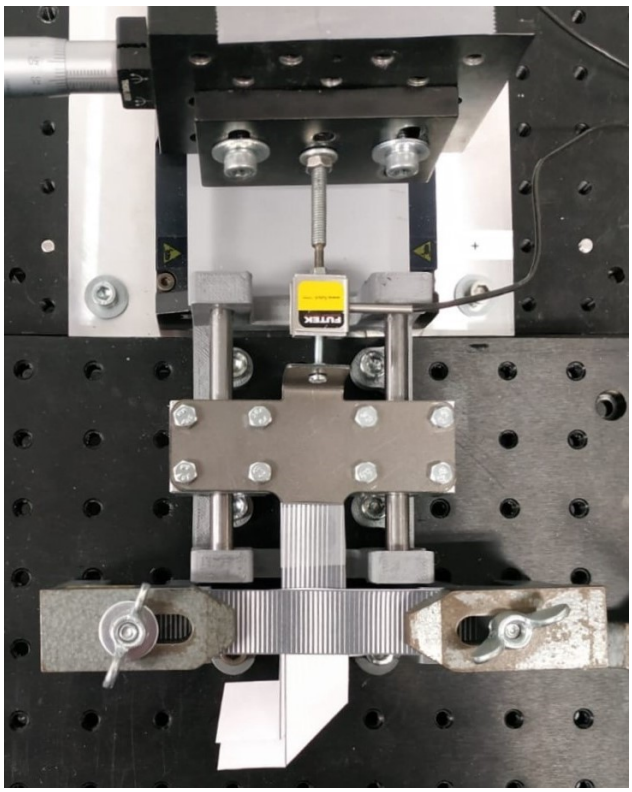

Fig. 8. The experimental setup; two sheets are folded into each other. One sheet is fixed to the solid ground and one sheet is attached to a template which is constrained by two linear bearings. The movement is performed with a PI Stage in combination with a FSH00104 Futek sensor for the measurements.

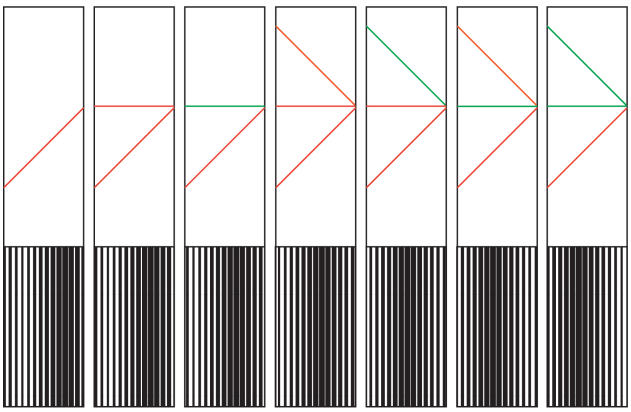

Fig. 9. The crease patterns for the experiment. Ordered alphabetically from left to right. A red line represents opposite folding and a green line represent a Jacobs ladder.

Tab. 1. The expected constraints in the direction x^+, x^-, y^+, y^- for each crease pattern are given. If the crease pattern is constrained then a "yes" is shown, else "no". This table refers to objective one.

	Creases						
Direction	A	B	C	D	E	F	G
x^+	no	yes	no	yes	yes	yes	no
x^-	yes	yes	yes	yes	yes	yes	yes
y^+	yes	yes	yes	yes	yes	yes	yes
y^-	no	no	no	yes	yes	yes	no

The hypothesis of objective two is shown in Tab. 2. Objective two involves the proportion of the constraints within a crease pattern compared to each other. A constraint into a direction is represented with a value, if the sheets are not constraint then a value zero is shown in the table.

From all measurements the highest peak (P) is determined, which represents the maximum resistance to unfolding. This has also been done with the baseline measurement (Q) which is subtracted from the actual measurements (P). Mathematically: $f(P,Q) = abs(P) - abs(Q)$ and $Var(F(P,Q)) = Var(P) + Var(Q)$.

The first hypothesis to be tested determines if the sheets are constrained or not, this is validated with a null hypothesis. If the sheets are not constrained then the expected value is $H_0 : \mu = 0$, if the sheets were constrained then $H_1 : \mu > 0$.

The hypothesis can only be rejected into one-direction, this is therefore a case of one-sided confidence inter-

Tab. 2. The expected constraints in the direction x^+, x^-, y^+, y^- for each crease pattern are given. If the crease pattern is constrained then a "yes is shown, else "no". This table refers to objective one.

	Creases						
Direction	A	B	C	D	E	F	G
x^+	0	2	0	4	4	4	0
x^-	2	2	4	4	2	4	6
y^+	2	2	2	4	2	2	4
y^-	0	0	0	2	2	4	0

Tab. 3. The rejection of null hypothesis is shown in the table for crease A and B. The determination of the rejection is accompanied by the test statistic (T) and the number of measurements. If the hypothesis is wrongly rejected, then the result will be indicated with a (!).

	Creases					
	A			B		
	T	n	*Rejected*	T	n	*Rejected*
x^+	2.3735	5	No	4.0149	5	yes
x^-	29.2020	5	Yes	34.5762	5	yes
y^+	20.5297	5	yes	32.0194	5	yes
y^-	1.7372	5	No	-3.9655	4	No

val. The allowable exceedance probability is set to be $p = 0.025$. "The null hypothesis will be rejected in favor H_1, if $T \geq t_{n-1,\alpha}$ [20]. If H_0 is rejected then the creases are constraint. The Tab. 3, 4 and 5 indicate whether the constraints are rejected or not.

4.1 Results of the experiment

The first hypothesis is confirmed with the experiment. However, three measurements differ from the expected results, namely; crease C into the x^+-direction, crease D into the y^+-direction and crease G into the x^+-direction.
Crease pattern C into the x^+-direction is rejected in contradiction with the hypothesis. But the data show no sign of unfolding. This measurement was influenced by a relatively high friction within the set-up. This may be because the experiment had to be rebuilt on a different day. Probably, an apparently negligible rotation of the setup results in a slightly higher non-negligible friction within the system.
Crease D into the y^+-direction is not rejected as expected. This measurement did require a second template which caused the origami object to be pulled too far out of its $\mathbb{R}^2$ plane into the $\mathbb{R}^3$ space. Because of that, the folds were not sharp enough. This induced a relatively high variance preventing the rejection of H_0.
Crease pattern E needed two templates to prevent deformation at the bottom of the strip. In combination with the fact that the final crease is part of a Jacobs ladder, it was not possible to take viable measurements. The final part of the strip remained in the $\mathbb{R}^3$ space. The crease pattern of E will be entirely neglected.
Crease pattern G in the x^+-direction is rejected in contradiction with the hypothesis. The H_0 has been rejected just above the threshold. The data do not indicate any unfolding behavior. This crease pattern has more Jacobs ladders then any other crease pattern. Although there should have been free movement, the physical interaction between the sheets, friction, has a negative influence on the measurement.

Although objective one is sound, no conclusion can be drawn about objective two. For example in case of crease B, the constraint of x^+, x^- and y^+ should be proportionally equal. Although the measurements of the y^+ and x^--direction are near each other they differ too much. The same is true for the measurement in the x^+-direction for

Tab. 4. The rejection of null hypothesis is shown in the table for crease C and D. The determination of the rejection is accompanied by the test statistic (T) and the number of measurements. If the hypothesis is wrongly rejected, then the result will be indicated with a (!).

	Creases					
	C			D		
	T	n	*Rejected*	T	n	*Rejected*
x^+	3.0368	5	yes (!)	3.5645	4	yes
x^-	20.8352	5	yes	60.7267	4	yes
y^+	16.1896	4	yes	1.8247	6	No (!)
y^-	0.3277	6	No	10.5634	5	Yes

Tab. 5. The rejection of null hypothesis is shown in the table for crease F and G. The determination of the rejection is accompanied by the test statistic (T) and the number of measurements. If the hypothesis is wrongly rejected, then the result will be indicated with a (!).

	Creases					
	F			G		
	T	n	*Rejected*	T	n	*Rejected*
x^+	3.2437	5	yes	3.9739	5	yes (!)
x^-	16.7574	4	yes	15.7683	5	yes
y^+	28.1274	6	yes	4.9214	5	yes
y^-	45.4043	5	yes	-5.7570	5	no

which can be said it is significantly larger than the y^+ and x^--direction. Therefore objective two could not be confirmed. Additional research should be done to include or exclude any conclusions about the ratio.
Concluding, the first objective of the hypothesis is confirmed. The direction of the constraints behaves as expected. The second objective could not be validated, additional research must be conducted. Further research could start with the introduction of physical elements into the model.

5 Optimization of a Crease pattern

In this section, the aforementioned mathematical framework will be used to optimize a crease pattern for a given situation. With an engineering application in mind, there is no need to have a unique solution, a range of best solutions will also satisfy.
As will be pointed out later on, the constraints are non-linear. Therefore the optimization problem is a multi-objective binary mixed-integer nonlinear problem (MOMINP). The constraints are not easy to differentiate. Accordingly the problem seems to be non-convex. A genetic algorithm can be used to solve these types of problems.
The number of creases which fits inside a strip depends on the orientation and location of the already laid creases. Accordingly, the number of variables is variable within this optimization problem. To avoid computational complications the number of creases for each subset is fixed before the implementation of the optimization. The accompanied algorithm handles only subset $\mathcal{H}$ and $\mathcal{V}^1$ although the set of rules should also apply to $\mathcal{V}^n$.

Depending on the subset the number of variables per crease differs. A crease of subset $\mathcal{H}$ can be defined with three variables, 1) the location on the y-axis ($x_1^{\mathcal{H}}$), 2) the angle between the incoming and outgoing strip ($x_2^{\mathcal{H}}$), and 3) the direction of the folding ($x_3^{\mathcal{H}}$). A crease of subset $\mathcal{V}$ is defined with four variables, 1) the location on the y-axis ($x_1^{\mathcal{V}}$), 2) the location on the x-axis, either left or right ($x_2^{\mathcal{V}}$), 3) the angle of the crease ($x_3^{\mathcal{V}}$), and 4) the direction of the folding ($x_4^{\mathcal{V}}$).
The folding can either be $\lambda = -1$ or $+1$ for both subsets. The location on the x-axis can be $x_{pos} = -\frac{D}{2}$ or $\frac{D}{2}$ for subset $\mathcal{V}$. All other variables are continuously within there domain. The feasible solutions space is defined as $\mathcal{G}^{\mathcal{H}}$: $\left\{0 \leq x_1 \leq L, \quad 0 \leq x_2 \leq \frac{pi}{2}, \quad x_3 = \pm 1\right\}$ and $\mathcal{G}^{\mathcal{V}}$: $\left\{0 \leq x_1 \leq L, \quad x_2 = \pm 1, \quad 0 \leq x_3 \leq \frac{pi}{2}, \quad x_4 = \pm 1\right\}$, with L as the total length of the strip. Note that the feasible solution space of higher subsets will be the same as for $\mathcal{G}^{\mathcal{V}}$.
The optimization problem can be formulated as shown in Eqn. (6) with the total objective function (d_p) and the constraints represented by $g(X)$ inside the feasible space $\mathcal{G}$.

$$\begin{aligned} &\min_X -d_p(X) \\ &\text{s.t.} \quad g(X) \leq 0 \\ &\qquad X \in \mathcal{G} \end{aligned} \tag{6}$$

5.1 Optimization: Objective

The individual objectives are represented with $F_i(x) = \left\{x^+, x^-, y^+, y^-, L\right\}$, the desired result with z_i. The designer could also place a certain emphasis on individual objectives with the use of weights, w_i. To give preference to the different objectives, the Weighted Metric Method [21] and the Global Criterion Method [22] are combined as is often done in Compromise Programming [22]. The total objective function (d_p) is shown in Eqn. (7), with p as "individual relative deviations can be raised to any power ($p = 1, 2, \ldots \infty$)" [22].

$$d_p(x) = \left(\sum_{i=1}^{5} w_i \left| \frac{F_i(x) - z_i}{z_i} \right|^p \right)^{1/p} \qquad \text{[22], [21]} \quad (7)$$

$$\text{with:} \quad 0 < w_i < 1, \quad \sum_{i=1}^{5} w_i = 1, \quad p = 1, 2, \ldots \infty \quad (8)$$

For the Pareto optimization the following objective is used:

$$d_p(x) = w_i \left| \frac{F_i(x) - z_i}{z_i} \right| \qquad \text{[22], [21]} \quad (9)$$

$$\text{with:} \quad 0 \leq w_i \leq 1, \quad \sum_{i=1}^{5} w_i = 1, \quad p = 1, 2, \ldots \infty \quad (10)$$

5.2 Optimization: Constraint

The optimized system is bounded by the axioms of flat origami which can be found in [17]. With the use of these axioms the folded ($\mathcal{F}$) and unfolded state ($\mathcal{F}^{-1}$) of a crease pattern can be determined [17]. The main goal of constraining strips is to join two kirigami sheets that are located on the x,z-plane. The strips are therefore not allowed to penetrate the x,z-plane. This is realised by constraining all the vertices to the first and second quadrant in folded state ($\mathcal{F}$), see Eqn. (11). Also the individual creases (E) within a subset are not allowed to intersect, see Eqn. (12).

$$g_1(x): \qquad V \geq \begin{bmatrix} -\infty \\ 0 \end{bmatrix} \quad \text{with} \quad V \in \mathcal{F} \qquad (11)$$

$$g_2(x): \qquad E_i \not\pitchfork E_j \quad \text{with} \quad E \in \mathcal{F}^{-1}, \mathcal{F} \qquad (12)$$

A constraint is imposed on opposite folding, Eqn. (13). A crease (E_k) which is part of opposite folding must be placed outside the already laid ($\prec$) faces (F_i).

$$g_3(x): \qquad \left(\bigcup_{i=0}^{n} F_i \right) \not\pitchfork E_k \qquad \text{for} \quad \begin{cases} F_i \prec E_k \\ E_k \in \mathcal{F} \\ \lambda_{k-1} = \lambda_k \end{cases} \tag{13}$$

The following constraints apply on the algorithm. Additional constraints for the algorithm are shown in Eqn. (14). Equation (14) defines that the order of folding operations happens

from the bottom of the strip into the upwards direction. In addition, Eqn. (15) prevents numerical error within the algorithm by setting a minimal distance between the vertices of an arbitrary distance.

$$g_4(x): \qquad V_{i,A,y} < V_{j,A,y} \quad \text{for} \quad i < j \quad \text{and} \quad V \in \mathcal{F}^{-1} \tag{14}$$

$$g_5(x): \qquad \text{if} \quad V_i \neq V_j \quad \Rightarrow \quad ||V_i - V_j|| > 7 \cdot 10^{-1} \tag{15}$$

The total nonlinear constraints of the optimization problem can be formulated as followed: $g(x) = \{g_1(x), g_2(x), g_3(x), g_4(x), g_5(x)\}$ for the subsets $\mathcal{X} = \mathcal{H}, \mathcal{V}^1, \mathcal{V}^2, \ldots$

6 Result of the optimization

The used algorithm to optimize a crease pattern does not involve the secondary constraints. The secondary constraints are an empirical result from the mathematical validation. The optimization algorithm was written before the validation and therefore lacking the secondary constraints.
The second important notion is the direction of the first opposite fold. The first opposite fold is folded upwards in such a way that the orientations of the sheets are pointing to each other. Mathematically $\lambda(p,q) = \lambda(q,p) = +1$.
The third important notion is that the algorithm does not allow any intersection of subset $\mathcal{H}$ with the top raw edge, but does allow one crease of subset $\mathcal{V}$ to intersect the top raw edge.
A genetic algorithm is used for which is true that the "convergence to the global optimum cannot be guaranteed, but will yield "good" solutions on average" [23]. Therefore the solutions found need to be examined more closely.

6.1 Optimized crease pattern

For illustration a crease pattern is optimized. The crease pattern will consist of six creases evenly divided over subset $\mathcal{H}$ and $\mathcal{V}$ with an objective of $\mathbf{C}: \{x^+, x^-, y^+, y^-\} = \{4,4,4,4\}$. All directions are set to be evenly important but the stacked layers are slightly more important, leading to the following weight factors $w = \{\frac{4}{25}, \frac{4}{25}, \frac{4}{25}, \frac{4}{25}, \frac{9}{25}\}$. The strip has the following dimension: a length of 3 and a width of 1.
The constraint tolerance is zero in order to have a feasible solution and the function tolerance is equal to 10^{-5} for subset $\mathcal{H}$ and 10^{-3} for subset $\mathcal{V}$. A solution is gained with a population size of 900 ($\mathcal{H}$) and 1000 ($\mathcal{V}$) with a maximum number of 300 ($\mathcal{H}$) and 100 ($\mathcal{V}$) generations. The resulting crease pattern from the optimization algorithm is shown in fig. 10.

The resulting crease pattern of subset $\mathcal{H}$ has the following variables: $x_{\mathcal{H}} = \begin{bmatrix}0.6147 & 0.2890 & 0.6896 & 0.8271 & 0.9896 & 1.2109 & 1.0000 & 0 & 0\end{bmatrix}$.

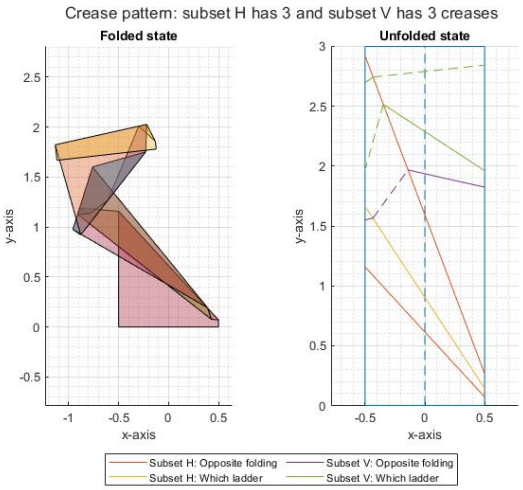

Fig. 10. An x-ray view of a possible solution from the optimization algorithm which has as objective $\mathbf{C}: \{4,4,4,4,4\}$. The true primary constraint is found to be $C^{\mathcal{V}} = \begin{bmatrix}-2.9741 & -2.7615 & -2.9535 & -2.8230 & -6.0000\end{bmatrix}$. Both subsets have three creases. The mountain valley assignment can be distinguished with a dashed and straight line.

The variables of subset $\mathcal{V}$ are set to be $x_{\mathcal{V}} = \begin{bmatrix}1.5504 & 1.9610 & 2.6963 & 0 & 1.0000 & 0 & 1.3488 & 0.9908 & 0.9579 & 1.0000 \\ 0 & 1.0000\end{bmatrix}$.
The optimization algorithm lacks a calculation for the secondary constraints but does include the primary constraints. The primary constraints of subset $\mathcal{H}$; $C^{\mathcal{H}} = \begin{bmatrix}-2.2104 & -2.1990 & -2.4338 & -1.7963 & -2.0000\end{bmatrix}$ and of subset $\mathcal{V}$ are $C^{\mathcal{V}} = \begin{bmatrix}-2.9741 & -2.7615 & -2.9535 & -2.8230 & -6.0000\end{bmatrix}$. If the secondary constraints had been known they would have been added to the constraint space. Therefore the actual constraint space will be higher.

6.2 Example of joining two Kirigami sheets

The found crease pattern can be used to join kirigami sheets. These sheets should have embedded strips of equal size in such a way that they can be folded into each other. Figure 11 and 12 represent a resulting joint result. The sheets have a different color so that the folding operations are clearly visible.

7 Discussion

A mathematical method is presented to constrain the discretized strips from a kirigami object in order to join a single continuous cut. From the mathematical validation it is evident that the mathematical model alone is not sufficient to describe the proportion of the constraints. But the mathematical model does correctly predict the direction of the constraints.
The deviations are presumably caused on a physical level. Although excluded on a mathematical level, the sheets

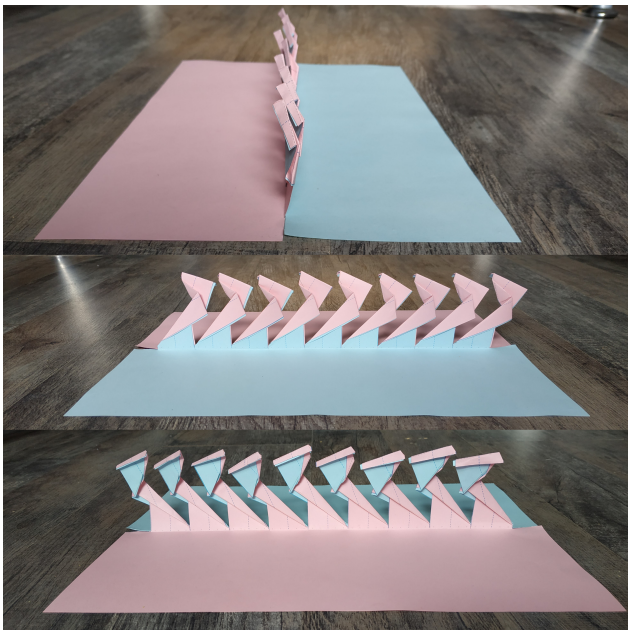

Fig. 11. Front and side views of the the joined Kirigami sheets. Two sheets are joined with nine strips from figure 10. Top figure; front view, second figure; side view one, third figure; side view two.

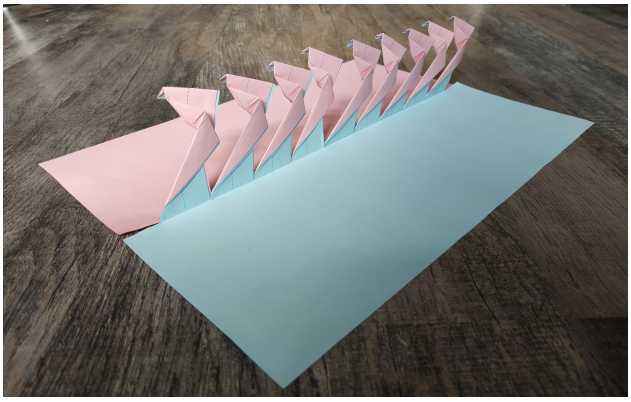

Fig. 12. Isometric view of the the joined Kirigami sheets. Two sheets are joined with nine strips from figure 10.

do interact with each other, for example through friction. While the mathematical model assumes that the constraints are additive and linear, a potential physical model does not necessarily have to be. Perhaps a comparison can be made for opposite folding with the capstan equation for friction [24] leading to an exponential set of constraints within the physical model. In order to determine an accurate physical model additional research should be conducted.

Closely related solutions to join kirigami sheets are designs as "the Zippermast" from the company Geo Systems [25], "the Spirallift" from the company Gala Systems [26] and the spiral robot arm [27]. In these systems the sheets are moving through a static zipper, which connects them to each other with a shape lock. The above mentioned systems have only one resulting form, either a cylinder or prism. But in combination with a zipper and the presented joining method a landscape of more divers shapes seems to be possible.
Although this paper only joins two flat sheets, which represent a kirigami object, more complex objects should be possible. The next step would include objects with an non-zero curvature, for instance a sphere or a paraboloid. A more interesting exercise can be found with the creation of large D-forms, as shown in [28], [29] and [30]. Large, in the order of room-sized kirigami structures with one single cut. This type of kirigami could be useful for example deployable antenna's up in space, inflatable habitats or free-form architecture.

8 Conclusion

Two kirigami sheets are joined. A mathematical model is presented on how two strips are able to constrain each other in order to constrain the entire kirigami object. Constraining due to folding can be divided into primary constraints and secondary constraints.
The primary constraints involve the contribution of individual creases and the secondary constraints involve the interaction between the creases. Excluding rotation, an individual crease acts as a unilateral constraint for the displacement. A combination of creases can be part of opposite folding or be part of a Jacobs ladder, and are therefore able to constrain the strips in multiple directions.
The conducted experiment did confirm that the strips of the Kirigami sheets are constrained in the expected directions. However the proportion of the constraints do not represent the full reality. Probably due to physical elements which are not part of the presented mathematical model.
An example crease pattern is found with an optimization algorithm and has been applied to two sheets which represent a kirigami object. The resulting joined kirigami object has resistance in all directions. However, the optimization algorithm excludes secondary constraints and only one crease from the second set of foldings ($\mathcal{V}$) can intersect with the top raw edge and none of the first set of foldings ($\mathcal{H}$).
Concluding, the mathematical description in combination with the optimization algorithm did find a viable crease pattern to join the Kirigami sheets. Additional research needs to be done in order to introduce physical elements into the model.

References

[1] K. Kuribayashi, K. Tsuchiya, Z. You, D. Tomus, M. Umemoto, T. Ito, and M. Sasaki, "Self-deployable origami stent grafts as a biomedical application of Ni-rich TiNi shape memory alloy foil," *Materials Science and Engineering A*, vol. 419, no. 1-2, pp. 131–137, 2006.

[2] S. A. Zirbel, B. P. Trease, S. P. Magleby, and L. L. Howell, "Deployment methods for an origami-inspired rigid-foldable array," in *Proceedings of the*

40th Aerospace Mechanisms Symposium. Greenbelt: NASA Goddard Space Flight Center, 2014, pp. 189–194. [Online]. Available: http://www.esmats.eu/amspapers/pastpapers/pdfs/2014/zirbel.pdf

[3] S. Felton, M. Tolley, E. Demaine, D. Rus, and R. Wood, "A method for building self-folding machines," *Science*, vol. 345, no. 6197, pp. 644–646, aug 2014. [Online]. Available: http://www.sciencemag.org/cgi/doi/10.1126/science.1252610

[4] S. J. Callens and A. A. Zadpoor, "From flat sheets to curved geometries: Origami and kirigami approaches," *Materials Today*, vol. 21, no. 3, pp. 241–264, apr 2018. [Online]. Available: https://doi.org/10.1016/j.mattod.2017.10.004https://linkinghub.elsevier.com/retrieve/pii/S1369702117306399

[5] J. Cui, F. R. Poblete, and Y. Zhu, "Origami/Kirigami-Guided Morphing of Composite Sheets," *Advanced Functional Materials*, vol. 28, no. 44, p. 1802768, oct 2018. [Online]. Available: http://doi.wiley.com/10.1002/adfm.201802768

[6] GRANTA DESIGN, "CES EduPack software," Cambridge, UK, pp. 1–2, 2019. [Online]. Available: www.grantadesign.com

[7] H. Strobl, "Knotology & Snapology." [Online]. Available: http://knotologie.de/

[8] "USC Libraries Unveils Amazing 3D Fractal Model Made of 49,000 Folded Business Cards," 2012. [Online]. Available: https://inhabitat.com/usc-libraries-unveils-amazing-3d-fractal-model-made-of-49000-folded-business-cards/

[9] S. Cicaló, "The PJS technique and the Construction of the First Origami Level-4 Menger Sponge," in *Origami7: Seventh International Meeting of Origami Science, Mathematics, and Education, Volume 2: Mathematics*. St Albans: Tarquin, 2018, pp. 653–668.

[10] Y. Yang and Z. You, "A modular origami-inspired mechanical metamaterial," in *Origami7, Seventh International Meeting of Origami Science, Mathematics, and Education, Volume 3: Engineering 1*. St Albans: Tarquin, 2018.

[11] F. Goldman, "Using the snapology Technique to Teach Convex Polyhedra," in *Origami 5: Fifth International Meeting of Origami Science, Mathematics, and Education*. Natick: Taylor & Francis Inc, 2016, pp. 99–110.

[12] M. Kawamura, "The Celes Family of Modular Origami," in *Origami4: Fourth International Meeting of Origami Science, Mathematics, and Education*. Taylor & Francis Inc, 2009, pp. 21–30.

[13] R. J. Lang and B. Hayes, "Paper Pentasia: An Aperiodic Surface in Modular Origami," *The Mathematical Intelligencer*, vol. 35, no. 4, pp. 61–74, dec 2013. [Online]. Available: http://link.springer.com/10.1007/s00283-013-9405-5

[14] E. Hennig, "ZEBRA – A Heteromodular Origami Technique for Constructing Large-Scale 3D Framework Architectures and Kinematic Linkages," in *Origami7, Seventh International Meeting of Origami Science, Mathematics, and Education, Volume 1: Design, Education, History, and Sience*. St Albans: Tarquin, 2018, pp. 47–62.

[15] J. Stewart, *Calculus Early transcendentals International Metric Version*, 7, Ed. Athenaeum Uitgeverij, 2008.

[16] E. D. Demaine and J. O'Rourke, *Geometric Folding*. Cambridge, UK: Cambridge University Press, 2007.

[17] J. Schneider, "Flat-Foldability of Origami Crease Patterns," pp. 1–18, 2004. [Online]. Available: https://organicorigami.com/

[18] J. B. Hopkins and M. L. Culpepper, "Synthesis of multi-degree of freedom, parallel flexure system concepts via Freedom and Constraint Topology (FACT) – Part I: Principles," *Precision Engineering*, vol. 34, no. 2, pp. 259–270, apr 2010. [Online]. Available: http://dx.doi.org/10.1016/j.precisioneng.2009.06.008https://linkinghub.elsevier.com/retrieve/pii/S0141635909000920

[19] FUTEK Advanced Sensor Technology, "LSB200 JR S-Beam Load Cell – FSH00104." [Online]. Available: https://datasheets.globalspec.com/ds/10/FutekAdvancedSensorTechnology/DD15764B-56A5-4AFC-8558-83E69B817F3A

[20] F. M. Dekking, C. Kraaikamp, H. P. Lopuhaä, and L. E. Meester, *A Modern Introduction to Probability and Statistics*, 1st ed., ser. Springer Texts in Statistics. London: Springer London, 2005. [Online]. Available: http://link.springer.com/10.1007/1-84628-168-7

[21] P. Cortez, "Multi-Objective Optimization," 2014, pp. 99–117. [Online]. Available: http://link.springer.com/10.1007/978-3-319-08263-9{_}6

[22] A. Gupta and A. Siakumar, "Simulation based multiobjective schedule optimization in semiconductor manufacturing," in *2002 Winter Simulation Conference*, 2002, pp. 1862–1870. [Online]. Available: https://brill.com/view/journals/njz/46/3-4/article-p163{_}1.xml

[23] T. van den Boom and B. De Schutter, "Optimization in Systems ans Control, dictation for the course SC42055, article nr: 06917680006," Delft, p. 198, 2018. [Online]. Available: www.dcsc.tudelft.nl

[24] R. Hibbeler, *Engineering Mechanics: Statics*, 13th ed. Singapore: Pearson Prentice Hall Pearson Education inc., 2013.

[25] G. Woodruff, P. Muench, and G. Witus, "Zipper mast for enhanced communications and surveillance," in *SPIE 8045, Unmanned Systems Technology XIII*, D. W. Gage, C. M. Shoemaker, R. E. Karlsen, and G. R. Gerhart, Eds., vol. 8045, no. May 2011, may 2011, pp. 1–6. [Online]. Available: http://proceedings.spiedigitallibrary.org/proceeding.aspx?doi=10.1117/12.885525

[26] GALA Systems INC, "GALA Systems INC." [Online]. Available: https://www.galasystems.com/en/

[27] F. Collins and M. Yim, "Design of a spherical robot arm with the Spiral Zipper prismatic joint," *Proceedings - IEEE International Conference on Robotics and Automation*, vol. 2016-June, pp. 2137–2143, 2016.

[28] R. R. Orduño, N. Winard, S. Bierwagen, D. Shell, N. Kalantar, A. Borhani, and E. Akleman, "A Mathematical Approach to Obtain Isoperimetric Shapes for D-Form Construction A Mathematical Approach to Obtain Isoperimetric Shapes for D-Form Construction Departments of Visualization & Computer Science and Engineering ," *Proceedings of Bridges 2016: Mathematics, Music, Art, Architecture, Education, Culture*, no. August, pp. 277–284, 2016.

[29] J. Sharp, "D-forms and developable surfaces," *Renaissance Banff: Mathematics, Music, Art, Culture*, pp. 121–128, 2005.

[30] Ö. Gönen, E. Akleman, and V. Srinivasan, "Modeling D-Forms," *Bridges: Mathematical Connections between Art, Music and Science*, pp. 209—-216, 2007.

3

Recommendations & Applications

The article presents a mathematical model to join a single continuous and smooth cut through a kirigami sheet by constraining additional discretized strips with origami. The article rounds off with an optimized crease pattern used to create a kirigami object.

The kirigami object of the article is rather simple. Two A4 paper sheets are joined together. It is a simplification for possible applications which can be found in a parabolic antenna for satellites, cylindrical habitats or arbitrary surfaces, for instance free form architecture.
The epilogue will first treat several applications, followed by a small discussion on future steps for the project.

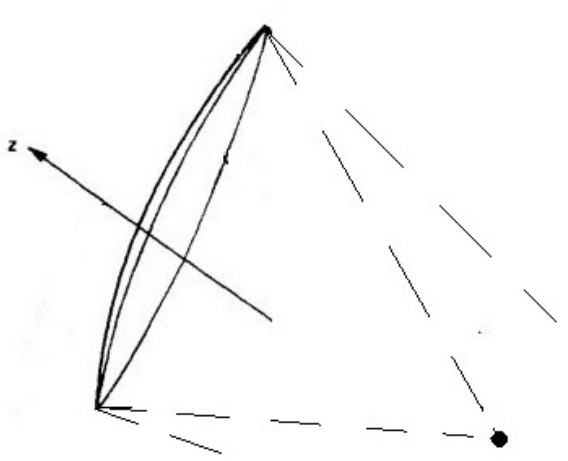

Figure 3.1: Standard parabolic reflector antenna. Modified from: [7]

3.1. Applications

As mentioned, there are several possible applications: parabolic antenna for satellites, cylindrical habitats or arbitrary surfaces, for instance free form architecture. These will be discussed separately.

3.1.1. Parabolic shape (antenna)

The whole project is aimed at producing an antenna for outer space. There are various options for antennas of small satellites as CubeSats, namely: wire, reflector, reflectarray, membrane, horn and patch antennas [30]. The reflector antenna has "the possibility of high gain and fine resolution"[30]. Compared to the other types of antennas. The reflector antenna can be divided into smaller segments: the standard parabolic reflector, the offset parabolic-reflector [7], the Cassegrain dual reflector [31] and the Gregorian dual reflector antenna [31]. These types of antennas are distinguished by an off-set of the sensor or the use of an additional conclave or convex reflection surface. Although a reflector antenna is preferred, it does not have an Euclidean shape, "i.e. cannot be realized in a flat configuration" [32]. Refreshed, a reflector antenna can not be created from a single sheet. Therefore A.D. Yellowhorse did research at the University of Delft to create a kirigami-based reflector antenna. With the ambition to reduce manufacturing costs and simplify implementation. Figure 3.1 shows an example of a standard parabolic reflector antenna.

In line with the situation of the article, a parabolic object can be described with a space curve. The space curve could represent the cut of the parabolic object, see Fig A.2. Although, an offset-parabolic reflector is described by a paraboloid with a domain created by the projection of a cone [7], the space curve of Fig. 3.1 gives a good indication of possible future shapes.

3.1.2. Cylindrical shape

The National Aeronautics and Space Administration (NASA) does a lot of research for space applications. NASA has as a goal to return to the moon in 2024 and wants to use the moon for deep-space explorations [33]. Different habitats have been designed to stay in space or on the moon for an extended period of time. Many of them are inflatable in order to safe space and have various geometries, such as spheres

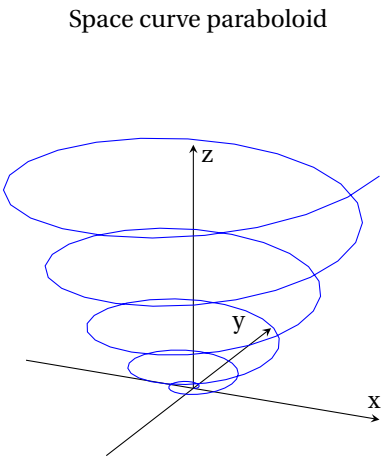

Plot 3.1: The space curve of a paraboloid as defined in formula A.9. This curve could be used with or without modification as a cutting line for a paraboloidal surface.

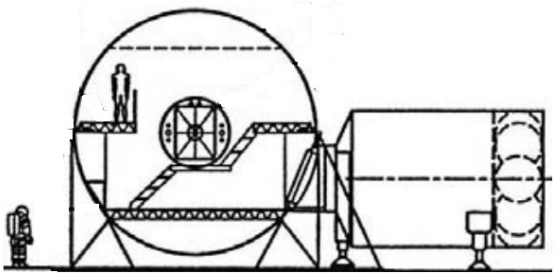

Figure 3.2: A design of a cylindrical lunar inflatable habitat by NASA. Modified from: [8]

or cylindrical shapes [8]. Figure 3.2 shows a lunar inflatable habitat designed by NASA [8]. Figure 3.3 shows a cylindrical habitat which is patented [9].

Although we don't aim to create an airtight connection for kirigami surfaces, these examples illustrate a discussion in literature on large cylindrical shapes. This makes a large and thin-walled cylinder suitable for further investigation.

3.1.3. Arbitrary shape

Large kirigami structures can be found for example in the architecture. Take for example the Bilbao's Guggenheim Museum, figure 3.4, or the Louvre's New Islamic Art Wing seen in figure 3.5 and 3.6 [34]. Both exist of a continual arbitrary surface. The building of the Bilbao's Guggenheim Museum by Frank Gehry actually exist of several finite surfaces with an arbitrary shape, while the Department of Islamic Arts at Musée du Louvre by Mario Bellini and Rudy Ricciotti just have one single arbitrary surface. The aimed kirigami joining method is for one surface. So a surface of the Department of Islamic Arts at Musée du Louvre could be created with such a method at once, while the surfaces of the Bilbao's Guggenheim Museum should be handled separately.

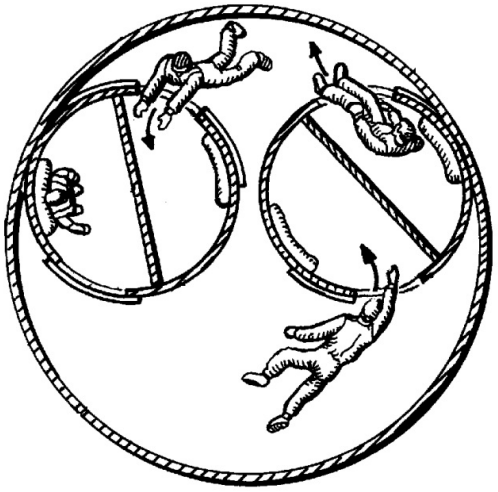

Figure 3.3: Patent US6216984B1, cylindrical habitat for space. Modified from: [9]

Figure 3.4: Example of free form architecture, the Bilbao's Guggenheim Museum by Frank Gehry. Source from: [10]

H. pottmann et al. describe in their article the relevance for architectural applications. They state that "For most of the materials used (glass panels, wooden panels, metal sheets, ...), it is very expensive to produce general double-curved shapes" [12]. In there article they describe a method for semi-discrete surface representations using D-strip models. In this model the surface is approximated by D-strips, which results in each strip having a single curvature. See for example figure 3.7 for which the surface is approximated with D-strips.

Although the method for making these types of strips does not fall within the scope of this report, it is clear that large structures that occur in architecture, for example, which can be made with D strips or similar methods, could benefit from a new kirigami joining technique.

Figure 3.5: Example of free form architecture: Side view of Department of Islamic Arts at Musée du Louvre. Source from: [11]

Figure 3.6: Example of free form architecture: Top view of Department of Islamic Arts at Musée du Louvre. Source from: [11]

3.2. Further recommendations and actions

There are several possibilities of future steps within this project. The first reasonable steps will be the creation of a physical model and a zipper design. Followed by the creation of 3D kirigami objects, discussed in the section "Applications". The physical model and the zipper design will be discussed next.

3.2.1. Physical model

The article states that the mathematical method, to constrain discretized strips from a kirigami object to join a single cut, is not sufficient to describe the proportion of the constraints. But the mathematical model does correctly predict the direction of the constraints. The deviations are presumably caused on a physical level. Therefore, the creation of an additional physical model is vital. Possible questions to answer: How do the sheets interact with each other outside the fold lines? Can a comparison be made for opposite folding with the capstan equation for friction [35]? The capstan equation could lead to an exponential set of constraints within the physical model. In order to determine an accurate physical model additional research should be conducted.

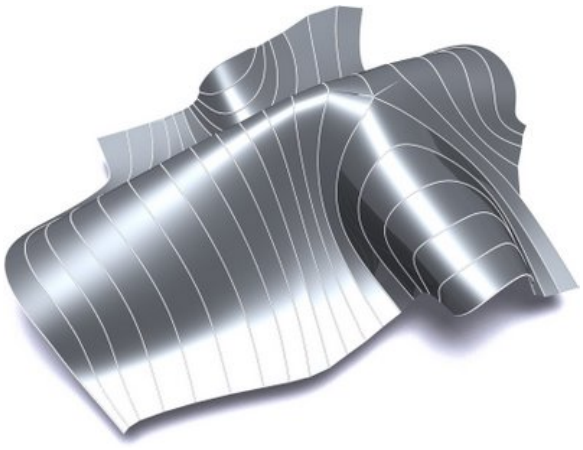

Figure 3.7: Example of free form architecture. "The shape of a piece of felt has been approximated by a D-strip model"[12]. Source from: [12]

3.2.2. Zipper design

Apart from the validation of a physical model the found crease patterns should also be implemented. The main idea is to automate the folding operations with a zipper design. The zipper design is assumed to be accurate, precise and fast in order to be a competitive alternative for adhesives, fasteners or welding. However, the zipper design is still hypothetical and

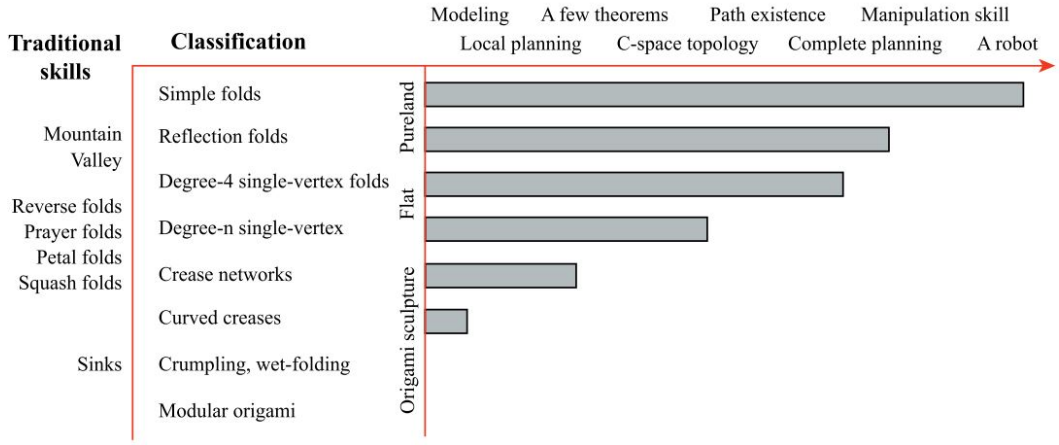

Table 3.1: "A map of the origami task domain". Source from: [16]

needs to be accomplished first in order to validate these claims.
The article joins two A4 papers. The discretized strips which are folded into each other have an identical crease-pattern. But for an actual kirigami design this will not be true in general. Take for example a large thin walled cylinder laying on its side that will need to carry its own weight, resulting in tensile stresses in the top of the cylinder while having compressive stresses in the bottom part of the cylinder. The different stresses that can occur within an object would result in a different optimal crease-pattern. Therefore each strip could have a distinctive creases-pattern. This leads to high demands for a zipper design.

Although there exist not yet a zipper design for arbitrary kirigami surfaces, there are closely related examples; "the Zippermast" by the company Geo Systems [5], "the Spirallift" by the company Gala Systems [26] and the spiral robot arm [36]. These systems do not involve origami or kirigami but snap-fits. These systems have therefore only one predetermined shape as output. The question remains how difficult it would be to create a zipper design for an arbitrary kirigami surface?

Table 3.1 is cited from the article "Robotic origami folding" published in 2008. The table gives a good indication of the development of automating folding operations from simple folds towards modular origami.
The proposed method to assemble kirigami sheets is in fact part of modular origami. The method connects two sheets together, which can be seen as the joining of two origami objects.
From table 3.1 could be concluded that automating folding operations for modular origami is still in its infancy. However, the presented article states clearly that misalignment gadgets are excluded. Resulting from this is that flaps and pockets, which are complicated to automate, are excluded from the crease-pattern of the strip. The intended crease patterns have similarities with the "Reflection folds" which are near full automation. By avoiding the difficulties of modular origami in general while making use of the developments from the "Reflection folds", a zipper design to join kirigami objects should be achievable within a reasonable amount of time and effort.

Appendices

A

Single continuous and smooth kirigami cut

This chapter explains how to define a cut on a 3D surface. The cut will be described with a space curve. The mathematical description of the parabolic antenna is also discussed in more detail.

A.1. Basic calculus

For the selection of materials, manufacture methods and joining techniques the cut of a surface must be defined with its properties. Although space vectors and curvatures are standard mathematics, a quick recap is necessary to get all readers on the same page.

A.1.1. Space curves

A potential cut can be described as a line on a certain surface. Therefor a space curve $\mathbf{r}(t)$ and not a surface $\mathbf{r}(u,v)$ is used thoughout this chapter. Parametric equations are defined as $(x,y,z) = \big(f(t),g(t),h(t)\big)$. From thereon a space curve C can be defined by a continuous vector function $\mathbf{r}(t)$ [18] which is defined as followed:

$$\mathbf{r}(t) = \begin{bmatrix} f(t) & g(t) & h(t) \end{bmatrix}^T \qquad [18] \qquad (A.1)$$

with $f(t)$,$g(t)$ and $h(t)$ as real valued functions and t the parameter of the parametric equations. The unit tangential line to C at point P is defined in formula A.2.

$$\mathbf{T}(t) = \frac{\mathbf{r}'(t)}{\left|\mathbf{r}'(t)\right|} \qquad [18] \qquad (A.2)$$

Note that $\mathbf{T}'(t)$ is othogornal with $\mathbf{T}(t)$, this results in normal vector $\mathbf{N}(t)$ as defined in formula A.3.

$$\mathbf{N}(t) = \frac{\mathbf{T}'(t)}{\left|\mathbf{T}'(t)\right|} \qquad [18] \qquad (A.3)$$

The binomial vector which is permedicular to $\mathbf{N}(t)$ and $\mathbf{T}(t)$ is defined as follwed:

$$\mathbf{B}(t) = \mathbf{T}(t) \times \mathbf{N}(t) \qquad [18] \qquad (A.4)$$

A.1.2. Curvature

For general joining techniques or fabrication of sheets it is important to determine the curvature of the space curve. The curvature is defined below. The curvature of "$\mathbf{r}(t)$ is called smooth on an interval I if $\mathbf{r}'(t)$ is continuous and $\mathbf{r}'(t) \neq 0$ on I"[18]. The curvature of a curve is given by formula A.5 and A.6, with s defined as the arc length of the curve.

$$\kappa = \left|\frac{\mathrm{d}\mathbf{T}(t)}{\mathrm{d}s}\right| = \left|\frac{d\mathbf{T}(t)/dt}{ds/dt}\right| = \frac{|\mathbf{T}'(t)|}{|\mathbf{r}'(t)|} \qquad [18] \qquad (A.5)$$

or

$$\kappa = \frac{|\mathbf{r}'(t) \times \mathbf{r}''(t)|}{|\mathbf{r}'(t)|^3} \qquad [18] \qquad (A.6)$$

Several cases are defined which are simplified as a paraboloid, cone and cylinder. Although they will be discussed later on, figure A.1 shows the curvature of all the cases. The curvatures are defined in formula A.10 for the paraboloid, in formula A.13 for the cone and in formula A.16 for the cylinder.

A.2. Parabolic object

An eliptic paraboloid is defined with the following formula:

$$\frac{z}{c} = \frac{x^2}{a^2} + \frac{y^2}{b^2} \qquad [18] \qquad (A.7)$$

For simplicity we assume that we have a perfect parabolic object, so c, a, b is equal to one. which results in:

$$z = x^2 + y^2 = r^2$$

This is true for:

$$x = r\cos\phi \quad y = r\sin\phi \quad z = r^2 = t^2 \qquad (A.8)$$

The simplification $\phi = t$ will result in a vector function with one variable, as shown in formula A.9. The resulting space curve is shown in figure A.2.

$$\mathbf{r} = \begin{bmatrix} t\cos t & t\sin t & t^2 \end{bmatrix}^T \qquad (A.9)$$

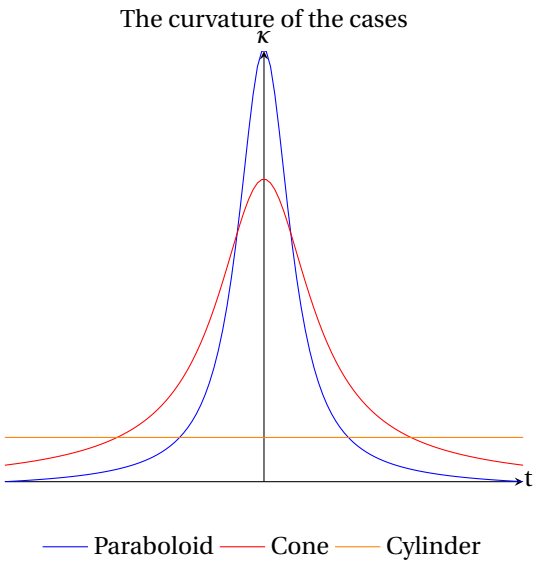

Plot A.1: The curvature (κ) of a parabolic (formula A.10), conical (formula A.13) and cylindrical (formula A.16) space curve for the parametric parameter t.

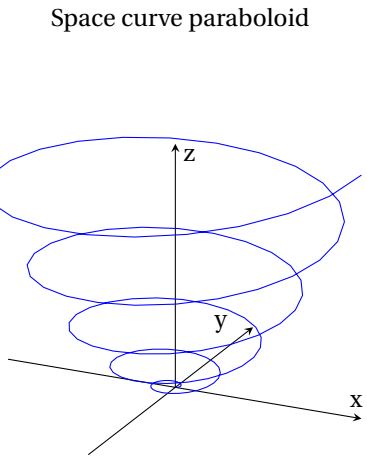

Plot A.2: The space curve of a paraboloid as defined in formula A.9. This curve could be used with or without modification as a cutting line for a paraboloidal surface.

With the use of formula A.6 the found curvature is stated in formula A.13.

$$\kappa(t) = \frac{\sqrt{5t^4 + 16t^2 + 8}}{5t^2 + 1^{3/2}} \tag{A.10}$$

A.3. Conical object

A cone is defined with the following formula:

$$\frac{z^2}{c^2} = \frac{x^2}{a^2} + \frac{y^2}{b^2} \qquad [18] \tag{A.11}$$

For a perfectly round cone a needs to be equal to b and for simplicity a,b,c will be equal to one.

$$z = \sqrt{x^2 + y^2} = r$$

That is true for

$$x = r\cos\phi \quad y = r\sin\phi \quad z = r = t$$

The simplification $\phi = t$ will result in a vector function with one variable, as shown in in formula A.12 and figure A.3.

$$\mathbf{r} = \begin{bmatrix} t\cos t & t\sin t & t \end{bmatrix}^T \tag{A.12}$$

With the use of formula A.6 the found curvature is stated in formula A.13.

$$\kappa(t) = \frac{\sqrt{4 + 8t^2 + 2t^4}}{(2t^2 + 1)^{3/2}} \tag{A.13}$$

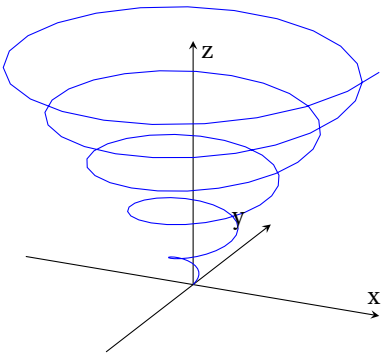

Plot A.3: The space curve of a cone as defined in formula A.12. This curve could be used with or without modification as a cutting line for a conical surface.

A.4. Cylindrical object

A cylinder is defined with the following formula:

$$x^2 + y^2 = \cos t^2 + \sin t^2 = 1 \quad \forall \quad z \in \mathbb{R} \qquad [18] \tag{A.14}$$

For more general situations it follows:

$$\mathbf{r}(t) = \begin{bmatrix} a\cos t & a\sin t & bt \end{bmatrix} \tag{A.15}$$

The space curved as defined in formula A.15 is shown in figure A.4. With the use of formula A.6 the found curvature is stated in formula A.16 and is constant.

$$\kappa = \frac{|a|}{\left|\sqrt{a^2 + b^2}\right|^3} \tag{A.16}$$

Space curve cylinder

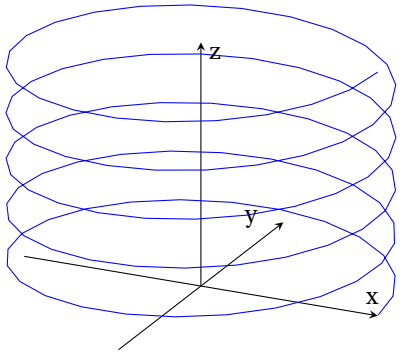

Plot A.4: The space curve of a cylinder as defined in formula A.15. This curve could be used with or without modification as a cutting line for a Cylindrical surface.

A.5. Case off-set antenna Paraboloid

The department of PME is doing research on a kirigami antenna. Parabolic antenna for satellites, describes several parabolic antennas namely: standard parabolic antenna, offset parabolic reflector, Cassegrain dual reflector and Gregorian dual reflector. From the project point of view the offset antenna will be the most interesting, it has a single surface and the focal point is not in the way of the signal. There for a mathematical description is of the offset antenna is shown below. Note that all mathematical rules as described in section A.1 also apply for the offset antenna.

A.5.1. Cartesian coordinates

An paraboloid ($\mathbb{R}^3$) or parabola ($\mathbb{R}^2$) will reflect all incoming signals, which are perpendicular to the directrix (for figure A.5, parallel to z), to the focal point. This makes paraboloids ideal for the design of antennas [7]. "A parabola is the set of points in a plane that are equidistant from a fixed point F (called focus) and the fixed line (called directrix)"[18] as is shown in figure A.5. The directrix can be described with $z = -p$ when the focus point is on point $(0,0,p)$. The parabola can be defined as followed:

$$z = \frac{x^2}{4p}, \text{ F: } (0,0,p), \text{ directrix: } z = -p \quad [18] \qquad (A.17)$$

Figure A.5 shows a parabola for the xz plane. To create a paraboloid for a $\mathbb{R}^3$ space, a parabola on the yz plane needs also be defined, $z = \frac{y^2}{4p}$. An elliptic paraboloid has a standard form as shown in formula A.18.

$$\frac{z}{c} = \frac{x^2}{a^2} + \frac{y^2}{b^2} \qquad [18] \qquad (A.18)$$

or

$$f(x,y) = z = c\frac{x^2}{a^2} + c\frac{y^2}{b^2} \qquad (A.19)$$

Parabola in 2D space

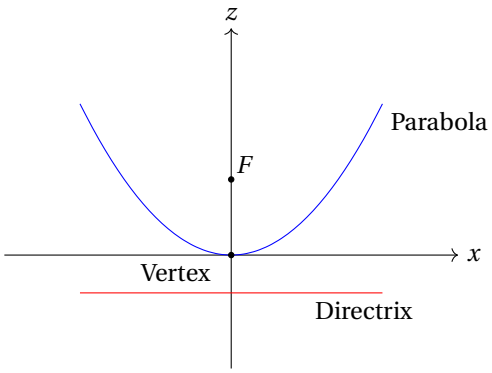

Plot A.5: Definition of a parabola, with parabola $z = \frac{x^2}{4p}$, directrix $z = -p$, focus point $(0,0,p)$ and the vertex $(0,0,0)$, source [18]

In formula A.17 the parabola is defined with the use of the focal point. Combining formula A.17 and A.18, A.19 results in $a = \sqrt{p}$, $b = \sqrt{p}$ and $c = \frac{1}{4}$, for symmetric purposes $a = b$. The paraboloid with the directrix plane is shown in A.6.

Eliptic paraboloid in 3D space

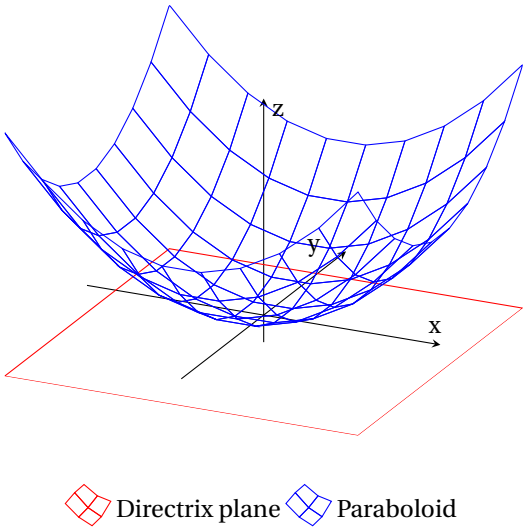

Plot A.6: A paraboloid with $a = \sqrt{p}$, $b = \sqrt{p}$ and $c = \frac{1}{4}$ and a directrix plane on $z = -1$. The focal point lays on F(0,0,p)

A.5.2. Cylindrical Coordinates

The cylindrical coordinates are defined in A.20 with $0 \leq \phi \leq 2\pi$ [18] and can be converted with the use of formula A.20.

$$\begin{cases} x = \rho\cos\phi \\ y = \rho\sin\phi \\ z = z \end{cases} \longleftrightarrow \begin{cases} \rho^2 = x^2 + y^2 \\ \tan\phi = \frac{y}{x} \\ z = z \end{cases} \tag{A.20}$$

Formula A.19 can be rewritten with the use of the definition A.20. This results in expression A.21, with $c = \frac{1}{4}$ and p the location of the focal point.

$$f(x,y) \rightarrow f(r,\phi) = z = \frac{c}{p}\rho^2 \tag{A.21}$$

A.6. Domain

A conventional sub-reflector has a sensor in the $F(0,0,p)$ focal point. The construction required for the sensor results in an aperture blocking for the received signal[7]. This "leads to scattered radiation which results in a loss of system gain on the one hand and a general degradation in the suppression of sidelobes and cross-polarized radiation on the other"[7]. A solution to this problem is the use of offset-parabolic reflector [7]. In figure **??** an offset-parabolic antenna is shown. The offset-parabolic reflector has some disadvantages, for example "the offset reflector will generate a cross-polarized component in the antenna radiation field"[7], more advantages and disadvantages can be found in [7].

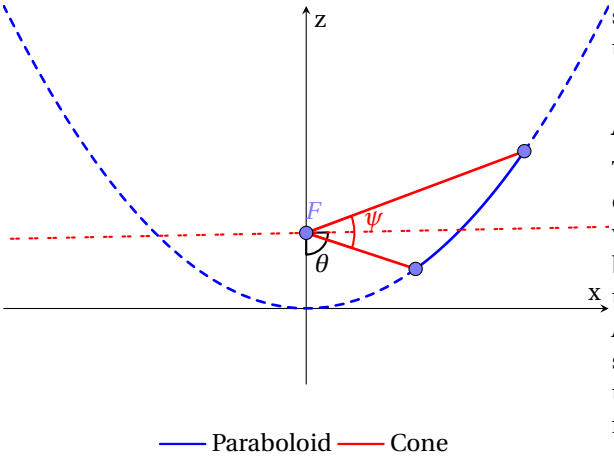

Plot A.7: Paraboloid with a focal point in $F(0,0,p)$ and a cone with the tip in the focal point. The location of the cone is set by θ and the sharpness of the cone is set by ψ. The paraboloid that is not part of the projection of the cone on the paraboloid is dashed. The bisector of the cone is also dashed.

The offset-parabolic reflector can be described by a paraboloid with a domain created by the projection of a cone [7]. It is clear that the tip of the cone needs to lay on the focal point (F) of the paraboloid. Figure A.7 shows a section of $\mathbb{R}^3$ onto the xy plane. The part of the paraboloid which is not part of the domain created by the the projection of the cone is dashed. The variables used in figure A.7 are explained lateron. Notice that "the projection of this contour onto the plane will produce a true circle"[7].

A cone in the negative direction and the tip in the origin can be defined with polar coordinates as described in formula A.22 [18].

$$z^2 = \rho^2 = x^2 + y^2 \quad \text{with} \quad \rho \leq 0 \tag{A.22}$$

For engineering purposes, it must be possible to adjust the sharpness (ψ) of the cone. The sharpness also defines the size of the final domain (read also area) of the off-set reflector. Formula A.22 will change into formula A.23.

$$z = \frac{\rho}{\sin\left(\frac{\psi}{2}\right)} \quad \text{with} \quad \rho \leq 0,\ \psi = C \tag{A.23}$$

There are two possible ways to define the area of the parabola which is suitable for the offset antenna. First rotate the cone around the focus point and the projection will be domain of the offset antenna. Secondly, the cone stays aligned with the z-axis end the parabola will rotate around the focal point. Once again the projection of the cone is the domain of the offset antenna. Notice that the incoming signal should be parallel to the normal vector of the directrix plane.

A.6.1. Rotation of the cone

The idea of the an off-set antenna is that the sensor does not converge with the path of the signals to prevent aperture blocking. Therefore the cone should be able to rotate around the focal point. The rotation equations are defined as determined in formula A.24. Due symmetric property's of a paraboloid, it is sufficient to rotate with an single angle θ to map $\mathbb{P}$ to $\mathbb{N}$ (maps the reference frame of the cone to main frame).

$$\begin{cases} x' = \cos(\theta)x + \sin(\theta)z \\ y' = y \\ z' = -\sin(\theta)x + \cos(\theta)z \end{cases} \quad \text{with } \theta = C \tag{A.24}$$

From equation A.23 is known that $z = \frac{\rho}{sin(\frac{\psi}{2})}$ for $\rho \leq 0$ and $\psi = C$. With this knowledge in combination of formula A.24, formula A.23 can be updated to for-

mula A.25.

$$\left.\begin{aligned} z' &= \tfrac{\rho}{sin(\frac{\psi}{2})} \text{ for } \rho \le 0 \\ z' &= -\sin(\theta)x + \cos(\theta)z \end{aligned}\right\} \Rightarrow$$
$$-\sin(\theta)x + \cos(\theta)z = \frac{\rho}{\sin\left(\frac{\psi}{2}\right)} \qquad \text{(A.25)}$$
$$\text{with } \rho \le 0 \quad \theta, \psi = C$$

Which results in:

$$\left.\begin{aligned} &-\sin(\theta)x + \cos(\theta)z = \tfrac{\rho}{sin(\frac{\psi}{2})} \text{ for } \rho \le 0 \\ &x = \rho\cos\phi \end{aligned}\right\} \Rightarrow$$
$$z = \frac{\rho\left(\sin(\theta)\sin(\phi) - 1\right)}{\sin\left(\frac{\psi}{2}\right)\cos(\theta)} \qquad \text{(A.26)}$$
$$\text{with } \rho \le 0,\ 0 \le \phi \le 2\pi \quad \theta, \psi = C$$

The cone needs to be translated with a distance p along the z-axis to such that the tip of the cone will intersect in the focal point. The formula of A.26 will change to A.27.

$$z = p + \frac{\rho\left(\sin(\theta)\sin(\phi) - 1\right)}{\sin\left(\frac{\psi}{2}\right)\cos(\theta)} \qquad \text{(A.27)}$$
$$\text{with } \rho \le 0, \quad 0 \le \phi \le 2\pi, \quad \theta, p = C$$

The offset-parabolic reflector can be described with

$$f(\rho,\phi) = z = \frac{\rho^2}{4p} \quad \text{on domain } D \qquad \text{(A.28)}$$

with:

$$D = \left\{(\rho,\phi,z) \quad | \quad 0 \le \phi \le 2\pi, \quad \rho \le 0, \qquad \text{(A.29)}\right.$$
$$\left. 0 \le z \le p + \frac{\rho\left(\sin(\theta)\sin(\phi) - 1\right)}{\sin\left(\frac{\psi}{2}\right)\cos(\theta)}\right\}$$

A.6.2. Rotation of the paraboloid

Formula A.19 describes the standard form of the paraboloid with $a = b = \sqrt{p}$ and $c = \frac{1}{4}$. The focal point is noted as $F(0,0,p)$. For the rotation of a paraboloid it needs to be translated first, such that the focal point collide with the origin. Secondly the paraboloid needs to be rotated with an angle θ. The domain of the offset antenna will be defined by the projection of a cone along the z-axis. Formula A.30 shows the first step. The paraboloid is translated with $-p$ along the z-axis.

$$f(x,y) = z = c\frac{x^2}{p} + c\frac{y^2}{p} - p \qquad \text{(A.30)}$$

The rotation equations are defined as determined in formula A.31. Due symmetric property's of a paraboloid, it is sufficient to rotate with an single angle θ to map $\mathbb{P}$ to $\mathbb{N}$ (maps the reference frame of the paraboloid to the main frame)

$$\begin{cases} x' = \cos(\theta)x + \sin(\theta)z \\ y' = y \\ z' = -\sin(\theta)x + \cos(\theta)z \end{cases} \quad \text{with } \theta = C \qquad \text{(A.31)}$$

With the use of formula A.30 and A.31 a rotated paraboloid can be determined, see formula A.32

$$y^2 = cos(\theta)z - sin(\theta)x - \frac{c}{p}\left(cos(\theta)x + sin(\theta)z\right)^2$$
$$\text{on domain} \quad E \qquad \text{(A.32)}$$

or

$$f(x,z) = y = \qquad \text{(A.33)}$$
$$\pm\sqrt{cos(\theta)z - sin(\theta)x - \frac{c}{p}\left(cos(\theta)x + sin(\theta)z\right)^2}$$
$$\text{on domain} \quad E$$

Domain E is defined by a cone along the z-axis. The cone is defined in formula A.22. Domain E can be described as formula A.34.

$$E = \left\{(x,y,z) | x^2 + y^2 = \rho^2 = z^2, z \le 0\right\} \qquad \text{(A.34)}$$

Example

For the example the software MATLAB [37] is used. For easy processing a rotation for the paraboloid will be used. The cone will be represented by a mesh in the shape of a cone. It seems to be difficult to rotate an entire circular mesh, that's why the paraboloid is rotated for this example and not the cone.

Firstly the entire paraboloid will be calculated on a certain domain e.g. $[-10:10, -10:10]$, using listing A.1 with P as $f(x,y) = z.$,

```
[X,Y] = meshgrid(-10:0.05:10,
                 -10:0.05:10);
P = @(x,y)((c/f)*(x.^2+y.^2)-f);
Z =P1(X,Y);
```

Listing A.1: Code: The definition of a paraboloid

The paraboloid needs to be rotated with angle "ϕ" with the use of formula A.31, this results in in the code A.2.

,

```
Xnew = cos(phi)*X+sin(phi)*Z;
Ynew = Y;
Znew = -sin(phi)*X+cos(phi)*Z;
```

Listing A.2: Code: Rotation of a paraboloid.

With the inbuilt function $surf$ the rotated paraboloid is plotted with an angle of $\phi = \frac{\pi}{3}$ as can be seen in figure A.8

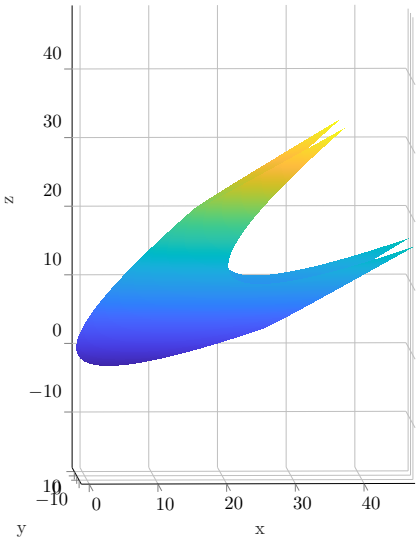

Plot A.8: Figure of the paraboloid created with MATLAB, Rotated with an angle of $\phi = \frac{\pi}{3}$

The domain which is defined by a cone, is equal to a circle the cone creates on the paraboloid. The cone is defined as $x^2 + y^2 = z^2 = \rho^2$ as stated in formula A.22. If the sharpness of the cone is known then also the radius on the projection is known. This can be realised with a for loop throughout all the datapoints as shown in listing A.3.

```
for i = 1:1:p
    for j=1:1:q

        if Xnew(i,j)^2+Ynew(i,j)^2 >r
            Ynew(i,j)= NaN;
            Xnew(i,j) = NaN;
            Znew(i,j) = NaN;
        end

      % Antenna beneath the z=0;
        if Znew(i,j)>0
            Ynew(i,j)= NaN;
            Xnew(i,j) = NaN;
            Znew(i,j) = NaN;
        end

       if j > length(Xnew)
           break;
       end
    end

     if i > length(Xnew')
         break;
     end
end
```

Listing A.3: Code: Domain of the paraboloid defined by an intersection of a cone but executed by a circle r with the same size as the projection.

The result of listing A.3 is shown in figure A.9, a radius of $r = 1$ is used.

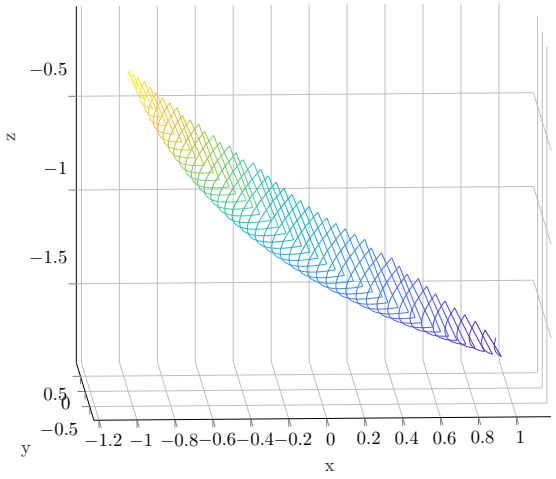

Plot A.9: The offset antenna created with MATLAB. A cone is projected on a paraboloid. The paraboloid has an angle of $\phi = \frac{\pi}{3}$.

B

Introduction to origami mathematics

The first stage of the project will involve the definitions and properties of a crease. This is obtained by conducting a literature search first. The literature search results into a mathematical model which is a skeleton for constraining sheets with the use of creases. This chapter also describes how to distinguish creases from different subsets with the use of map folding.

B.1. Elements of folding

The first stage of the thesis is based based on the article "Flat-Foldability of Origami Crease Patterns" by J. Schneider [14]. The first thing he defines is the sheet S, "as a compact connected region of the plane bound by simple closed curves" with a finite area. On sheet S an crease pattern G is defined, which consists of "the vertices (V), edges (E), and faces (F)". "A c-net, C, is a sheet of paper S with a crease pattern G embedded on it. The elements of C and S are the same, they are the points of the sheet S" [14].
He also defines two types of edges; "An edge lying in the interior of S is called a crease, whereas an edge on the boundary of S is called a raw edge" [14].

A vertex (V) is a point were several edges (often creases) (E) intersect. By definition an edge (E) is defined by a starting point (V_i) and an end point (V_j) . The angle between the edges are defined as α. While the faces (F) are bounded by the edges (E). Note that often the raw edge is not mentioned in the set of edges.

B.1.1. Folding axioms for flat origami

Flat origami models are in reality in $\mathbb{R}^3$ and satisfy the five origami axioms [14]. For mathematical reasons the sheet thickness is assumed to be near zero. Therefore the origami model will be mapped to the folding space $\mathbb{R}^2$.
In the field of flat origami there exist five axioms for polyhedral folding [14]. These axioms form the basic rules of origami and are listed below[14]:

Axiom B.1.1. *"The crease pattern faces retain their shapes when the paper is folded". Mathematically: "The image ϕ acts as an isometry on each face" [14] meaning the distance is preserved.*

Axiom B.1.2. *"The paper is folded at every crease". Mathematically: "If F_1 is adjacent to F_2, then $i_{F_1} \neq i_{F_2}$" with "face isometry $i_f : \mathbb{R}^3 \to \mathbb{R}^3$" [14]*

Axiom B.1.3. *"In the folded model, the paper cannot self-intersect". Mathematically: "ϕ is one-to-one". "Even if the origami is "flat", there is still a small space between overlapping layers". So "Technically, axiom 3 prohibits any fold from being truly flat. The dihedral angle of any fold cannot go to zero without violating the one-to-one principle." [14]*

Axiom B.1.4. *"The paper never tears". Mathematically: "ϕ is continuous". in other words "any discontinuity in folding corresponds with a cut or tear made in the paper" [14].*

Axiom B.1.5. *"During the folding process, the paper cannot self-intersect".*

B.1.2. Implication of the mathematical model

Figure B.1 shows two sheets (S_1 and S_2). Both have several vertices on different positions on the raw edge, $V = \{V_1, V_2, V_3, V_4\}$ each V_i has an (x_i, y_i) component. A crease between the two vertices $V_1(x_1, y_1)$ and $V_2(x_2, y_2)$ can be defined as shown in formula B.1.

$$E_{12} = \overline{V_1 V_2} = \left\{ (x, y) \quad | \quad y = \frac{y_2 - y_1}{x_2 - x_1} x + y_1 \in \left[V_1, V_2 \right] \right\} \tag{B.1}$$

A crease E_{ij} defines the faces border between the F_i and F_j. For example S_1, E_{12} lies between F_1 and F_2, see figure B.1.

B.2. Map folding

The methodology of map folding is closely related to the intended model for strips. Both models includes

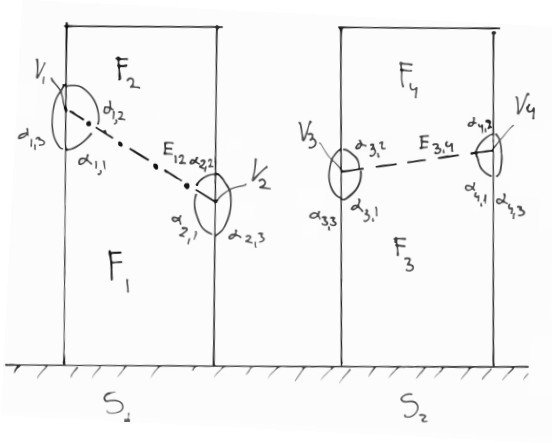

Figure B.1: Two sheets are fixed to the ground each having a single latitudinal crease E throughout the sheet which is accompanied with two vertices V. As defined by [13] and [14].

intersecting creases. For map folding the creases are either parallel or perpendicular, while folding with strips the creases do not have to. Following Demaine and Rourke [15] map folding needs to have at least one continuous crease which is labeled valley or mountain throughout the sheet. In case of map folding for each subset can be said that "all creases must be parallel; otherwise the vertex of intersections between crossing crease lines violate Maekawa's Theorem" [15]. A continuous mountain or valley is part of subset $\mathcal{H}$ or $\mathcal{V}$. Creases from the same subset can be folded independently from each other. The letter $\mathcal{H}$ is inherited from map folding for which creases are aligned with the horizontal, likewise $\mathcal{V}$ for the vertical. For the presented model the creases are not necessarily aligned with the horizontal of vertical, but for conventional reasons we will stick to the labels $\mathcal{H}$ and $\mathcal{V}$.

Figure B.2 from [15], shows an example of map folding. The main vertical crease of figure B.2 is folded first, therefore part of subset $\mathcal{V}_1$. Secondly the horizontal crease is folded, which is part of subset $\mathcal{H}_1$. Notice the mountain valley transition in order to satisfy Maekawa's Theorem. The final fold is part of of subset $\mathcal{V}_2$. For this example the independent creases are part of subset $\mathcal{V}_1$. The creases from subset $\mathcal{H}_1$ are and only are depending of subset $\mathcal{V}_1$. In the same way the creases of subset $\mathcal{V}_2$ depends on $\mathcal{V}_1$ and $\mathcal{H}_1$.

B.3. Strip folding

As mentioned earlier, our strip model will exclude the condition of perpendicular and parallel creases while including the requirement of independent creases within a subset, with 'independently' defined only within a strip. Reformulated, by definition the creases may not intersect inside the strip. For conventional reasons the completely independent creases will be placed in subset $\mathcal{H}$. Afterwards the creases of subset $\mathcal{V}_1$ will be folded. Because the creases are not parallel nor perpendicular, the upcoming subset are also called $\mathcal{V}$ and are accompanied with an index number. The first set of creases are labeled differently with $\mathcal{H}$ because it has distinctive number of variables per crease compared to $\mathcal{V}$. At first sight subset $\mathcal{V}_1$, $\mathcal{V}_2$ etc. do not differ in constraints, and are therefore characterized with the same label $\mathcal{V}$ accompanied with a unique index number. The following lemma is adopted from [15]

Lemma B.3.1. *"All crease lines in set $\mathcal{H}$ must be folded before any other creases"[15]*

B.3.1. Creating creases of subset $\mathcal{V}$

A crossing crease is part of subset $\mathcal{V}$ and is literally crossing a crease of a different subset. Figure B.3 shows the process to create creases from different subsets. The folding sequence $\mathcal{F}^1$ leads from an unfolded state to a folded state were only creases of subset $\mathcal{H}$ are folded. The second set of folding $\mathcal{F}^2$ introduces the subset $\mathcal{V}_1$ into the folded state, as is shown with the green line in figure B.3.

A side affect of the the stated above, a subset should not introduce creases which can be placed in lower subsets. As described in lemma B.3.2, which should be extended to all subsets.

Lemma B.3.2. *Subset $\mathcal{H}$ contains the optimal set of creases which are continuously a mountain or valley fold from one raw edge to another raw edge. Therefore the subset $\mathcal{V}$ can not induce a continuous mountain or valley fold from one raw edge to another raw edge.*

Proof. If the subset $\mathcal{V}$ would have a continuous mountain or valley fold from one raw edge to another raw edge then the subset $\mathcal{H}$ is not optimal, lacking this specific fold. □

B.4. More in depth: Creases of subset $\mathcal{H}$

In unfolded state all creases of subset $\mathcal{H}$ will go from one raw edge to a raw edge parallel to it, excluding the fixed ground as shown in figure B.1. This is not true for origami in general but only for our strips (flaps). The creases will be straight lines, in order to satisfy the axioms B.1.1, B.1.2, B.1.4 [14].

Definition B.4.1. *The crease pattern consist of straight creases going from and to parallel raw edges*

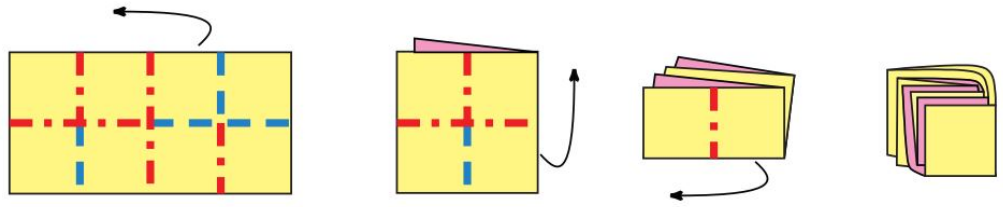

Figure B.2: Example of mapfolding. The first fold is part of $\mathscr{V}_1$, the second fold is part of $\mathscr{H}_1$ and the third fold is part of subset $\mathscr{V}_2$. The mountain assignment is shown in red while the valley assignment is shown in blue. Source: [15]

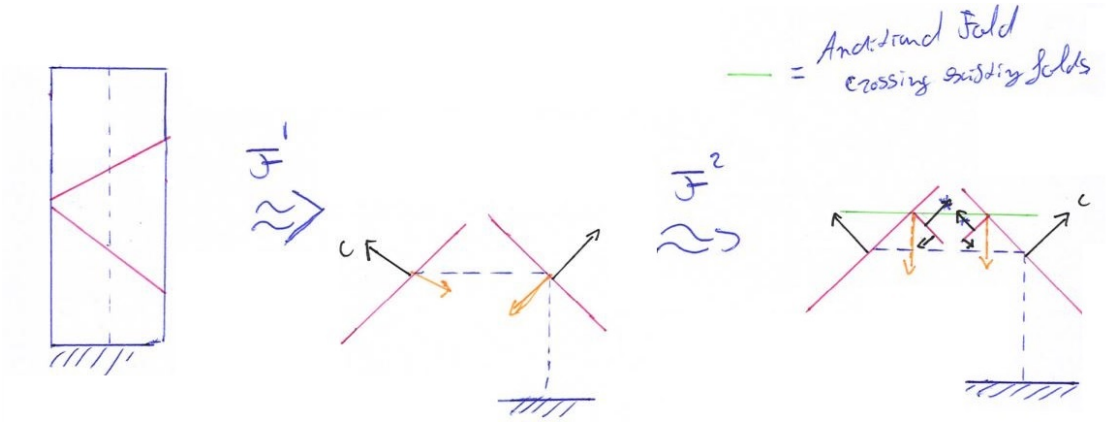

Figure B.3: A process to create crossing creases. The folding sequence $\mathscr{F}$ leads from unfolded to folded states of the strip.

excluding the fixed base. Strip (flaps) emerges perpendicular from the fixed ground.

Proof. If definition B.4.1 were not true then a crease line would intersect with the fixed ground which should also be folded. The ground can not be folded because it is fixed.

If creases were not straight lines the origami axioms B.1.1, B.1.2, B.1.4 would be violated [14] □

The strip itself can be defined with a constant width (D) of the strip and a constant length (L). The centerline of the crease is at a distance of $\frac{D}{2}$ from the raw edges and is often aligned with the origin of the axis, as shown in figure B.4. Although the foldable models are in reality in $\mathbb{R}^3$ and meet the 5 origami axioms. It is mathematically advantageous to use a mapping of ω which will map the folding to the space $\mathbb{R}^2 \times \mathbb{Z}$. The map ω can be divided in two semifolding maps μ and σ. The folded and unfolded state are related by the "*semifolding map* $\mu : C \to \mathbb{R}^2$ that determines only the final position of the sheet in a plane and *superposition ordering* $\sigma : C \to \mathbb{Z}$ determines only the overlap order of the layers"[14] of folded sheets. In figure B.4 the outgoing sheet of crease E_1 is mapped to the other side of the crease line as shown in the left figure.

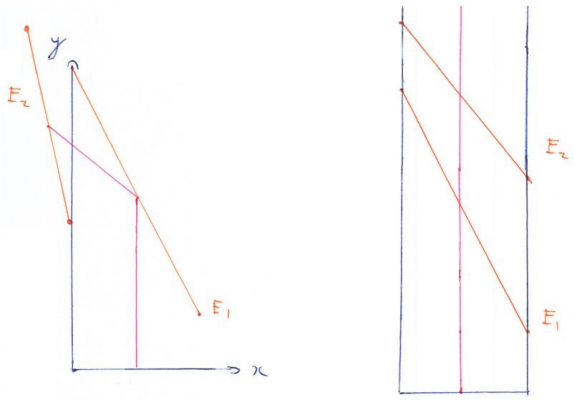

Figure B.4: Left folded strip and right unfolded strip with creases numbered. The centerline of the strip is shown in pink. The axes are located on the left hand side of the strip, but can also be located in the middle.

Before mapping the crease, it needs to be defined first. A crease of subset $\mathscr{H}$ can be defined with three variables, 1) the location on the y-axis ($x_1^{\mathscr{H}}$), 2) the angle between the incoming and outgoing strip ($x_2^{\mathscr{H}}$), 3) and the direction of the folding ($x_3^{\mathscr{H}}$).

B.4.1. Direction of the folding

This section deals with the direction of a crease. What direction does the incoming and outgoing strip come from and to?
Figure B.5 includes a folded sheet into the $\mathbb{R}^3$ space. If

the crease is defined inside the xy-plane, if folded the angle around the x-axis would ≈ 0, in such a way the faces touches. The angle around the x-axis $= \pi$ when unfolded. For flat foldability the angle around the x-axis is either 0 or π otherwise it would pop up into the $\mathbb{R}^3$ space. Including the fact that mathematically speaking the sheet is infinitely small, the crease can be represented as a line in a plane with a normal vector $\vec{N}$ indicating the direction of the fold and tangent vector $\vec{T}$ indicating the direction of the crease itself as shown in figure B.5. This is a direct result from simple vector calculus [18]. For completeness the $\vec{N}$ and $\vec{T}$ are defined in the center of the crease.

Definition B.4.2. *The normal vector ($\vec{N}$) and the tangent vector ($\vec{T}$) are located in the center of the crease E. Crease E has its endpoints in two vertices (V_i, V_j). The vector $\vec{N}$ determines the direction of the folding, therefore laying on the same side as the incoming and outgoing strip. Next $\vec{T} \perp \vec{N}$. And $\vec{T}$ denotes the tangent direction of the crease E with $|\vec{T}| = \frac{1}{2}|E|$*

It is worth to mention that normal vector ($\vec{n}$) is used to determine the orientation of the sheet, see chapter 11 of [15], these normal vectors are defined from the facets and not from the crease. Both definitions will be used with in this thesis.

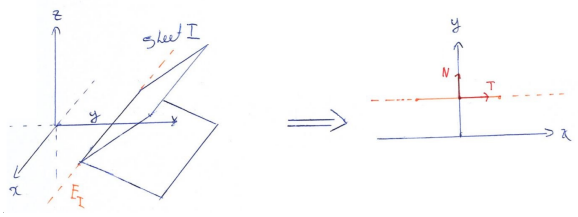

Figure B.5: Left a folded sheet with a creaseline. Right the crease itself on the xy-plane with the normal vector $\vec{n}$ and the tangent $\vec{T}$.

B.4.2. Behavior of a crease

A crease acts like a mirror, the incoming strip is reflected by crease what results into an outgoing strip. This is clearly shown in figure B.6, the centerline touches the origin of the normal vector before it is reflected. Mathematically shown in definition 8 of [14], which is cited in definition B.4.3.

Definition B.4.3. *"Let C be a c-net with straight-line creases. Let p be a path in C. The isometry induced by p, denoted $i_p : \mathbb{R}^2 \to \mathbb{R}^2$, is defined as follows. Suppose p crosses the creases $E_1, E_2, ..., E_n$, not necessarily all distinct, in that order. Let R_{E_j} denote the reflection of the plane across the line containing the crease E_j. Then i_p is defined to be the composition $R_{E_1} \bullet R_{E_2} \bullet ... \bullet R_{E_n}$ "[14]*

The reflection R of B.4.3 depends on the variable α.

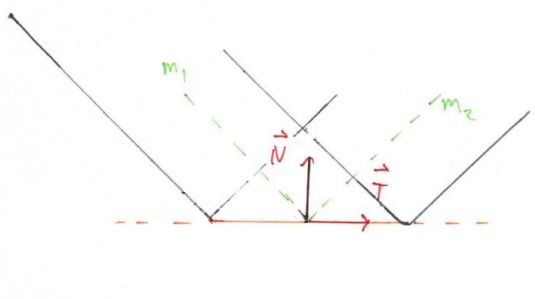

Figure B.6: The incoming strip is mirrored on the crease resulting in an outgoing strip.

which is defined by the angle between the incoming centerline and the normal vector of the crease.

Corollary B.4.1. *The angle α between $\vec{N}$ and the centerline $\vec{l}$ (in figure B.6 noted as m) is constrained by $-\frac{\pi}{2} \leq \alpha < \frac{\pi}{2}$.*

Proof. If $\alpha > \frac{\pi}{2}$ then the incoming strip would be at the back of the crease. As a result also the reflection would also be at the back of the crease. Therefore definition B.4.2 is violated, which states that the $\vec{N}$ needs to be on the same side as the incoming and outgoing strip.

If $\alpha = \frac{\pi}{2}$ then the strip is parallel to the crease. Which is in violation with definition B.4.1.

□

B.4.3. Strip Model of subset $\mathscr{H}$

The strip is folded from the bottom to the top raw edge. The therefore the folding operations within a strip have an ordering.
The basic idea of the strip model; if the distance between the center of the creases $|\vec{l}_n|$ and the angle α_n between the normal vector and the centerline are known in combination with the constant width of the strip (D) then all the vertices and center points of of all the creases can be calculated. In other words this model has as input the lengths of the centerlines and the angles of the crease and the model gives as output the coordinates of all important points, see also figure B.4 and figure B.7.

From corollary B.4.1 is known that α is the angle between $\vec{N}_n$ and $\vec{l}_n$. So the angle between two centerlines are equal to 2α, see also figure B.7. In a more generalised form, $\angle\vec{l}_n, \vec{l}_{n+1} = 2\alpha_n$. A crease is able to reflect π, therefore can be said that $\beta_n = \pi - 2\alpha_n$ which will be the the variable of the reflection matrix from definition B.4.3. The reflection matrix is stated below:

$$\mathbf{R}(\beta_n) = \begin{bmatrix} \cos\beta_n & -\sin\beta_n \\ \sin\beta_n & \cos\beta_n \end{bmatrix} \tag{B.2}$$

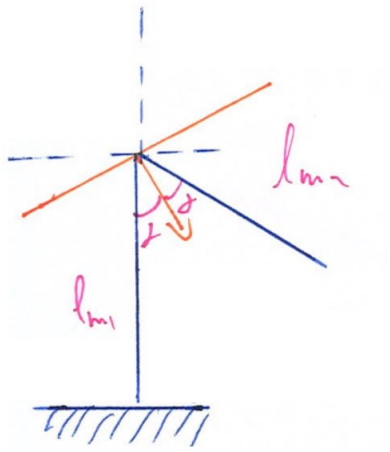

Figure B.7: The centerline is mirrored at the center of the crease line with an angle α to the normal vector $\vec{n}$.

The endpoint of $\vec{l}_{m2}$ of figure B.7 can be determined if α, $\vec{l}_{m1}$ and the $|\vec{l}_{m2}|$ are known, then:

$$\vec{l}_{m2} = \underbrace{|\vec{l}_{m2}|}_{\text{New length}} \underbrace{\mathbf{R}(\beta)\hat{l}_{m1}}_{\text{direction}} + \underbrace{\vec{l}_{m1}}_{\text{begin position}}$$

In a more generalised form:

$$\vec{l}_{n+1} = |\vec{l}_{n+1}|\mathbf{R}(\beta)\hat{l}_n + \vec{l}_n \quad \text{with} \tag{B.3}$$

$$\mathbf{R}(\beta) = \mathbf{R}_{n+1}(\beta_{n+1})\mathbf{R}_n(\beta_n)\mathbf{R_{n-1}}(\beta_{n-1})\dots\mathbf{R_0}(\beta_0)$$

Formula B.3 is a bit of cumbersome. For a clear and more intuitive definition, formula B.3 is rewritten into a matrix notation as shown in formula B.4.

$$\begin{bmatrix} \vec{l}_1 \\ \vec{l}_2 \\ \vec{l}_3 \\ \vdots \end{bmatrix} = \begin{bmatrix} \hat{l}_1 & \mathbf{0} & \mathbf{0} & \cdots & \mathbf{0} \\ \hat{l}_1 & \mathbf{R}(\alpha_1)\hat{l}_1 & \mathbf{0} & \cdots & \mathbf{0} \\ \hat{l}_1 & \mathbf{R}(\alpha_1)\hat{l}_1 & \mathbf{R}(\alpha_2)\mathbf{R}(\alpha_1)\hat{l}_1 & \cdots & \mathbf{0} \\ \vdots & \vdots & \vdots & \ddots & \vdots \end{bmatrix} \begin{bmatrix} |l_1| \\ |l_2| \\ |l_3| \\ \vdots \end{bmatrix} \tag{B.4}$$

Note: That the total length of the subset α is smaller with one then subset $|l|$. This is a locigal result because α only exist between two centerlines.
Note: That from definition B.4.1 the strip originate perpendicular from the fixed base. If the fixed base would be aligned with the x-axis, then $\hat{l}_1 = \begin{bmatrix} 0 & 1 \end{bmatrix}^T$.
Note: This model does not satisfy origami axiom B.1.3 and B.1.5, which prevents intersection of the sheet. Keep these axioms in mind.

B.4.4. Implications of the strip model

With the information of the strip model and the known constant width of the strip the location of the vertices can be calculated. This is realised by the fact that the centerline is parallel with the vertex line with $\frac{D}{2}$, see also figure B.6. Note that $\vec{l}_n$ is located on the center of a crease.

$$V = \begin{bmatrix} x \\ y \end{bmatrix} = \vec{l}_n \pm \frac{D}{2}\hat{l}_n^T \tag{B.5}$$

with:

$$\hat{l}_n^T = \mathbf{R}_\perp \hat{l}_n = \begin{bmatrix} \cos\frac{\pi}{2} & -\sin\frac{\pi}{2} \\ \sin\frac{\pi}{2} & \cos\frac{\pi}{2} \end{bmatrix} \hat{l}_n \tag{B.6}$$

From definition B.4.2 $\vec{T} = V$ and $\vec{N} \perp \vec{T}$. The vector $\vec{N}$ can also be described as the bisector between the incoming strip and the outgoing strip. Therefore $\hat{N}$ can be formulated as followed:

$$\vec{N}_n = ||\hat{l}_{n+1}||\hat{l}_{n-1} + ||\hat{l}_{n-1}||\hat{l}_{n+1} = \hat{l}_{n-1} + \hat{l}_{n+1} \tag{B.7}$$

With the above information and formulations lemma B.4.1 can be defined.

Lemma B.4.1. *If the the strip model is used in $\mathbb{R}^2$, the normal vector $\hat{N}$ and the tangent $\hat{T}$ can be described as a function of l_i with $i = 1 \dots n$ as followed:*

$$\hat{N} = \frac{\hat{l}_{n-1} + \hat{l}_{n+1}}{|\hat{l}_{n-1} + \hat{l}_{n+1}|} \quad \textit{and} \quad \hat{T} = \mathbf{R}_\perp \hat{N} \tag{B.8}$$

B.5. More in depth: Creases of subset $\mathcal{V}$

Figure B.8 shows a close view of a part of a crease pattern with creases of subset $\mathcal{H}$ and $\mathcal{V}$. The creases of subset $\mathcal{V}$ intersect with subset $\mathcal{H}$, resulting that the a crease of subset $\mathcal{V}$ consist of several partial creases. In order to determine if a partial crease is mountain or valley, Kawasaki theorem can be used.

Back to figure B.8. The outer vertical line is the raw edge of the strip itself. While the vertical black line is midline of the strip. The crease of $\mathcal{H}$ is shown in orange and is defined before subset $\mathcal{V}$, therefore the angle and position of this crease is known. The angle α_3 is defined by angle between the normal vector of the existing crease and the incoming crossing crease. The crossing crease can be introduced to the strip model when the the starting position and the angle α_3 are known.

The starting position position of the crossing crease is a vertex $V_1^{\mathcal{V}}$ on a raw edge which can be defined with a vertex $V^{\mathcal{H}}$ of subset $\mathcal{H}$ with a certain length $l_1^{\mathcal{V}}$. See also formula B.9.

$$V_1^{\mathcal{V}} = V^{\mathcal{H}} + |l_1^{\mathcal{V}}|\hat{V}^{\mathcal{H}} \tag{B.9}$$

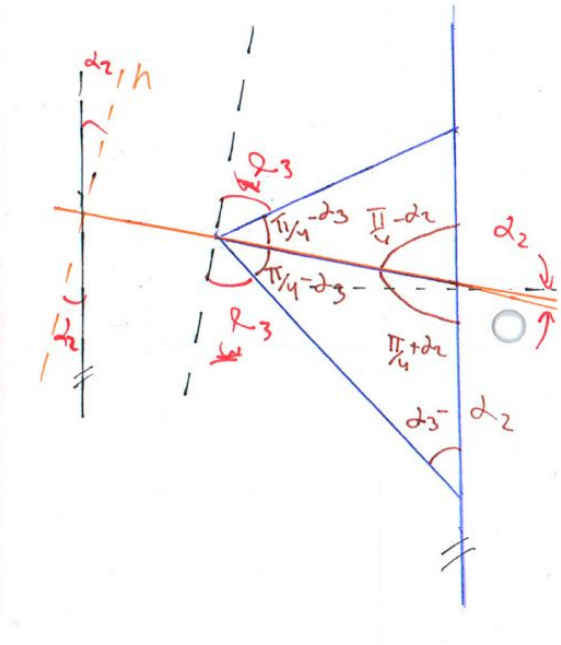

Figure B.8: A part of a crease pattern in unfolded state. The angle of the crossing crease of the raw edge. The variable α_2 is known from the previous subsets. The raw edge is shown with a blue line as well as the crossing crease. The middle line of the strip is shown in black. The variable α_3 can be freely chosen.

which is accompanied with a direction β:

$$\beta = \alpha_3 - \alpha_2 \quad \text{with:} \quad \frac{-D}{2} \leq V_1^{\mathcal{V}} \quad V_1^{\mathcal{V}} \leq \frac{D}{2} \tag{B.10}$$

The limitations of β are needed in order for vertices to lay inside the strip. With this information the entire line of the crease can be drawn. In order to determine if the crease is mountain or valley, Kawasaki theorem can be used.

Note that the normal vector $\vec{n}$ of a crease from subset $\mathscr{H}$ is defined. By the fact the crease line is refracted, formula B.11 is true from the fact that $\theta_1 = \theta_2$. With i is the incoming crossing crease and t is the outgoing crease.

$$\left(\vec{n} \wedge t\right) = \left(\vec{n} \wedge i\right) \tag{B.11}$$

A crease of subset $\mathcal{V}$ can be defined with four variables, 1) the location on the y-axis ($x_1^{\mathcal{V}}$), 2) the side of the strip ($x_2^{\mathcal{V}}$), 3) the angle of the crease ($x_3^{\mathcal{V}}$), 4) and the direction of the folding ($x_4^{\mathcal{V}}$)

C

Degrees of freedom in folded state

The basic principle of flat origami is that the resulting object could "be pressed between the pages of a book" [14]. Physically the layers have a certain thickness and would therefore popup into the $\mathbb{R}^3$-space. However, mathematically the sheet thickness is neglected, hence it spans a $\mathbb{R}^2$-space in unfolded state [14]. If the origami object is also flat foldable then also in folded state the crease pattern can be mapped to the same space of $\mathbb{R}^2$.
The physical ordering can be tracked with the space $\mathbb{Z}$. Concluding that mathematically flat origami can be described in a space $\mathbb{R}^2 \times \mathbb{Z}$ [14].
Although the mathematical model neglect the fact that a sheet has a thickness, the true thickness of a strip will be in the order of 0.01 mm to 1 mm. As is stated in section 1, compared with the total size of the object which is several meters, from a designer point of view it would also be appropriate to neglect the thickness of the sheets. Therefore all creases will lay in the same $\mathbb{R}^2$ plane as is shown in figure C.1.
Following Hopkins [38] a plane can be described by

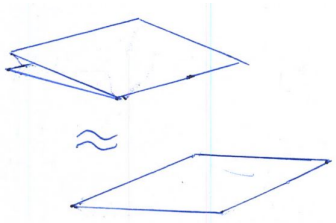

Figure C.1: With the mathematical origami principles all creases of a flat-folded object lie on the same plane.

constraints on a plane called the constraint-space. Figure C.2 shows this constraint-space and its corresponding freedom-space, following the topology of Hopkins. If the plane were aligned with the x and y-axis, then the resulting freedom-space would consist of translation into the z-direction and rotation around the x-axis and y-axis.
If one side of the sheet is fixed and the other side has a crease. The freedom of rotation would be parallel and perpendicular to the fold as is shown in figure C.3. While the largest displacement due translation

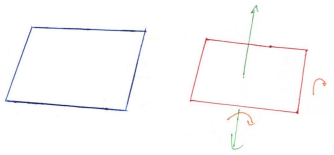

Figure C.2: Left the constraint space and right the freedom space of one single sheet , as defined by Hopkins [**?**]

into the z-direction would occur at the tail of the facet on the crease itself.
In figure C.4 the ground is replaced with the final

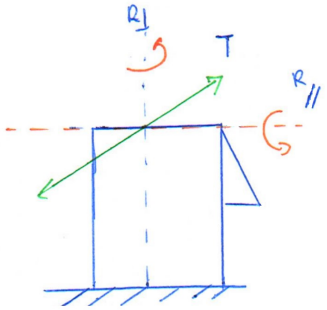

Figure C.3: One fold with the resulting DoF, which is attached to the ground.

object, which is shown in yellow. From the point of view of the object, the degree of freedom will be defined on same location as in figure C.3.
Summarizing, from the mathematical definition of flat origami, all creases lay inside one single plane $\mathbb{R}^2$. If the plane is spanned by x-axis and y-axis, the plane has a constraint-space of x, y, R_z and a freedom-space of z, R_x, R_y.

By taking in account that in the physical world the sheets can not intersect with itself and the fact that the sheets have a finite thickness, the freedom-space can be reduced. Once again the topology of Hopkins is considered [**?**], by stacking the flat constraint-spaces unto each other, as shown in figure C.5, the freedom-space can be reduced to only a translation into the z-direction.

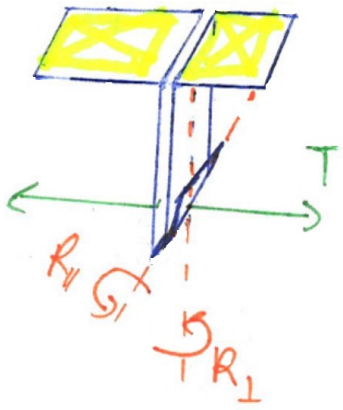

Figure C.4: One fold with the resulting DoF, which is attached to the object which is shown in yellow.

By assuming that the object resembles a fixed

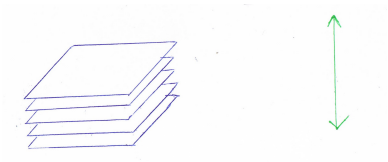

Figure C.5: Left the constraint space and right the freedom space of stacked sheets, as defined by Hopkins [**?**]

ground, a stacked strip of paper will have a DoF translation into the z-direction as shown in figure C.6. Note that translation into z-direction counts for the resulting folded state but not for individual facets which will "stick" to each other as explained in section D.

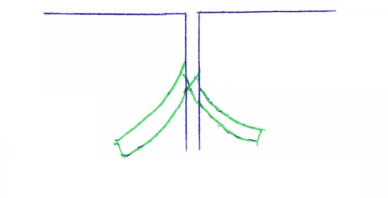

Figure C.6: The influence of the resulting DoF for stacked sheets.

D

Primary constraints

D.1. The bricks of constraining sheets

Remember from a mathematical point of view, the sheets are infinitely thin in such a way that all the creases lay inside one plane. This should also be true if a crease involves more then one sheet. This chapter restricts itself to two sheets which folded into each other, namely sheet I and sheet II.

In figure D.1, sheet I is folded inside the fold of

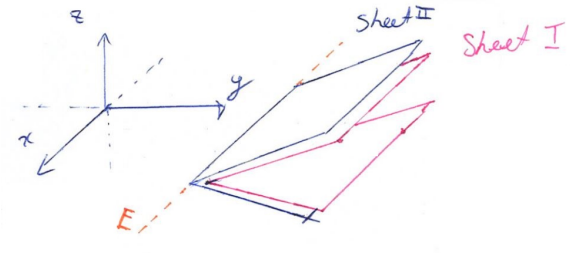

Figure D.1: Coordinate system with sheet one folded into sheet two. The creases of both sheets lay on the same plane.

sheet II in such a way that the crease $E = E_{II} \approx E_I$ is parallel to the x-axis inside the xy-plane. Let's say that one of the two sheets is fixed. Then there are two options, A) sheet I constrains sheet II, or B) sheet II constrains sheet I. For both situations it is true that:

Lemma D.1.1. *If the crease $E_{ij,I}$ of sheet I and $E_{ij,II}$ of sheet II lay both inside $\mathbb{R}^2$ and are folded into each other. And if $det(E_{ij,II}, E_{ij,I}) < 0$, $E_{ij,II}$ is on the left of $E_{ij,I}$, then the sheets are constraint by $\vec{E}_{ij,II} \preceq \vec{E}_{ij,I}$. Or if $det(E_{ij,II}, E_{ij,I}) > 0$, $E_{ij,II}$ is on the right of $E_{ij,I}$, then the sheets are constraint by $\vec{E}_{ij,II} \succeq \vec{E}_{ij,I}$. Independent of which sheet is fixed or which orientation the creases have:*
If $E_{ij,II} \neq E_{ij,I}$ then sheet I or II is somewhere in the freedom-space
If $E_I = E_{ij,II}$ and $E_{ij,I} \parallel E_{ij,II}$ then the creases are on the constraint
If $E_I = E_{ij,II}$ and $E_{ij,I} \nparallel E_{ij,II}$ then the creases have a collision

Proof. Lets say E_{II} lies left of E_I for $E_I \parallel E_{II}$. Then E_I can be rewritten as $E_I = \vec{d} + \hat{E}_{II}|E_I|$ with $\vec{d} \geq 0$ as the distance between E_I and E_{II}. In that case $det(E_{II}, \vec{d} + \hat{E}_{II}|E_I|) \leq 0$. If $det(\ldots) < 0$ then E_I is located on the right of E_{II} and if $det(\ldots) = 0$ then E_I and E_{II} lay into each other. So $E_{II} \leq \vec{d} + \hat{E}_{II}|E_I|$ results in $E_{II} - \hat{E}_{II}|E_I| \leq \vec{d}$. Indeed if $d = 0$ then E_I and E_{II} are equal to each other and are therefore laying on the same location and if $d > 0$ then E_I lies indeed right of E_{II}. □

Note that lemma D.1.1 states that sheets needs to be folded into each other. This can be checked with algorithms of chapter 11 of the book [15]. Section F will discuss ordering in in depth. As shown in the proof the creases E_I and E_{II} can be expressed in each other namely: if $E_I \parallel E_{II}$ then $E_I = \vec{d} + \hat{E}_{II}|E_I|$ and if $E_I \nparallel E_{II}$ then $E_I = \vec{d} + \hat{e}_I|E_I|$. This also complies with the strip model of section B.4.3 for which $\vec{d} = \vec{l}_n$.

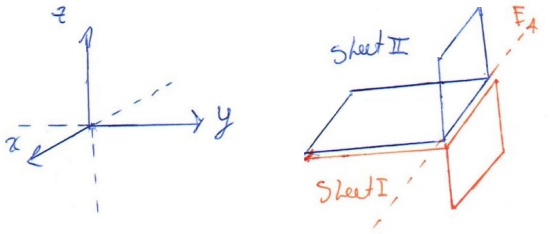

Figure D.2: Coordinate system with two sheets. The corresponding creases have an opposite direction. Also called a misalignment gadget.

Figure D.2 shows a folding with opposite creases. Note that in flat folding this fold is literally not allowed due the fact it pops up in $\mathbb{R}^3$ space. Figure D.2 is shown for illustration for a fold which is folded back. While folding back both sheets are not folded into each other. This fold could be used as a misalignment gadget, by creating different directions for each sheet.

Lemma D.1.2. *If the crease E_I of sheet I and E_{II} of sheet II lay both inside $\mathbb{R}^2$ and are **not** folded into each other. Independent of the location and orientation of*

the creases, the sheets are not constrained. Mathematically: $-\infty \leq E_I \leq \infty$ *and* $-\infty \leq E_{II} \leq \infty$.

Note, that this report will not include misalignment gadget and will assume that the sheets will remain sticky. That is a logical assumption if you were able to use multiple folds to lock the sheets into each other with the use of flat folding.

Figure D.3 shows a which ladder which includes twice a fold from lemma D.1.1. Although figure D.3 seems to pop up in $\mathbb{R}^3$ it is not, due the fact of sharp fold angles and infinite thin sheets. In this example sheet I lays on the left of sheet II both having crease A and B. The constraints of creases stated as $\vec{E}_{II,A} \leq \vec{E}_{I,A}$ and $\vec{E}_{II,B} \leq \vec{E}_{I,B}$. The total constraint is into the same direction. In other words there is a one directional constraint in figure D.3. With this idea in mind lemma D.1.3 is defined.

Lemma D.1.3. *If* $E_{II,i} \leq E_{I,i}$ *with* $i \in A \ldots n$ *and* $E_{II,i} \parallel E_{I,i}$ *then all constraints contribute to the same constraint. The same is true for* $E_{II,i} \geq E_{I,i}$.

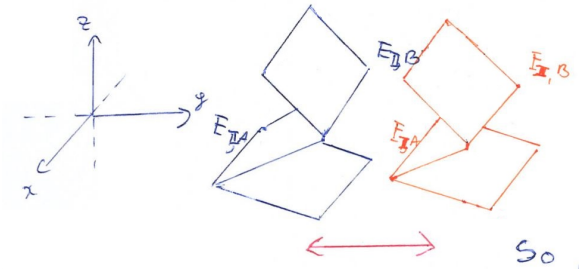

Figure D.3: Coordinate system with two sheets folded in a zigzag shape. The corresponding creases lie in the same plane.

Lemma D.1.4 involves a fold combination of opposite folds and how those folds can constrain the sheets. An example a fold combination can be seen in figure D.4.

Lemma D.1.4. *If there are two sheets (I, II) with both two crease (A,B) which have an opposite folding direction, e.g.* $\hat{N}_A = -\hat{N}_B$ *and* $\vec{d}$ *is distance between* $E_{II,A}$ *and* $E_{II,B}$. *Then:*
if $d(E_{I,A}, E_{I,B}) = \vec{d}$ *then the sheets are constraint in both directions, also called locked*
if $d(E_{I,A}, E_{I,B}) < \vec{d}$ *then the sheets can move freely between the creases of the fixed sheet.*

Proof. Figure D.4 two sheets with two opposite folds which agree with lemma D.1.1. For the independent constraints is true that $\vec{E}_{II,A} \leq \vec{E}_{I,A}$ and $\vec{E}_{II,B} \geq \vec{E}_{I,B}$. Lets assume that the distance between the creases A and B is equal to $\vec{d}$. In such a way that $\vec{E}_{II,A} = \vec{E}_{II,B} + \vec{d}$ and $\vec{E}_{I,A} = \vec{E}_{I,B} + \vec{d}$. Which results into the following

$$\begin{cases} \vec{E}_{II,A} \leq \vec{E}_{I,A} \\ \vec{E}_{II,B} \geq \vec{E}_{I,B} \\ \vec{E}_{II,A} = \vec{E}_{II,B} + \vec{d} \end{cases} \rightarrow \begin{cases} \vec{E}_{II,B} + \vec{d} \leq \vec{E}_{I,A} \\ \vec{E}_{II,B} \geq \vec{E}_{I,B} \end{cases}$$

$$\rightarrow \left\{ \vec{E}_{I,A} - \vec{d} \geq \vec{E}_{I,B} \right.$$

Reformulated to $\vec{E}_{I,A} - \vec{E}_{I,B} \leq \vec{d}$.
If $\vec{E}_{I,A} - \vec{E}_{I,B} = \vec{d}$ then sheet I is fixed between the creases of Sheet II. Note, the creases of sheet I may be parallel or have an collision.
If $\vec{E}_{I,A} - \vec{E}_{I,B} < \vec{d}$ then sheet I is able to move freely on the domain between the creases of sheet II which are defined by $\vec{d}$. □

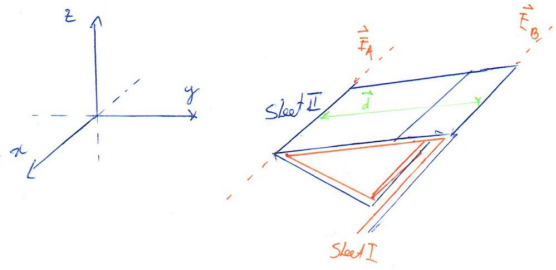

Figure D.4: Coordinate system with two sheets folded with two opposite creases. The corresponding creases lie in the same plane.

D.2. Projection of the constraints

Lemma D.1.4 shows how opposite creases are able to constrain/lock sheets. However, figure D.1 shows multiple creases which are not aligned with each other and have also different lengths. Physically the bending strain of a fold does depend on its length [39], therefore it is important to take the lengths of individual creases into account. To have an indication of the added value of those creases, they can be projected to a body fixed orthogonal base x y-axis. From section B.4 is known that the $\vec{N}$ represents the folding direction, or the direction of freedom and the vector $\vec{T}$ represents the direction of the crease. So sheets are able to move freely along this line.
So the constraint-space can be defined by $-||\vec{N}||\hat{n}$. From lemma D.1.1 it is clear that on the crease there is an one directional constrain. If the sheets are locked, as defined in lemma D.1.4, it will be sufficient to split the $\mathbb{R}^2$-space into four subsapces, namely: x^+, x^-, y^+, y^- in such a way we can track individual directions.

Lemma D.2.1. *Each individual crease has a freedom space:* $F = \{-\vec{T}, \vec{T}, \vec{N}\}$ *and a constraint space:* $C = \{-||\vec{N}||\hat{n}\}$ *in* $\mathbb{R}^2$. *The* $\mathbb{R}^2$*-space is the union of the subsets* $\{x^-, x^+, y^-, y^+\} = F \cup C$ *for which* $F \not\subset C$.

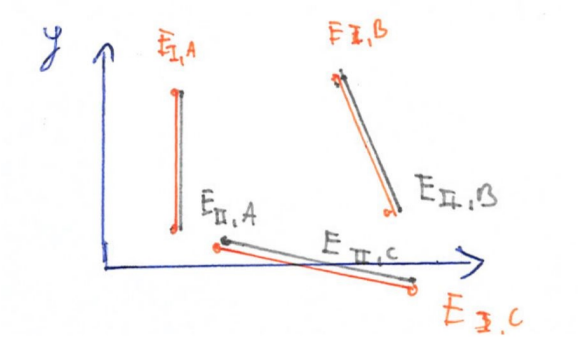

Plot D.1: Two sheets with each 3 creases which have different lengths and different directions.

D.3. Distinguishing the whichladder and opposite folding

This section will determine when a crease is part of a whichladder or opposite folding.

D.3.1. Distinguishing by ordering following Demaine and Rourke

Demaine and Rourke [15] describe a way to define the order of stacking of faces for one single sheet. They are able to tell whether point p or q, both on the same sheet, is on the top. This is realized by defining p and q on a faces with corresponding normal vectors of a sheet. See for example figure D.5, a sheet is represented with the blue line and the orange arrows represent the normal vectors. By folding, the sheets are mapped in such a way that "for every pair of distinct noncrease points $p, q \in P$ that $f(p) = f(q)$, we assign a value of $+1$ or -1 to $\lambda(p,q)$, with the intent that λ disambiguates whether p is stacked "above" $q(\lambda(p,q)) = +1)$ or p is stacked "below" $q(\lambda(p,q)) = -1)$" [15]. The normal vectors are defined as followed [15].

$$\mathbf{n}_f = \left(\frac{f'(r)}{||f'(r)||}\right)^{\perp} \quad \text{where} \quad f'(r) = \left.\frac{df(x)}{dx}\right|_{x=r} \tag{D.1}$$

$$\text{and} \quad <x,y>^{\perp} = <-y,x> \quad [15]$$

So, "$\lambda(p,q) = +1$ says that p touches q on q's top side, and $\lambda(p,q) = -1$ says that p touches$q$ on q's bottom side" [15], see figure D.6 Note that Demaine and Rourke defined this method in such a way that there may exist other sheets between point p and q. In our situation we are not using one sheet but two sheets which remain sticky, e.g. the pink line of figure D.5. With the normal vector of both sheets pointing into the same direction. Figure D.6 shows the normal vectors near a fold. If the normal vectors are pointing to each other $(\lambda(p,q) = +1, \lambda(q,p) = +1)$ then the normal vector of the fold (N_E) is pointing inwards. And if $(\lambda(p,q) = -1, \lambda(q,p) = -1)$ then the normal vector of the fold (n_E) is pointing outwards. The corresponding constraint space is still defined as $C = \{-||\vec{N}||\hat{n}\}$. A physical fold can be seen in figure D.7. The folds of figure D.6 are schematically shown in figure D.8.

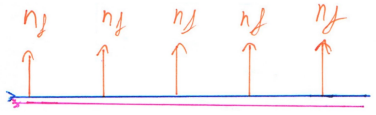

Figure D.5: Two flat sheets which are "sticky" shown in pink and blue. The corresponding normal vectors of the blue sheet are shown.

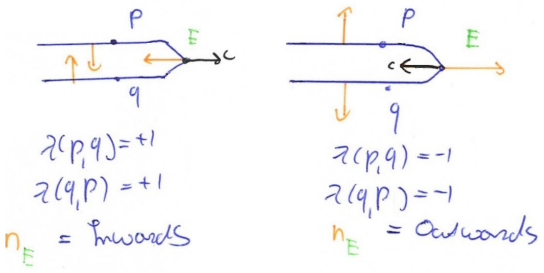

Figure D.6: The orientation of a sheet after folding with the corresponding resulting value of the λ-function. This figure is only true if no more then one crease is located between p and q. Partially adapted from [15]

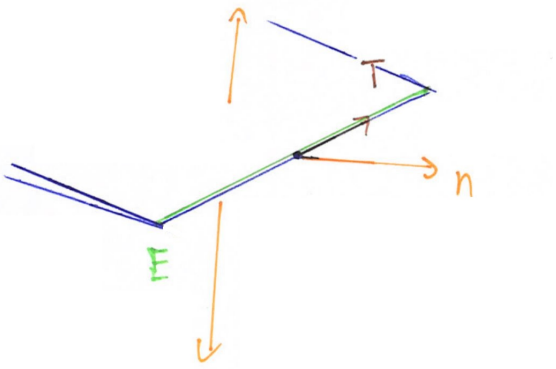

Figure D.7: A fold in the physical world. The sheet and the crease have a normal normal vector.

A ladder is shown in figure D.9 which is a schematically representation of figure D.3 with one additional crease. The creases of figure D.9 introduces constraints (C) which are pointing into the same direction.

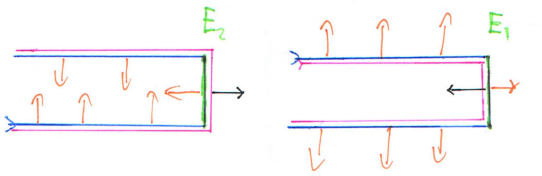

Figure D.8: A systematic way of drawing the orientation of the sheet after folding. Left: inward folding with $\lambda = +1$. Right: outward folding with $\lambda = -1$. The constraint is shown with a black arrow.

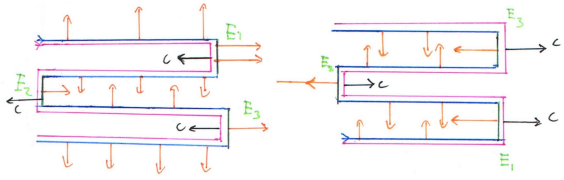

Figure D.9: Two which ladders with a different direction are shown including the normal vectors of the blue sheet. The constraint is shown with black arrows.

In contrary to the ladder you can fold around the base with opposite folding as is shown in figure D.4 and D.10. The resulting crease pattern have constraints in opposite directions.

Figure D.11 shows a combination of a ladder

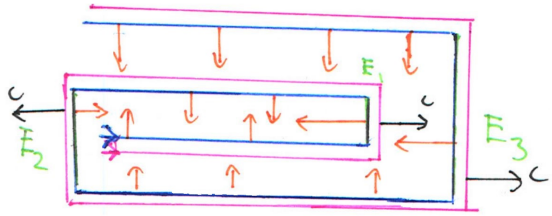

Figure D.10: Opposite folding. Includes three creases which fold around the base. The normal vector and constraint vectors are shown.

and opposite folding. The recurring question is which fold is a which ladder and which is part of opposite folding? From the eye its clear the the first crease is part of opposite folding, second crease is a which ladder, third crease is opposite folding as well as the fourth crease. The basic idea is that with the knowledge of the previous crease you can determine if the current crease is whichladder or part of opposite folding. The first crease of figure D.11 has normal vector (n_f) pointing to each other resulting in a $\lambda(p,q) = +1$. Due the fact we are only determining the orientation just after and just before a crease, we know that $\lambda(q,p)$ will also be equal to $+1$. The orientation of the previous crease (λ_{n-1}) compared to the current crease (λ_n) will tell if you have a which ladder or opposite folding.

Lemma D.3.1. *One single crease E_n will map two points p and q, laying on sheet S, in such a way that $n_p = -n_q$ independently whether $\lambda(p,q), \lambda(q,p) = +1$ or $\lambda(p,q), \lambda(q,p) = -1$ [15].*

Proof. If $\lambda(p,q) \neq \lambda(q,p)$ e.g. $\lambda(p,q) = +1$ or $\lambda(q,p) = -1$ then $n_p = n_q$ which is true if there are multiple creases between p and q. However, lemma D.3.1 states that there is one crease and logically $\lambda(p,q), \lambda(q,p) = +1$ or $\lambda(p,q), \lambda(q,p) = -1$ resulting to $n_p = -n_q$. More specific information can be found in [15]. □

Lemma D.3.2. *There are two creases next to each other, namely: E_{n-1} and E_n. From lemma D.3.1 is known that $\lambda(p,q) = \lambda(q,p)$ for two points with one intermediate crease E_j will be reformulated as λ_j. The creases E_{n-1} has an corresponding λ_{n-1} and E_n has a corresponding λ_n. Note; that λ_n is located on the crease E_n and is therefore aligned with the folding direction, positive or negative.*

- *if $\lambda_{n-1} = \lambda_n$ then E_n is part of opposite folding*
- *if $\lambda_{n-1} \neq \lambda_n$ then E_n is part of a whichladder*

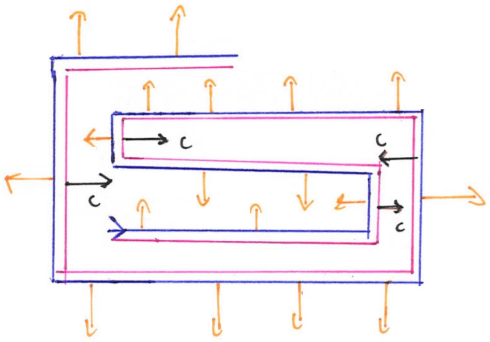

Figure D.11: A combination of the which ladder and opposite folding. The normal vector and constraint vectors are shown.

D.3.2. Relation of the constraint and the folding direction

A crease pattern in unfolded state is a roadmap to the folded state, it consist of vertices (V), edges (E), and faces (F) [14]. But it lacks a representation of the orientation of the sheet ($\vec{n}$) in folded ($\mathscr{F}$) and unfolded state ($\mathscr{F}^{-1}$). It becomes even more complex with the introduction of multiple creases. In order to keep track of the orientation of the sheet, the set of variables (Λ) is introduced. The variable Λ will help to relate the type of folding with the orientation of the sheet.

The variable Λ will recall if a crease is part of opposite folding or part of a Jacobs ladder. If a crease is

part of a Jacobs ladder then it will be represented with a 1, if not then the crease will be represented with a 2. The folding direction $\vec{N}$ and the orientation of the sheet ($\vec{n}$) can be related to each other on crease m as is shown in Eqn. (D.2).

$$\vec{n}_m = \vec{N}_m(-1)^{\sum_{i=1}^{m}\Lambda} \tag{D.2}$$

The resulting constraint can be formulated as $C_m = -\vec{n}_m = -\vec{N}_m(-1)^{\sum_{i=1}^{m}\Lambda}$ for crease m.

E

Crossing of creases

Till so far we only discussed crease patterns of a strip including creases going from one raw edge to the other, which is parallel. Till this moment they were not allowed to intersect. This chapter will involve the crossing of several creases and how it influences the constraint space.

E.1. Properties of crossing creases

The crossing creases of subset $\mathcal{V}$ have the following properties:

- The creases are subsequently folded with the order $\mathcal{H}$, $\mathcal{V}_1$, $\mathcal{V}_2$, etc.
- A crossing crease can be defined with 4 variables in unfolded state. 1) The start position defined from the horizontal axis. 2) The start position defined from the vertical axis. 3) The direction of the crease. 4) The folding direction (folding around the base or whichlader).
- In unfolded state the creases of a subset will be refracted by by lower subsets.
- In folded state the partial creases of a crossing crease will be co-linear.
- In folded state the crossing crease will be the most outer crease of the crease it does not intersect within a certain band spanned by itself.
- Creases of subset $\mathcal{V}$ do not necessarily go to another parallel raw edge.
- Crease may not intersect a crease from the same subset.

E.1.1. Projection method for subset $\mathcal{V}$.

A crease of subset $\mathcal{V}$ exist by definition of several sub creases, which are bounded by the rawedge or creases of earlier subsets. Due Maekawa's theorem the partial creases will be alternating between mountain and valley. Although the creases of subset $\mathcal{V}$ are refracted by lower subsets in folded state. The partial creases of a crossing of subset $\mathcal{V}$ are co-linear in folded state, as can clearly be seen in figure E.1.

While the partial creases of subset $\mathcal{V}$ are co-linear, the resulting constraints, which are induced by folding, are not but are opposite depending on the mountain valley assignment. Also the value linked to the constraints differs in size depending on the length of a partial crease. For clarification see also figure E.2. In this figure it is clear that the partial crease E_{II} results into a weaker constraint and is opposite to the constraint resulting from E_I which is quite large. From this example lemma E.1.1 is created.

Lemma E.1.1. *A crease from subset $\mathcal{V}$ creates a constraint in the normal direction, positive and negative, of the creases in folded state. The size of the constraint into the positive or negative direction may differ.*

Proof. First, remember that a mountain or valley assignment results into opposite constraints.
Secondly, the subset $\mathcal{V}$ will always intersect a crease from a lower subset or a raw edge. A lower subset or raw edge will have a continuous assignment of mountain or valley. In order to satisfy Maekawa's theorem the outgoing crease of subset $\mathcal{V}$ needs to have a different mountain valley assignment then the incoming crease. □

With the knowledge that a mountain or valley assignment results into opposite constraints, the projection method of subset $\mathcal{H}$ can be updated for subset $\mathcal{V}$. The mountain-valley assignment of the projection method for subset $\mathcal{V}$ will represented by an alternation, $(-1)^{index+1}$ with $index = \{I, II, III, \ldots\} \in \mathbb{N}_1$ as index number of the partial crease of a crease from subset $\mathcal{V}$. For example see figure E.2 which has subset $\mathcal{V}$ including $\{E_1^V\}$ with $E_1^V : \{E_I, E_{II}\}$.

The first partial crease $(E_{m,1})$ of crease (m) determines the direction of all other partial creases due the mountain valley sequence. The direction $(n_{m,i})$ of the partial crease $(E_{m,i})$ is mathematically shown in Eqn. (E.1). Note that i corresponds with

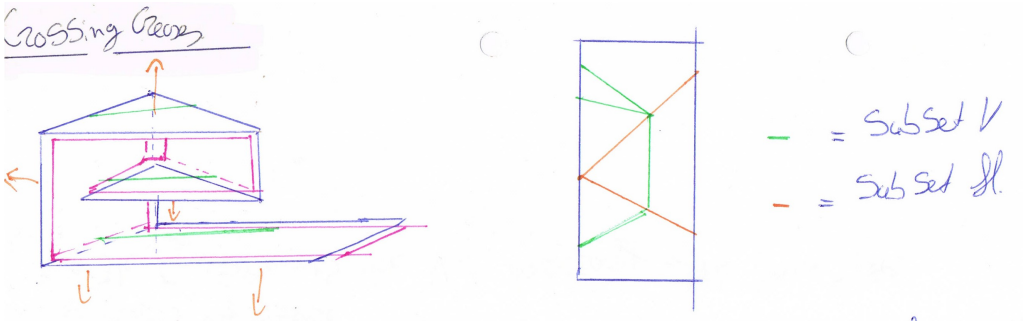

Figure E.1: Part of an unfolded strip accompanied with a schematic view of the folded state. Subset $\mathscr{H}$ is shown in orange and $\mathscr{V}$ is shown in green. Note: the orange arrows indicate the orientation of the sheet.

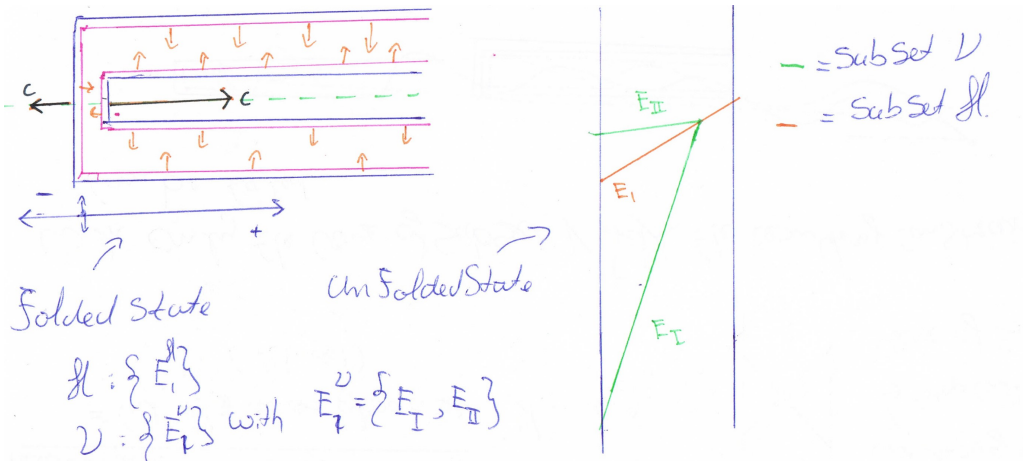

Figure E.2: Part of an unfolded strip accompanied with a schematic view of the folded state. Subset $\mathscr{H}$ is shown in orange and $\mathscr{V}$ is shown in green. The subsets are $\mathscr{H}$: $\{E_1\}$ and $\mathscr{V}$: $\{E_1^V\}$ with E_1^V : $\{E_I, E_{II}\}$. Note: the orange arrows indicate the orientation of the sheet.

the indexation number, previously called $index$.

$$\vec{n}_{m,i} = (-1)^{1+i} ||E_{m,i}|| \vec{n}_{m,1} \tag{E.1}$$

Although it is not validated yet, it is expected that also the secondary creases play a role in constraining subsets of $\mathscr{V}$. Further research should determine a correct formulation.

F

Stacking of sheets

Sheets can be constrained into the x,y-direction with folding. In order to constrain into the z-direction the sheets must be stacked, see section C. Note that from section C is known that when folded the degree of freedom of the z-direction is maintained. Due folding itself the sheets will remain sticky. The idea of stacking: keep track of the total number of layers, the more layers the stronger the stickiness will be.

F.1. Ordering by the literature

There are several ways to keep track of stacking following the literature. Stacking can relate to the order of faces (Following Schneider) or the "top" "bottom" determination between partial sheets which are on top of each other (Following Demaine and Rourke). Both methods will be discussed.

F.2. Following Schneider

The article "Flat-foldability of Origami Crease pattern" by J. Schneider [14] discusses the mathematics of flat polyhedral origami. The assumptions of the mathematical model differ from the physical physical model. The folded state with infinite thin sheets remains inside the $\mathbb{R}^2$ space. Due the infinite thin sheets, the stacking will not result into a mapping into the $\mathbb{R}^3$ space but into the integer space $\mathbb{Z}$. Summarizing, the folded space of flat polyhedral origami spans the $\mathbb{R}^2 \times \mathbb{Z}$-space[14].

To create a folded state there is "a *semifolding map* $\mu : C \to \mathbb{R}^2$ that determines only the final position of the paper in the plane, and a *superposition ordering* $\sigma : C \to \mathbb{Z}$ that determines only the overlap order of the layers"[14]. Schneider formulates a definition for superposition ordering in definition F.2.1. S-faces can be defined as identical faces. In folded state the S-faces will lay exactly on top of eachother.

Definition F.2.1. *"Let C be a semifoldable c-net. A superposition ordering $\sigma : C \to \mathbb{Z}$ is any map that acts as a constant on each S-face and has the following property: For every F-face F, the n s-faces in the set $\mu^{-1}(F)$ are mapped to distinct integers between 0 and $n-1$, inclusive". [14]*

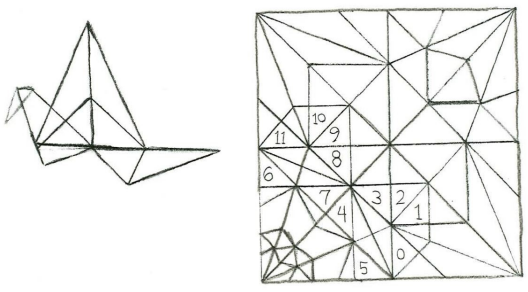

Figure F.1: Crane in unfolded state on the right and in folded state on the left. The identical faces are labeled analogous with σ and are part of the $\mathbb{Z}space$. Source: [14]

Definition F.2.1 is applied to figure F.1[14]. In figure F.1 eleven identical faces are shown and enumerated. The enumeration of the faces corresponds with the order of stacking of this specific S-face. For strip folding the f-faces are seldom identical. It is therefore difficult to adopt the definition of F.2.1. However, the main principle of using faces can be introduced in order to find the maximum number of layers within a folded crease pattern. The maximum number of layers on top each other is sufficient enough to say something about constraint of the rotation into the R_x and R_y direction.

An example of numbering faces for stripfolding is shown in figure F.2. In total there are fourteen faces, the majority of those face are unique. The faces (F) are defined with the edges (E) which can be either creases or raw-edges. In folded state the highest number of stacked layers can be found in a area composed of the intersection of the faces F_1, F_2, F_3, F_4, F_5, F_7, F_8. Accordingly, the number of stacked faces is equal to seven.

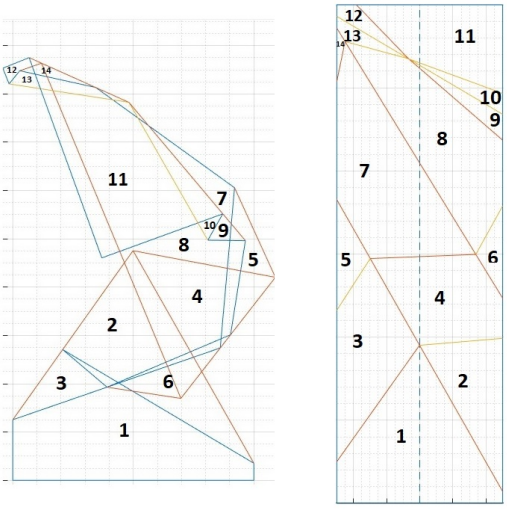

Figure F.2: A possible crease pattern for a strip. On the left a X-ray view of the strip in folded state and on the right in unfolded state. Each face numbered independently.

Definition F.2.2. *A set of faces, F_i, composes a crease pattern C. After a mapping, μ, into folded state the number of layers, L, can be determined by counting, n, the number of intersections of the faces. Mathematically:*

$$\bigcap_{i=0}^{n} F_i \quad for \quad F_i \cap F_{i+1} \neq 0 \quad \rightarrow \quad L = max(n) \qquad \text{(F.1)}$$

Note: This statement is only used in combination with opposite folding.

F.3. Following Demaine and Rourke.

Demain and Rourke [15] keep track of ordering with the orientation and points which lay on the same location. Their method is different from Schneider [14]. Schneider places the superposition ordering into the integer $\mathbb{Z}$-space. So, Schneider takes the total set of ordering of a identical S-faces while Demain and Rourke "consider the relative stacking order of collocated layers of paper"[15]. In section D.3 the method of Demain and Rourke is used in order to distinguish a whichlader from opposite folding. Therefore the method of Demaine and Rouke is futher elaborated in section D.3.

F.4. Algorithm

The final algorithm will use the approach of Schneider. The folded state is calculated with the use of creases instead of faces. Therefore the algorithm is accompanied with the piece of code to recompose the faces from the vertices in folded state.

G

Validation of the mathematical method

G.1. Introduction

This experiment has as goal to verify the projection method. The projection method should be a useful tool for determining where to place folds. The verification of the projection method can be divided into two separated objectives. First, is the crease pattern constraint as expected? Secondly, are the crease pattern constraints in portion?

Both objectives are achieved within the same experiment. The experiment has the following layout; two sheets are folded into each other. One sheet is fixed to the ground. The second sheet is moved. This relates to the objectives into the following way. If the second sheet can not move into a certain direction then it is constraint in that direction. For the second objective, the proportion between the constraints will be found by the determining the deformation of the crease pattern into a certain direction.

To have a reliable result, the projection method will only be validated for subset $\mathscr{H}$. Subset $\mathscr{H}$ has for each crease one single constraint into one single direction, which makes it more convenient to verify.

G.2. Hypothesis

There are seven creases in total. The crease pattern differ in number of creases and whether they are part of opposite folding or not. All creases are shown in figure G.1.

For each crease pattern from figure G.1 the constraints are calculated. For the calculation the function "total_constraint_of_creases" from the optimization algorithm is used. The width of the strip is set to be 2 and its length to be 6. The crease patterns of figure G.1 can be defined with the following variables; Note that the algorithm excepts only crease patterns with at least two creases. Crease pattern A is

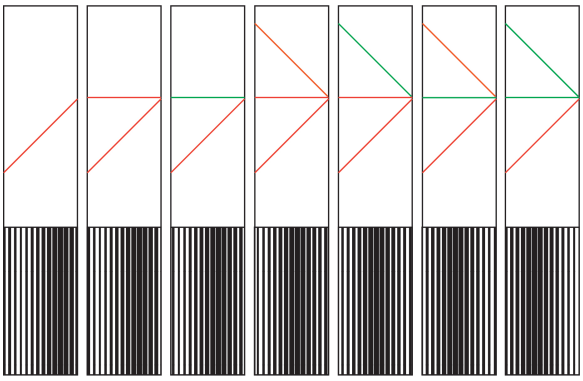

Figure G.1: The used strips for the experiment. Ordered alphabetically from left to right. A red line represents opposite folding and a green line represents a which ladder.

calculated by hand.

Crease A: $x_H = \begin{bmatrix} 3 & -\pi/4 & 1 \end{bmatrix}$

Crease B: $x_H = \begin{bmatrix} 3 & 1 & -\pi/4 & 0 & 1 & 1 \end{bmatrix}$

Crease C: $x_H = \begin{bmatrix} 3 & 1 & -\pi/4 & 0 & 1 & 0 \end{bmatrix}$

Crease D: $x_H = \begin{bmatrix} 3 & 1 & 1 & -\pi/4 & 0 & \pi/4 & 1 & 1 & 1 \end{bmatrix}$

Crease E: $x_H = \begin{bmatrix} 3 & 1 & 1 & -\pi/4 & 0 & \pi/4 & 1 & 1 & 0 \end{bmatrix}$

Crease F: $x_H = \begin{bmatrix} 3 & 1 & 1 & -\pi/4 & 0 & \pi/4 & 1 & 0 & 0 \end{bmatrix}$

Crease G: $x_H = \begin{bmatrix} 3 & 1 & 1 & -\pi/4 & 0 & \pi/4 & 1 & 0 & 1 \end{bmatrix}$

Table G.1 shows the hypothesis for objective one into all directions. Objective one determines if the sheets are constraint into a certain direction. A constraint into a direction is represented with a "yes", if the sheets are not constraint then a "no" is shown in the table. Table G.1 refers to objective one of the experiment.

Table G.2 shows the hypothesis for objective two for each direction. Objective two involves the proportion of the constraints within a crease pattern. A constraint into a direction is represented with a value, if the sheets are not constraint then a value zero is shown in the table. Table G.2 refers to objective two of the experiment.

Direction	Creases						
	A	B	C	D	E	F	G
x^+	no	yes	no	yes	yes	yes	no
x^-	yes	yes	yes	yes	yes	yes	yes
y^+	yes	yes	yes	yes	yes	yes	yes
y^-	no	no	no	yes	yes	yes	no

Table G.1: The expected constraints in the directions x^+, x^-, y^+, y^- for each crease pattern. If the crease pattern is constraint then a "yes" is shown or else a "no". This table refers to objective one. *Note, this table includes the secondary constraints. The discussion is written without the knowledge of the secondary constraints and has therefore has different table.*

Direction	Creases						
	A	B	C	D	E	F	G
x^+	0	2	0	4	4	4	0
x^-	2	2	4	4	2	4	6
y^+	2	2	2	4	2	2	4
y^-	0	0	0	2	2	4	0

Table G.2: The expected constraints in the directions x^+, x^-, y^+ and y^- for each crease pattern. If the crease pattern is constraint then a "yes" is shown or else a "no". This table refers to objective one. *Note, this table includes the secondary constraints. The discussion is written without the knowledge of the secondary constraints and has therefore has different table.*

G.3. Method

The hypotheses are tested in practice. Both objective one and two are checked in one experiment. In this experiment one sheet is fixed to the ground and one sheet is attached to the linear stage. Both sheets are folded into each other with the crease patterns shown in figure G.1. A constraint within the crease pattern can be seen as a resistance against deformation. It is sufficient for objective one to determine if there is resistance against movement or not. However for objective two the resistance should be quantified.

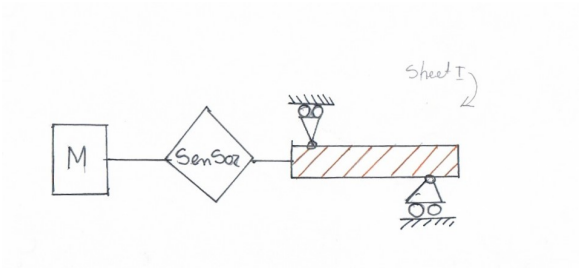

Figure G.2: Schematic overview of the experimental setup.

To quantify the constraints the resistance against deformation is measured. The measurement is taken with a "PI Stage Tensile test" which is able to measure the displacement and the needed force if a sensor is attached. Figure G.2 gives a schematic overview of the experimental setup. The sheet I is shown with a obliquely striped square. Sheet I can only move into one direction, x or y, and is constraint for every other. The sheet is attached to the sensor, which is connected to the linear stage.

The figures G.3, G.4, G.5, G.6 and G.7 show the experimental setup in real life. Sheet I is attached to a moving template while sheet II is fixed with two bolts. The linear bearings align the seet I with the linear stage and prevents movement of all other directions. The setup can be orientated in two different directions, x and y as can be seen in figure G.4 and G.5. This makes it possible to measure into the x and y-direction. In total, all measurements are measured five times.

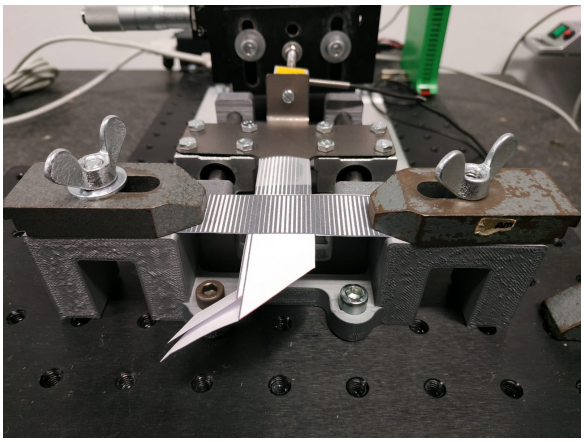

Figure G.3: Front view of the experimental setup.

The figures G.8 and G.9 show the used sensor. The FSH00104 Futek sensor for 10 lbs is used. It has a full scale accuracy of -0.1 to$0.1 \pm$ % [40]. The measurements are taken in Newtons (N) and the displacements in μm.

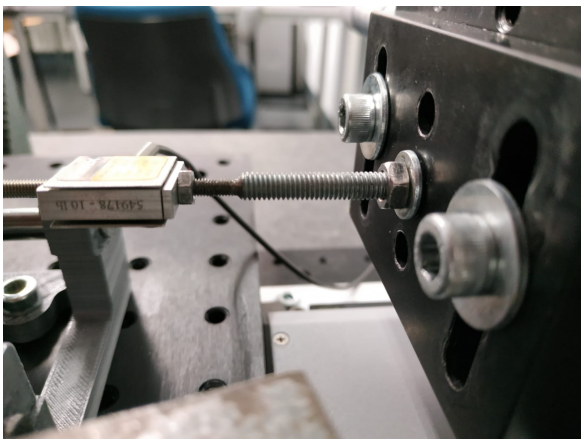

Figure G.9: Side view of the sensor

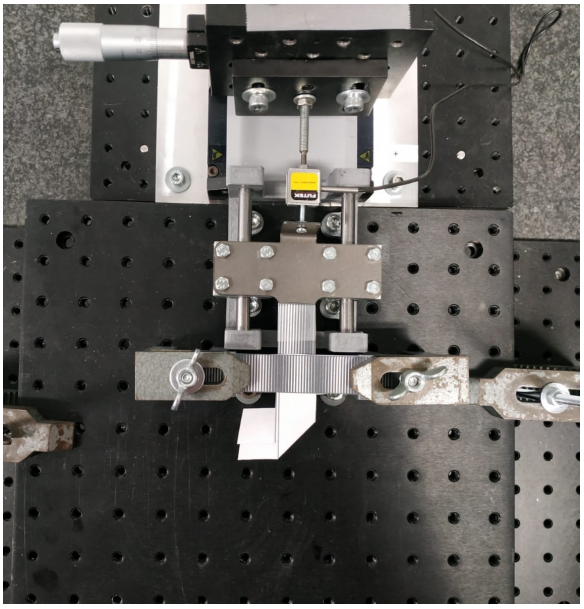

Figure G.4: Top figure of the experimental setup for the y-direction.

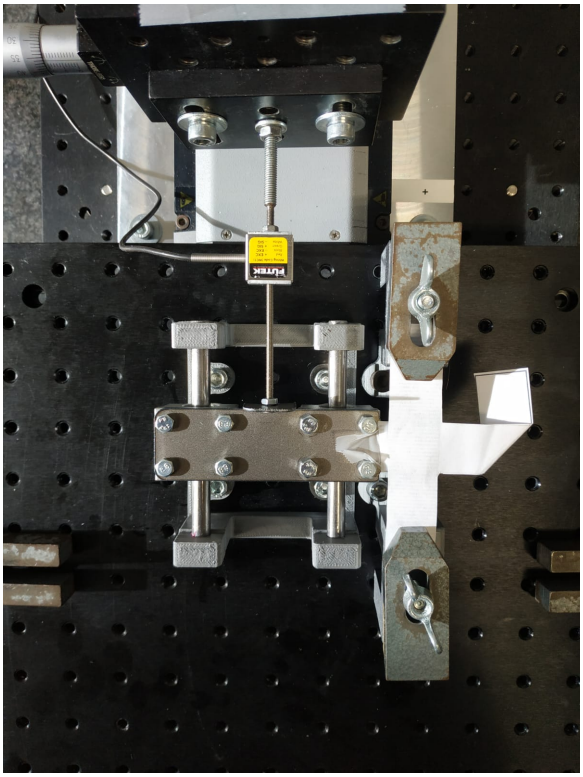

Figure G.5: Top figure of the experimental setup for the x-direction.

For some measurements the deformation did not happen on the crease but on on a different location, often at the base of the strip, see figure G.10. If the deformation happens on the wrong location the strip can even tear instead of unfolding. In order to prevent this problem a second template will be used if needed, see figure G.11. The second template will support the fixed sheet (II). If the second template is used, then this will be indicated in the results.

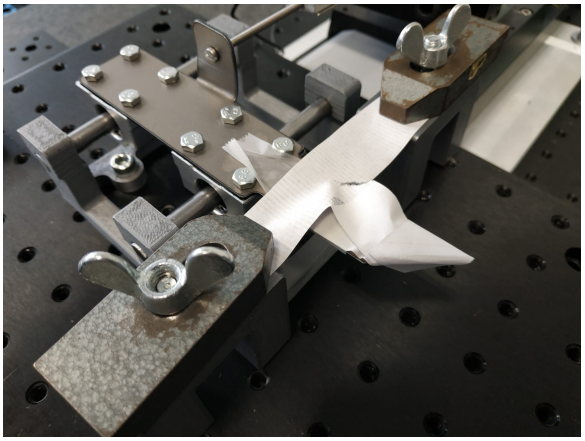

Figure G.10: A deformation strip is deforming in the wrong location. The crease pattern is also tearing apart instead of unfolding.

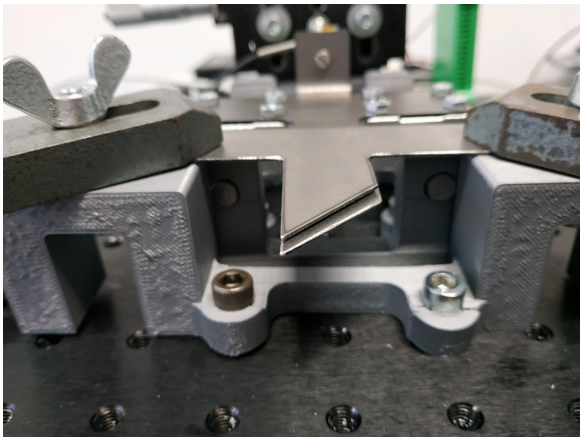

Figure G.11: Experimental setup with two templates. This setup is only used if deformation occurs in the wrong place. The crease pattern is not unfolding.

G.4. Implementation

The raw data will be plotted in order to check if all data is correct. The measurements are taken in Newtons (N) and the displacements in μm, the data will be plotted with these quantities. In order to find the peaks with the inbuilt Matlab function "findpeaks", the absolute value is taken and squared. With this approach the peaks within the data-set will be enlarged which makes it easier to find them. The manipulated date will also be plotted.

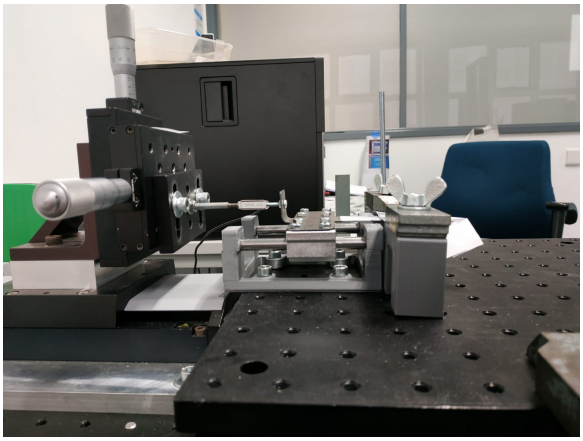

Figure G.6: Side view of the experimental setup.

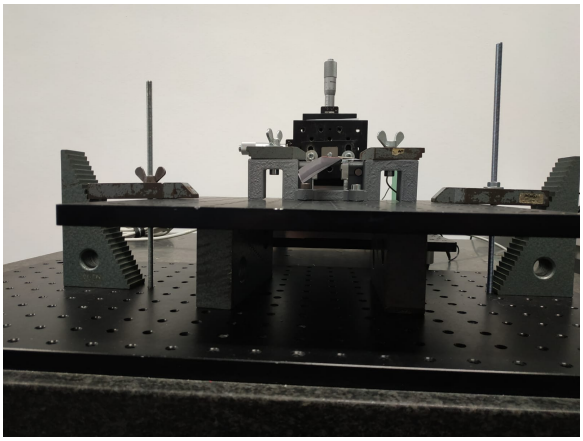

Figure G.7: The front view including the the fixation of the platform

The average and the deviation of the peaks from the raw data will be determined. With this information a conclusion will be drawn from the hypothesis.

G.5. Results

This section includes the data of the clean measurements and the individual creases.

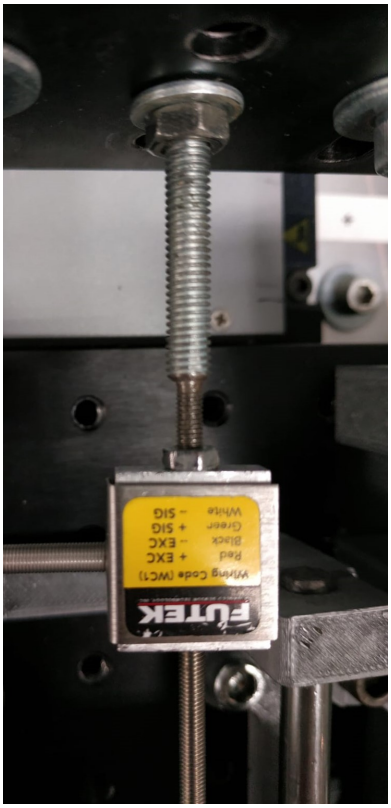

Figure G.8: Top view of the sensor.

G.5.1. Clean measurement

The clean measurement is a measurement without any sheets. The measurement reveals information about the friction of the system. This information will be used as a threshold if something is constraint or not. The raw data of the clean measurement is shown in figures G.1, G.2, G.3 and G.4. The manipulated data are also shown below. There are 1200 data points for a distance of 8000 μ m. The found peaks are shown in table G.3.

Direction	Mean value	Standard Deviation
x^+	-0.62360	0.0705216278881876
x^-	-0.19660	0.313464990070662
y^+	-0.52400	0.0589364064055487
y^-	0.41080	0.0566718625068914

Table G.3: Clean measurement; The mean value peak values from the measurements accompanied by the Standard Deviation.

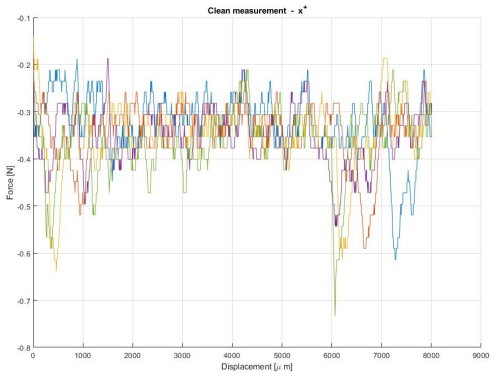

Plot G.1: Clean measurement with no sheets: Raw data into the x^+ direction. Vertical axis, force N. Horizontal axis, displacement μm.

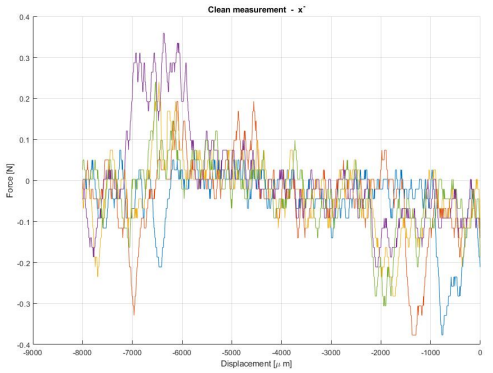

Plot G.2: Clean measurement with no sheets: Raw data into the x^- direction. Vertical axis, force N. Horizontal axis, displacement μm

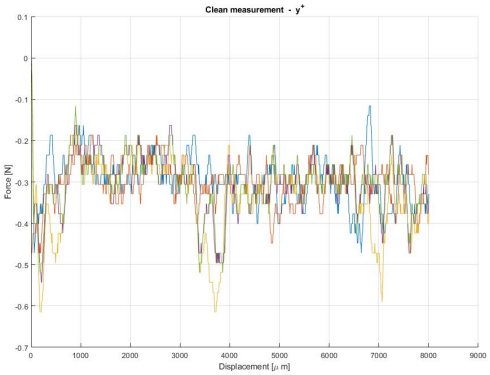

Plot G.3: Clean measurement with no sheets: Raw data into the y^+ direction. Vertical axis, force N. Horizontal axis, displacement μm.

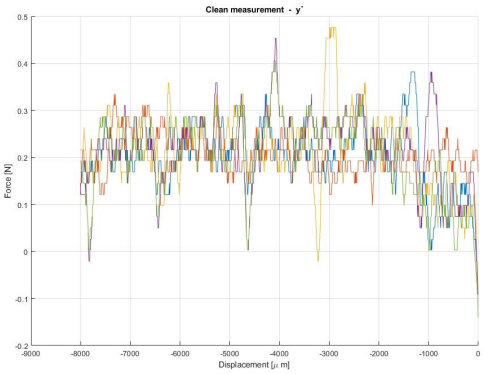

Plot G.4: Clean measurement with no sheets: Raw data into the y^- direction. Vertical axis, force N. Horizontal axis, displacement μm

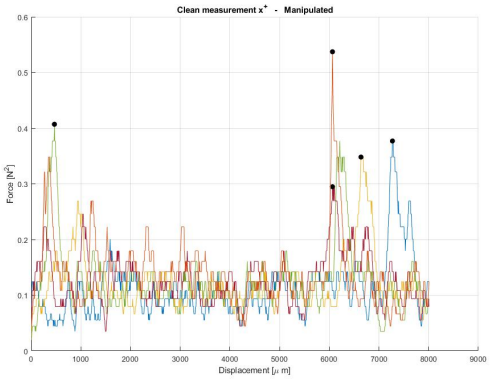

Plot G.5: Clean measurement with no sheets: Manipulated data into the x^+ direction. Vertical axis, force N. Horizontal axis, displacement μm.

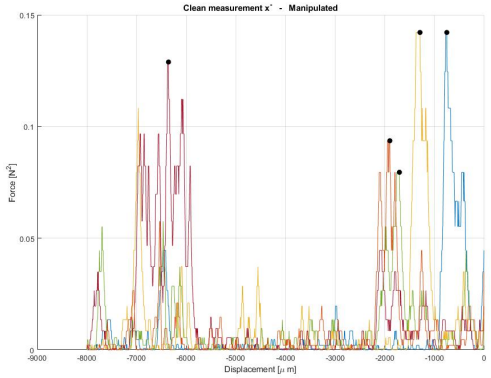

Plot G.6: Clean measurement with no sheets: Manipulated data into the x^- direction. Vertical axis, force N. Horizontal axis, displacement μm

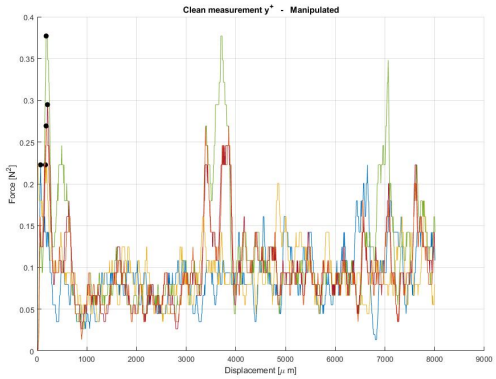

Plot G.7: Clean measurement with no sheets: Manipulated data into the y^+ direction. Vertical axis, force N. Horizontal axis, displacement μm.

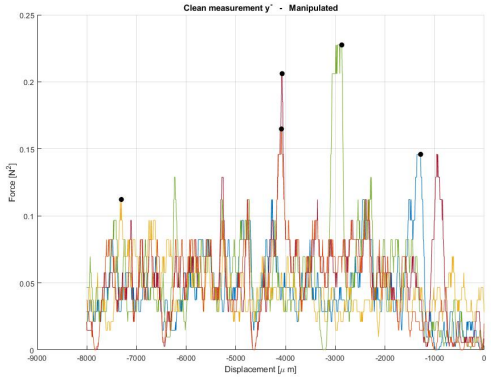

Plot G.8: Clean measurement with no sheets: Manipulated data into the y^- direction. Vertical axis, force N. Horizontal axis, displacement μm

G.5.2. Crease A

Crease Pattern A consist of one single fold; opposite folding.

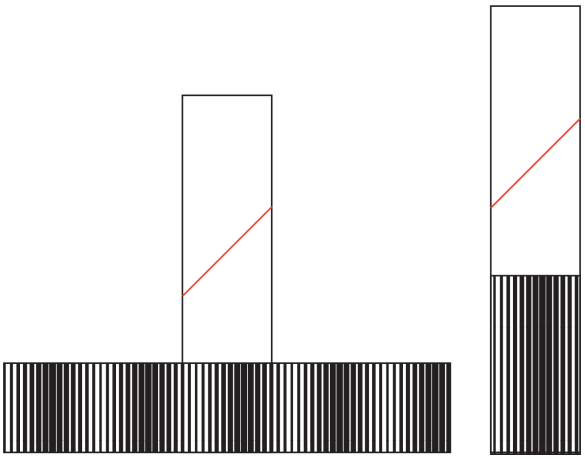

Plot G.9: Crease pattern A: top and bottom sheet. Opposite folding is indicated with the red line. Which ladder is indicated with a green line.

For both x-directions there are 1200 data points for a distance of 8000 μ m. The y^--direction has 1000 data points for a distance of 6000 μ m. And the y^+-direction has 1000 data points for a distance of 12 000 μ m. The found peaks are shown in table G.4. The graphs of the raw data and the manipulated data are shown below.

Direction	Mean value	Standard Deviation
x^+	-1.20180	0.121590295665403
x^-	0.56520	0.238727250225021
y^+	-0.90380	0.122609950656543
y^-	0.43460	0.102524631186852

Table G.4: Crease A; The mean value peak values from the measurements accompanied by the Standard Deviation.

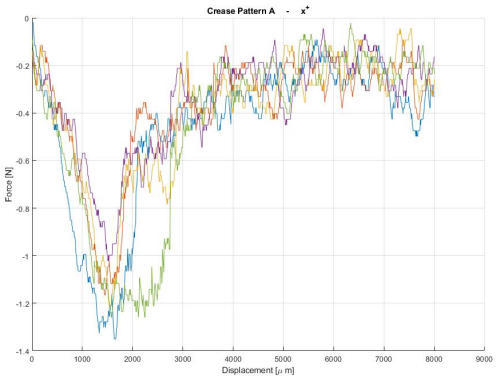

Plot G.10: Crease pattern A: Raw data into the x^+ direction. Vertical axis, force N. Horizontal axis, displacement μm.

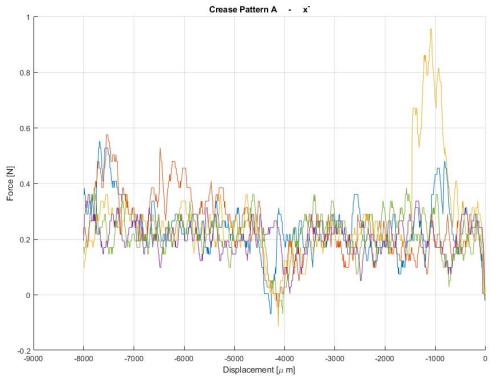

Plot G.11: Crease pattern A: Raw data into the x^- direction. Vertical axis, force N. Horizontal axis, displacement μm

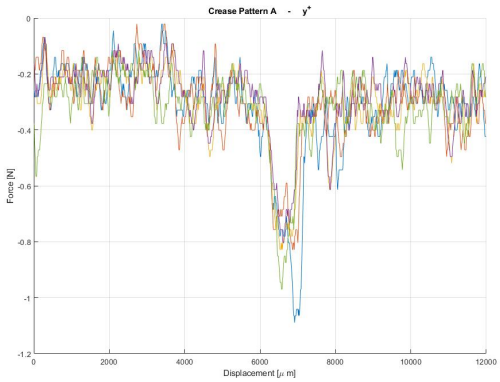

Plot G.12: Crease pattern A: Raw data into the y^+ direction. Vertical axis, force N. Horizontal axis, displacement μm.

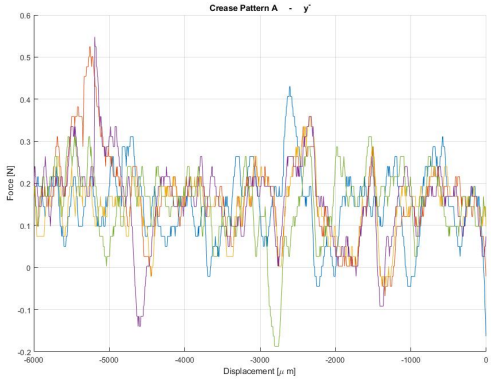

Plot G.13: Crease pattern A: Raw data into the y^- direction. Vertical axis, force N. Horizontal axis, displacement μm.

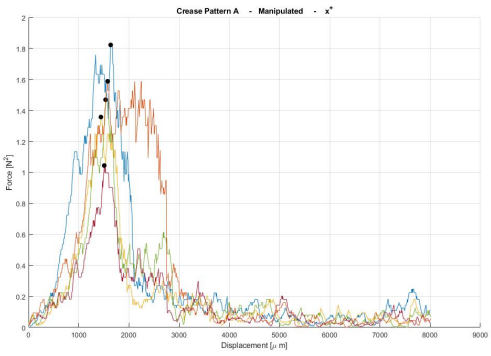

Plot G.14: Crease pattern A: Manipulated data into the x^+ direction. Vertical axis, force N. Horizontal axis, displacement μm.

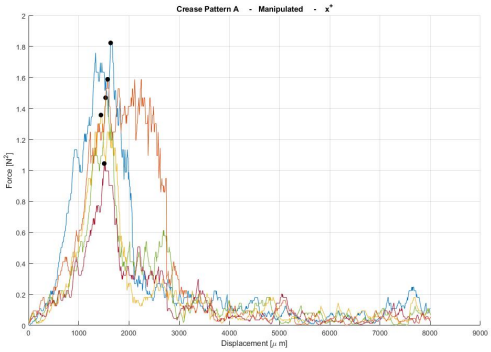

Plot G.15: Crease pattern A: Manipulated data into the x^- direction. Vertical axis, force N. Horizontal axis, displacement μm

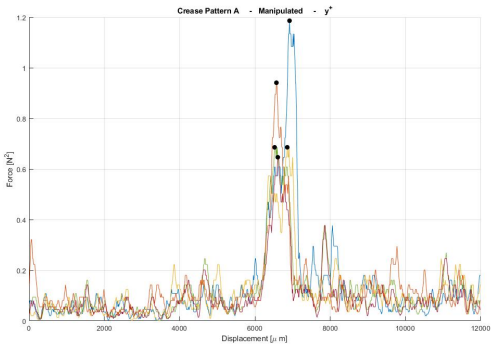

Plot G.16: Crease pattern A: Manipulated data into the y^+ direction. Vertical axis, force N. Horizontal axis, displacement μm.

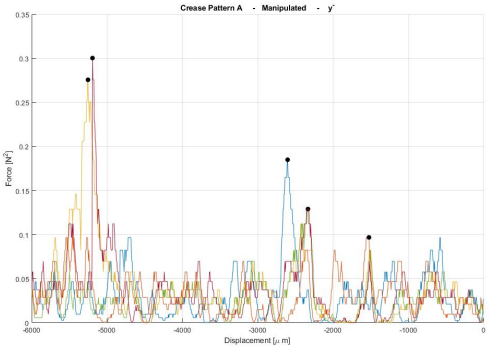

Plot G.17: Crease pattern A: Manipulated data into the y^- direction. Vertical axis, force N. Horizontal axis, displacement μm.

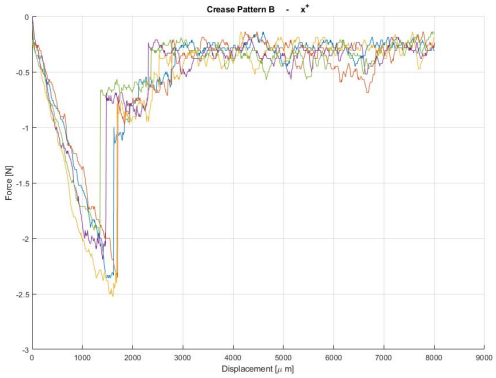

Plot G.18: Crease pattern B: Raw data into the x^+ direction. Vertical axis, force N. Horizontal axis, displacement μm.

G.5.3. Crease B

Crease Pattern B consist of two folds both of opposite folding.

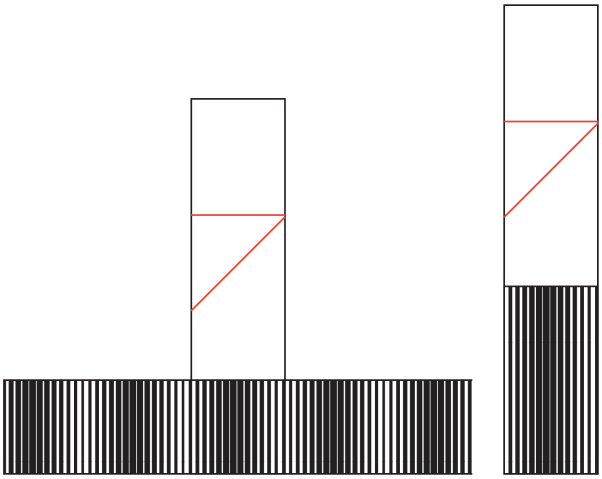

Figure G.12: Crease pattern B, top and bottom sheet. Opposite folding is indicated with the red line. Which ladder is indicated with a green line.

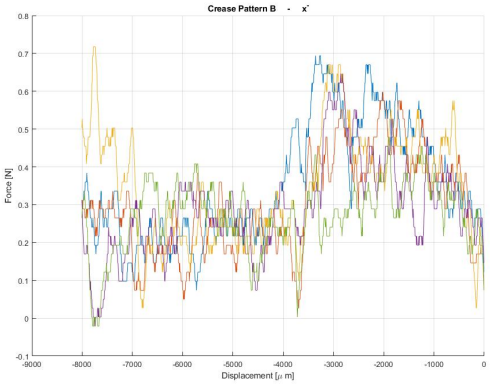

Plot G.19: Crease pattern B: Raw data into the x^- direction. Vertical axis, force N. Horizontal axis, displacement μm.

For both x-directions there are 1200 data points for a distance of 8000 μ m. The y^--direction has 1000 data points for a distance of 6000 μ m. And the y^+-direction has 1000 data points for a distance of 12 000 μ m. The found peaks are shown in table G.5.The graphs of the raw data and the manipulated data are shown below.

Direction	Mean value	Standard Deviation
x^+	-2.27980	0.207308224631827
x^-	0.62700	0.094704804524375
y^+	-1.18360	0.130733698792622
y^-	0.364750	0.091765552723594

Table G.5: Crease B; The mean value peak values from the measurements accompanied by the Standard Deviation.

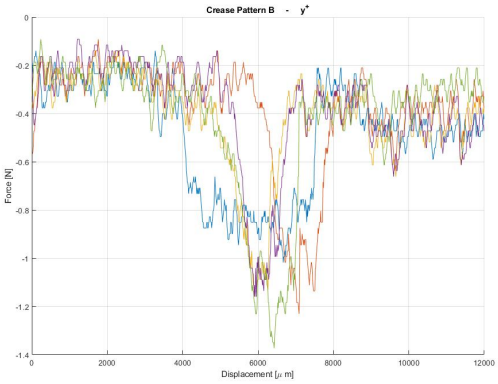

Plot G.20: Crease pattern B: Raw data into the y^+ direction. Vertical axis, force N. Horizontal axis, displacement μm.

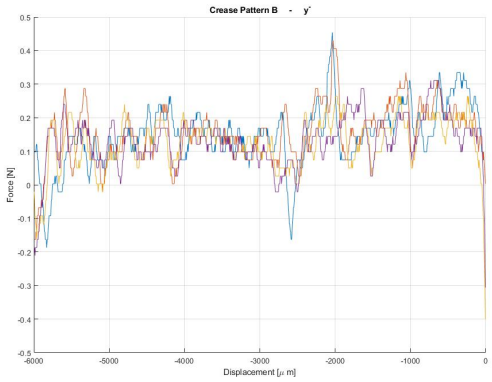

Plot G.21: Crease pattern B: Raw data into the y^- direction. Vertical axis, force N. Horizontal axis, displacement μm.

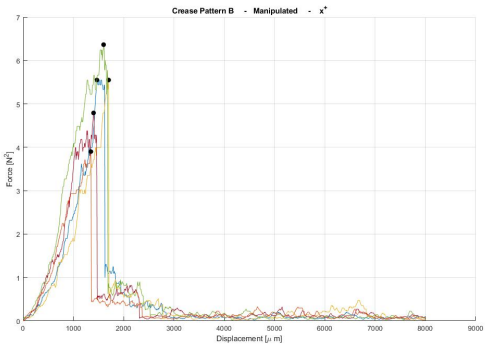

Plot G.22: Crease pattern B: Manipulated data into the x^+ direction. Vertical axis, force N. Horizontal axis, displacement μm.

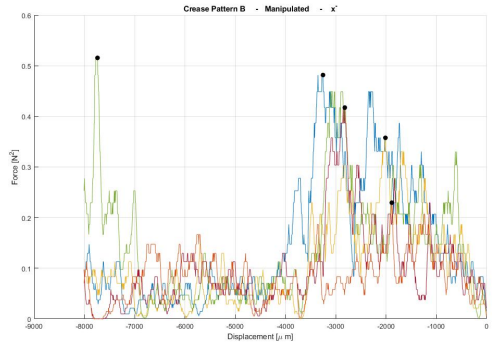

Plot G.23: Crease pattern B: Manipulated data into the x^- direction. Vertical axis, force N. Horizontal axis, displacement μm

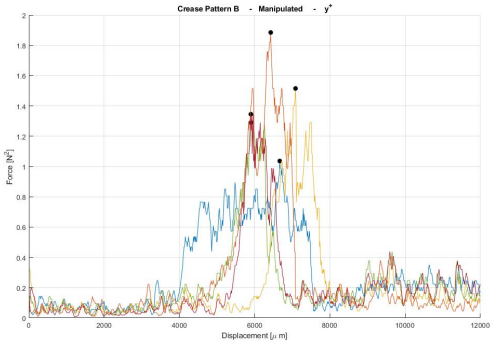

Plot G.24: Crease pattern B: Manipulated data into the y^+ direction. Vertical axis, force N. Horizontal axis, displacement μm.

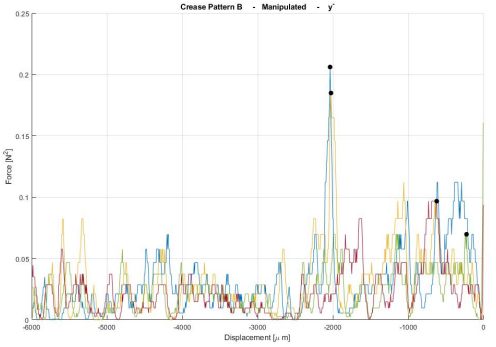

Plot G.25: Crease pattern B: Manipulated data into the y^- direction. Vertical axis, force N. Horizontal axis, displacement μm.

G.5.4. Crease C

Crease Pattern C consist of two folds one of opposite folding and one not.

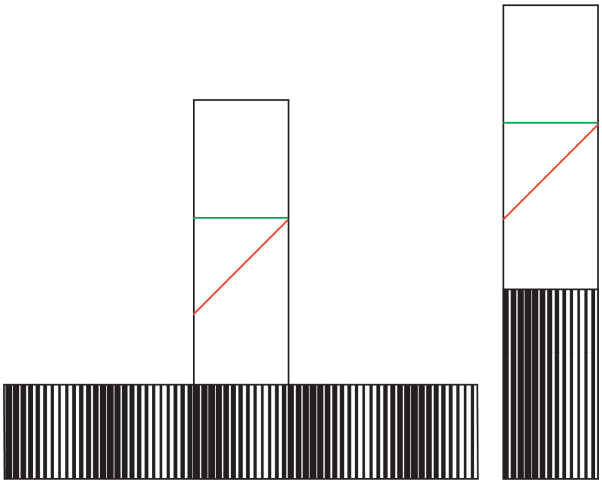

Figure G.13: Crease pattern C, top and bottom sheet. Opposite folding is indicated with the red line. Which ladder is indicated with a green line.

The measurement of the raw data of figure G.26 seems to be with one more then expected, for every direction there should be five measurements. This figure include six measurements. Due the initial absence of the x^--direction the light blue measurement from figure G.26 is probably part of the x^--direction. Therefore this measurement is ignored in the manipulated data.
Figure G.29, the raw data into the y^--direction, has once again six measurements where there should be five. There is one clearly deviating measurement which has a offset of 0.5 and is shown with a dark red line. This measurement is deleted from the set for the manipulated data.

For both x-directions there are 1200 data points for a distance of 8000 μ m. The y^--direction has 1000 data points for a distance of 6000 μ m. And the y^+-direction has 1000 data points for a distance of 12000 μ m.The found peaks are shown in table G.6.The graphs of the raw data and the manipulated data are shown below.

Direction	Mean value	Standard Deviation
x^+	-1.00280	0.114924757994089
x^-	0.52700	0.102588985763580
y^+	-1.207250	0.196664477388945
y^-	0.4573	0.372431291202373

Table G.6: Crease C; The mean value peak values from the measurements accompanied by the Standard Deviation.

Plot G.26: Crease pattern C: Raw data into the x^+ direction. Vertical axis, force N. Horizontal axis, displacement μm.

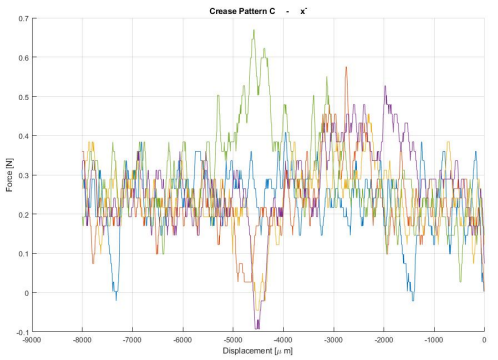

Plot G.27: Crease pattern C: Raw data into the x^- direction. Vertical axis, force N. Horizontal axis, displacement μm.

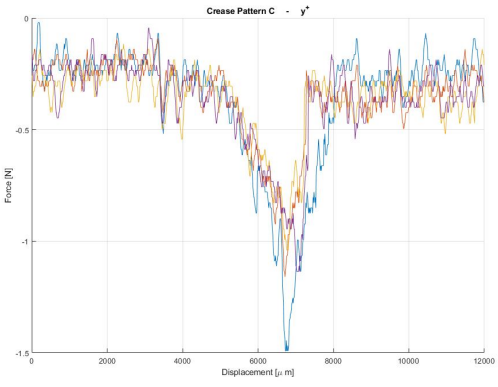

Plot G.28: Crease pattern C: Raw data into the y^+ direction. Vertical axis, force N. Horizontal axis, displacement μm.

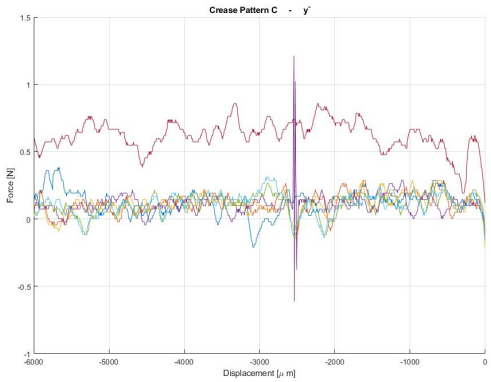

Plot G.29: Crease pattern C: Raw data into the y^- direction. Vertical axis, force N. Horizontal axis, displacement μm.

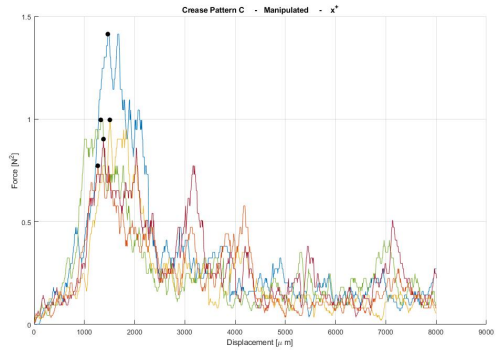

Plot G.30: Crease pattern C: Manipulated data into the x^+ direction. Vertical axis, force N. Horizontal axis, displacement μm.

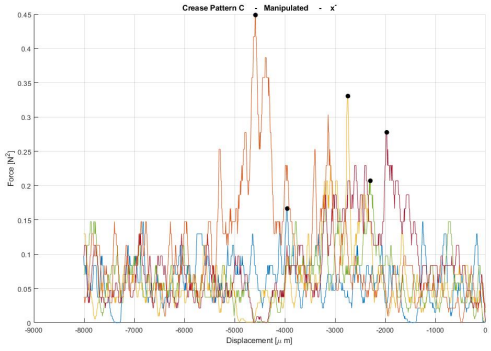

Plot G.31: Crease pattern C: Manipulated data into the x^- direction. Vertical axis, force N. Horizontal axis, displacement μm

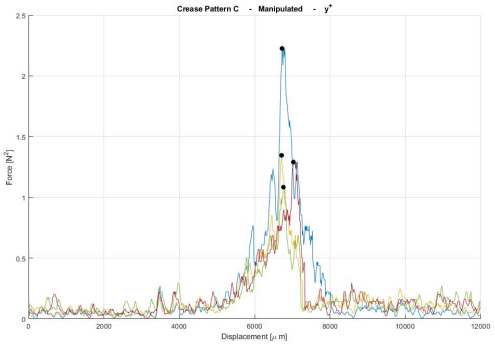

Plot G.32: Crease pattern C: Manipulated data into the y^+ direction. Vertical axis, force N. Horizontal axis, displacement μm.

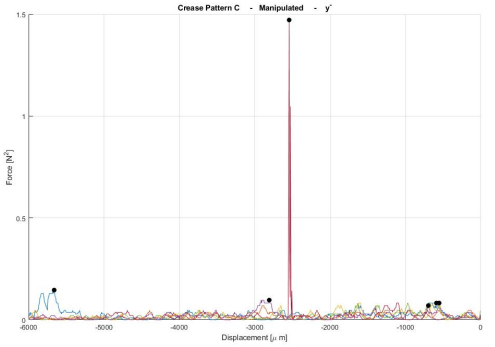

Plot G.33: Crease pattern C: Manipulated data into the y^- direction. Vertical axis, force N. Horizontal axis, displacement μm.

G.5.5. Crease D

Crease Pattern D consist of three folds all are part of opposite folding.

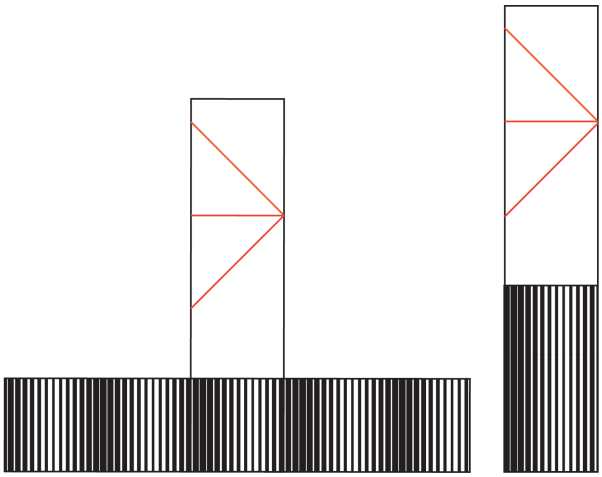

Figure G.14: Crease pattern D, top and bottom sheet. Opposite folding is indicated with the red line. Which ladder is indicated with a green line.

Crease pattern D has deformation near the bottom of the strip. In order to prevent deformation an additional template is used.

The measurements from the rawdata of figure G.34 shown in yellow and dark blue are removed from the complete data set. Due to the downwards trend it is clear that this data is corrupted. Also due the fact that there at most five measurements the yellow and dark blue measurements are not part of this measurement. Because these measurements are labeled as crease D, they are shown in figure G.34.
The plot with the rawdata into the x^-, figure G.35, shows has a different offset per measurement. The entire measurement of x^- needs to be redone.

For both the x-directions there are 1500 data points for a distance of 10 000 μ m. And for both the y-directions there are 1200 data points for a distance of 8000 μ m.The found peaks are shown in table G.7. The graphs of the raw data and the manipulated data are shown below.

Direction	Mean value	Standard Deviation
x^+	-2.51225	0.161755731480114
x^-	1.71725	0.573052280919173
y^+	-8.3768	2.073707927039550
y^-	0.78580	0.179714217578911

Table G.7: Crease D; The mean value peak values from the measurements accompanied by the Standard Deviation.

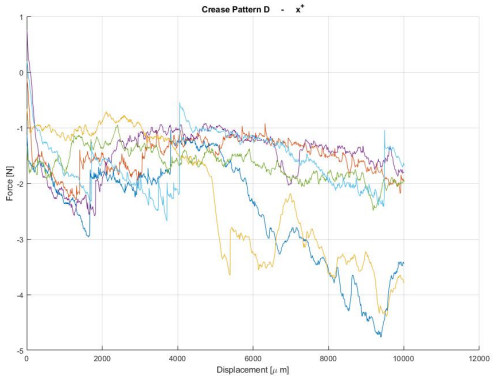

Plot G.34: Crease pattern D: Raw data into the x^+ direction. Vertical axis, force N. Horizontal axis, displacement μm.

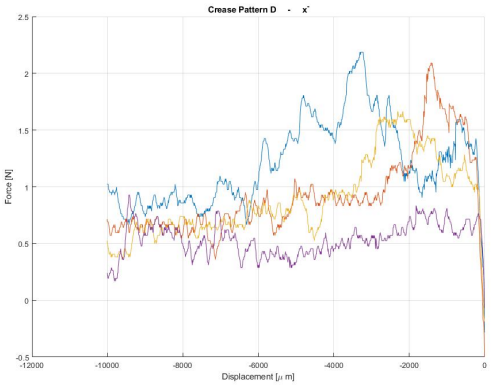

Plot G.35: Crease pattern D: Raw data into the x^- direction. Vertical axis, force N. Horizontal axis, displacement μm.

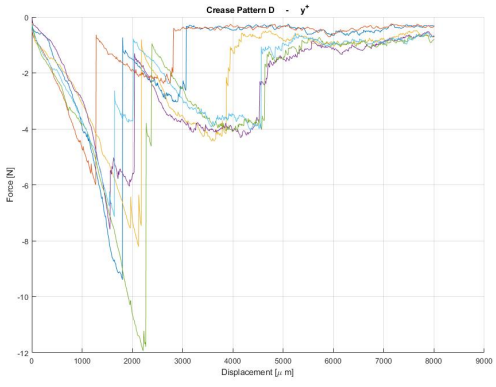

Plot G.36: Crease pattern D: Raw data into the y^+ direction. Vertical axis, force N. Horizontal axis, displacement μm.

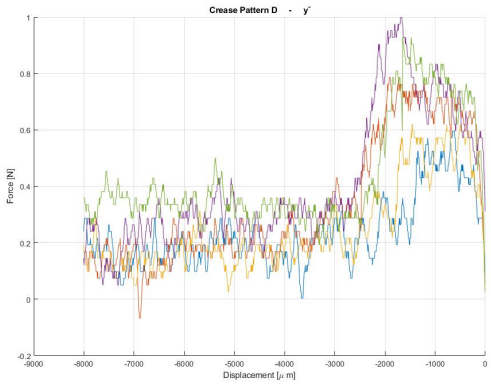

Plot G.37: Crease pattern D: Raw data into the y^- direction. Vertical axis, force N. Horizontal axis, displacement μm.

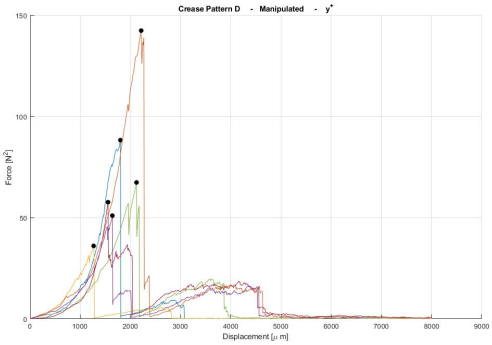

Plot G.40: Crease pattern D: Manipulated data into the y^+ direction. Vertical axis, force N. Horizontal axis, displacement μm.

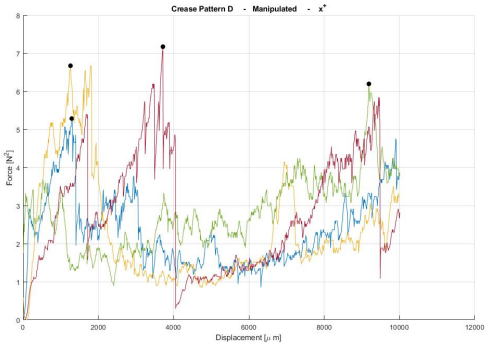

Plot G.38: Crease pattern D: Manipulated data into the x^+ direction. Vertical axis, force N. Horizontal axis, displacement μm.

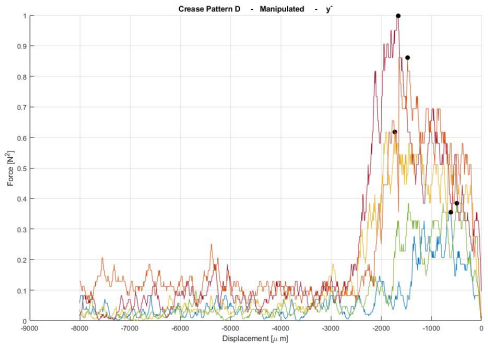

Plot G.41: Crease pattern D: Manipulated data into the y^- direction. Vertical axis, force N. Horizontal axis, displacement μm.

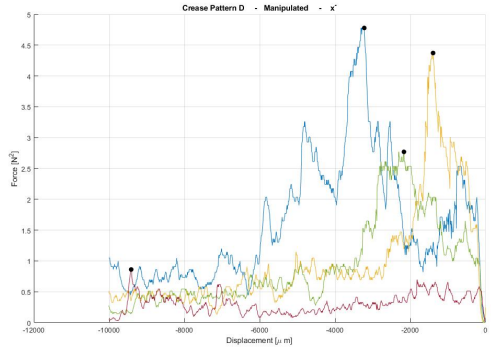

Plot G.39: Crease pattern D: Manipulated data into the x^- direction. Vertical axis, force N. Horizontal axis, displacement μm

G.5.6. Crease E

Crease Pattern E consist of three folds two of opposite folding and the final not.

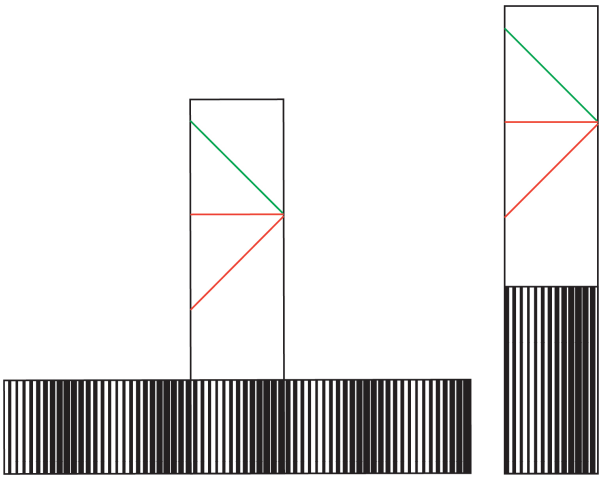

Figure G.15: Crease pattern E, top and bottom sheet. Opposite folding is indicated with the red line. Which ladder is indicated with a green line.

Crease pattern E consist of two creases of opposite folding (red) and a final crease which is not (green). For the measurement it is preferred to have all the creases inside a single plane. Two templates where needed to take the measurements, due to the deformation near the bottom of the strip. The final crease, the whichlader, is not folded around the base but tends to pop out into the 3D world. While being into the 3D world it did not seem possible to have a viable measurement. Concluding, the crease pattern E will be neglected in this experiment.

G.5.7. Crease F

Crease Pattern F consist of three folds, the first and final is part of opposite folding, the middle not.

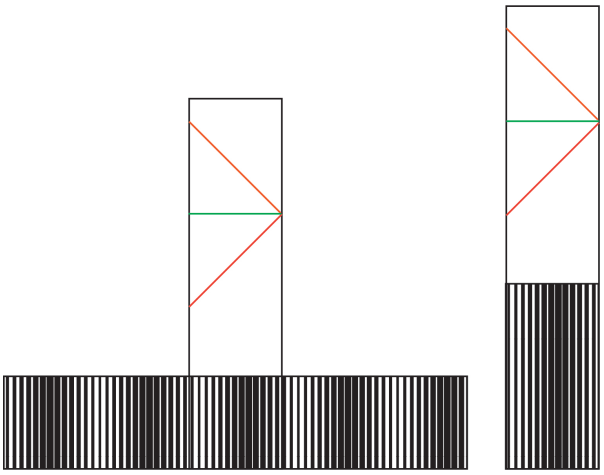

Figure G.16: Crease pattern F, top and bottom sheet. Opposite folding is indicated with the red line. Which ladder is indicated with a green line.

For all measurements there are 1200 data points for a distance of 8000 μ m. The found peaks are shown in table G.8. The graphs of the raw data and the manipulated data are shown below.

Direction	Mean value	Standard Deviation
x^+	-0.85150	0.092702031621031
x^-	0.52940	0.065824007778317
y^+	-1.12033	0.133036335888609
y^-	0.62420	0.0389191469587914

Table G.8: Crease F; The mean value peak values from the measurements accompanied by the Standard Deviation.

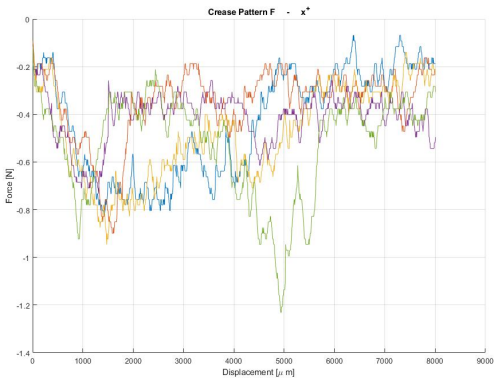

Plot G.42: Crease pattern F: Raw data into the x^+ direction. Vertical axis, force N. Horizontal axis, displacement μm.

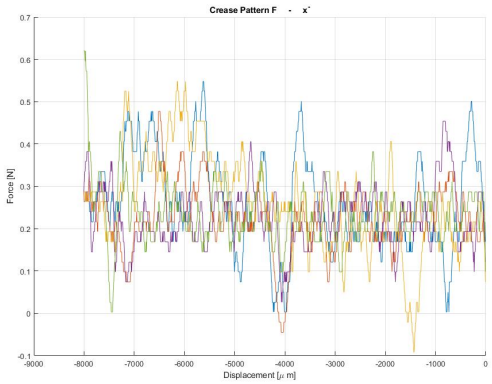

Plot G.43: Crease pattern F: Raw data into the x^- direction. Vertical axis, force N. Horizontal axis, displacement μm.

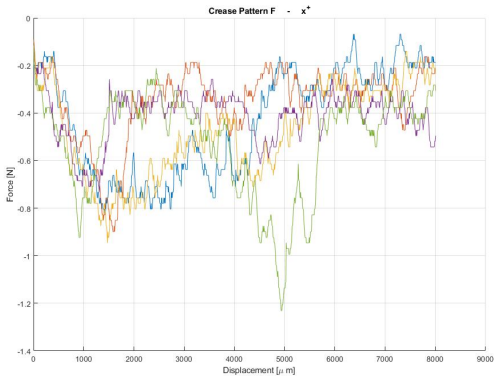

Plot G.44: Crease pattern F: Raw data into the x^+ direction. Vertical axis, force N. Horizontal axis, displacement μm.

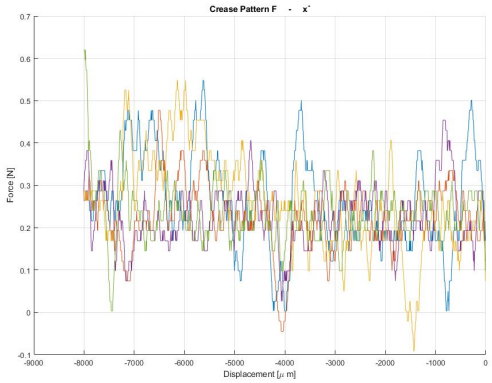

Plot G.45: Crease pattern F: Raw data into the x^- direction. Vertical axis, force N. Horizontal axis, displacement μm.

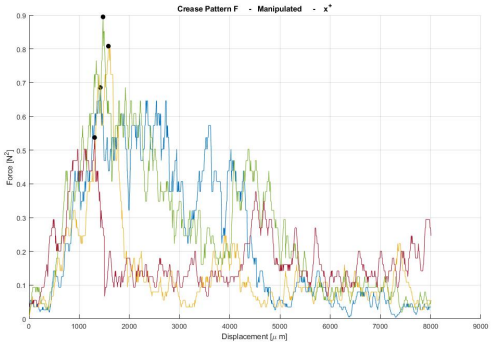

Plot G.46: Crease pattern F: Manipulated data into the x^+ direction. Vertical axis, force N. Horizontal axis, displacement μm.

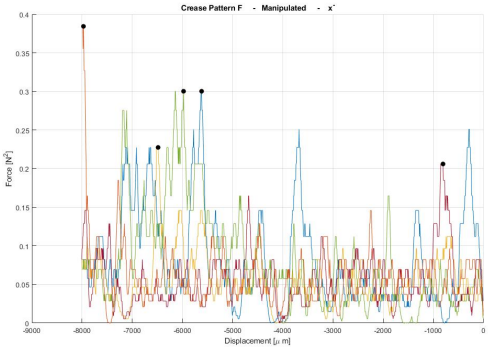

Plot G.47: Crease pattern F: Manipulated data into the x^- direction. Vertical axis, force N. Horizontal axis, displacement μm.

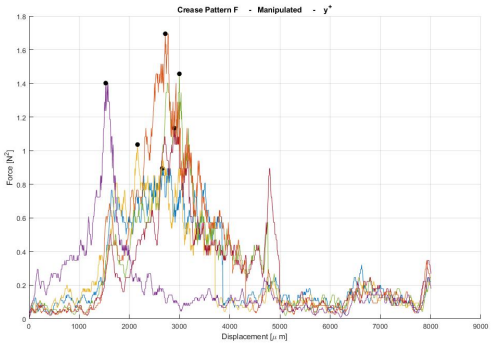

Plot G.48: Crease pattern F: Manipulated data into the y^+ direction. Vertical axis, force N. Horizontal axis, displacement μm.

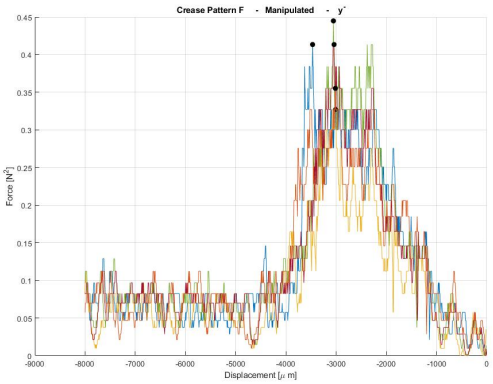

Plot G.49: Crease pattern F: Manipulated data into the y^- direction. Vertical axis, force N. Horizontal axis, displacement μm.

G.5.8. Crease G

Crease Pattern G consist of three folds, the first is part of opposite folding the other two are not.

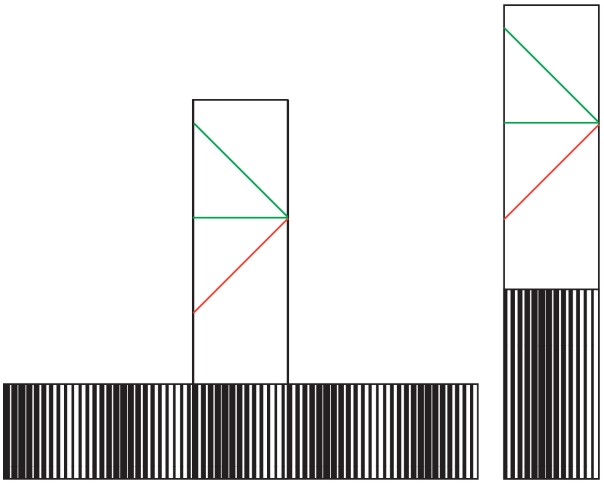

Figure G.17: Crease pattern G, top and bottom sheet. Opposite folding is indicated with the red line. Which ladder is indicated with a green line.

For all measurements there are 1200 data points for a distance of 8000 μ m. The found peaks are shown in table **??**. The graphs of the raw data and the manipulated data are shown below.

Direction	Mean value	Standard Deviation
x^+	-1.14080	0.166714426490331
x^-	0.62220	0.094043606906584
y^+	-0.79960	0.229091248195997
y^-	0.34920	0.086745028676000

Table G.9: Crease G; The mean value peak values from the measurements accompanied by the Standard Deviation.

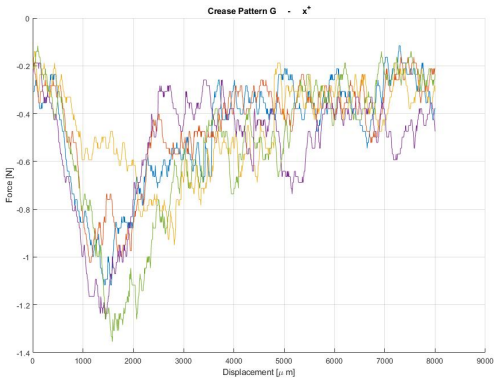

Plot G.50: Crease pattern G: Raw data into the x^+ direction. Vertical axis, force N. Horizontal axis, displacement μm.

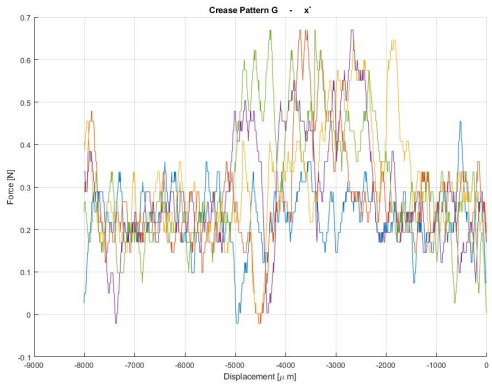

Plot G.51: Crease pattern G: Raw data into the x^- direction. Vertical axis, force N. Horizontal axis, displacement μm.

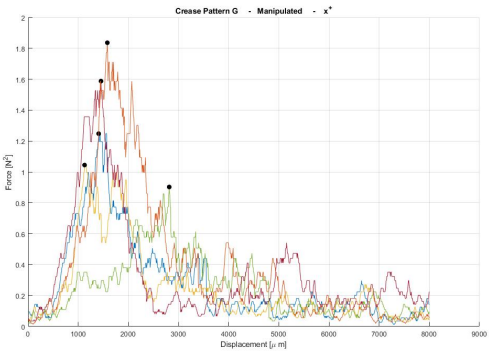

Plot G.54: Crease pattern G: Manipulated data into the x^+ direction. Vertical axis, force N. Horizontal axis, displacement μm.

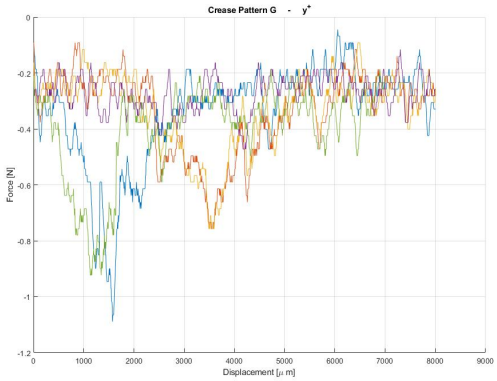

Plot G.52: Crease pattern G: Raw data into the y^+ direction. Vertical axis, force N. Horizontal axis, displacement μm.

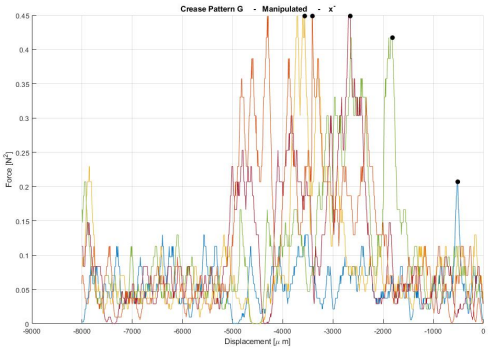

Plot G.55: Crease pattern G: Manipulated data into the x^- direction. Vertical axis, force N. Horizontal axis, displacement μm.

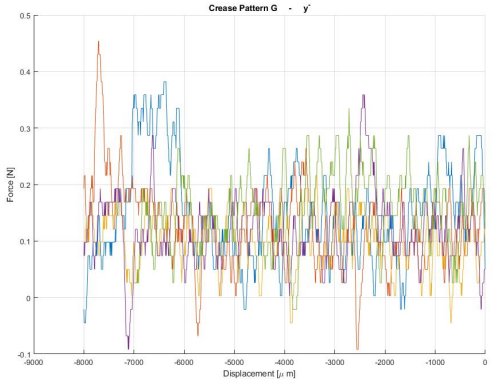

Plot G.53: Crease pattern G: Raw data into the y^- direction. Vertical axis, force N. Horizontal axis, displacement μm.

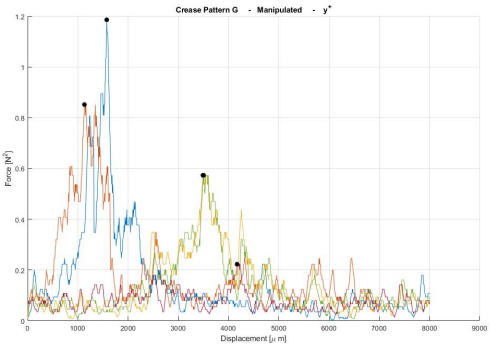

Plot G.56: Crease pattern G: Manipulated data into the y^+ direction. Vertical axis, force N. Horizontal axis, displacement μm.

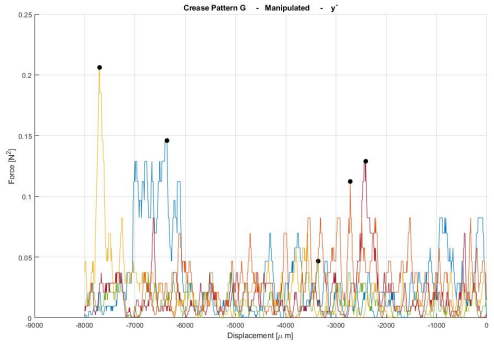

Plot G.57: Crease pattern G: Manipulated data into the y^- direction. Vertical axis, force N. Horizontal axis, displacement μm.

G.6. Discussion - Data evaluation

Note: at the time of writing the discussion, the secondary creases were not yet known. The secondary creases will be part of the conclusion in the experiment.

After analysing the data, it seems that that all measurements into the x-direction are mirrored. Although it was not that obvious during the experiment it can clearly be seen in the figures G.4 and G.5. The crease patterns are folded with the use of the template. The template of the x-axis was accidentally mirrored. The hypothesis can be easily updated by switching the x^+ and x^--direction as is shown in table G.10.

	Creases						
Direction	A	B	C	D	E	F	G
$M(x^+)$	yes	yes	yes	yes	yes	yes	yes
$M(x^-)$	no	yes	no	yes	yes	no	no
y^+	yes	yes	yes	yes	yes	yes	yes
y^-	no	no	no	no	yes	no	no

Table G.10: The expected constraints in the directions x^+, x^-, y^+, y^- for each crease pattern. If the crease pattern is constraint then a "yes" is shown or else a "no". This table refers to objective one and is updated to the new situation for which a mirrored crease pattern is used for the x^+ and x^--directions. Note: this table is without the consideration of the primary creases. The secondary creases will be the solution in the article.

Examining hypothesis one is done with the following approach; Determine significantly if the sheets can move freely. If there is not enough evidence that the sheet can move freely then we will reject the claim that it can move freely resulting in the claim that the sheet is constraint.
To do so, the measurement of the clean movement will be subtracted, canceling the noise of the measurement. If the resulting value is near zero then the sheet can move freely. If the resulting value is relatively large then it is constraint.

Formula G.1 shows the measurement subtracted of the clean movement accompanied with the variance under the assumption that P and Q are uncorrelated. P is equal to the measurement of a crease pattern. Q is equal to the the measurement of clean movement.

$$f(P,Q) = abs(P) - abs(Q) \tag{G.1}$$
$$Var(F(P,Q)) = Var(P) + Var(Q)$$

Formula G.1 resulted in table G.11 and G.12. The rounded are rounded to four digits.

The first hypothesis to be tested determines if the sheets are constraint or not. Formula G.1 subtracted the clean measurement. So if the sheets are not constraint then $H_0 : \mu = 0$ if the sheets are constraint then $H_1 : \mu > 0$. "The probability distribution of T under the null hypothesis"[41] needs to be determined with the test statistic defined in formula G.2 and μ_0 as the value of the null hypothesis.

$$T = \frac{\bar{f} - \mu_0}{S_n/\sqrt{n}} = \frac{\bar{f} - \mu_0}{Var(\bar{f})} \quad [41] \tag{G.2}$$

The hypothesise can only be rejected into one-direction, this is a case of one-sided confidence interval. The allowable exceedance probability is set to be $p = 0.025$. "The null hypothesis will be rejected of favor H_1, if $T \geq t_{n-1,\alpha}$ [41]. The tables G.13 and G.14 show the probability distribution and if the hypothesis H_0 may be rejected. If H_0 is rejected then the creases are constraint.

G.7. Discussion - Data meaning

The hypothesis stated two objectives. Both objectives will be discussed separately.

G.7.1. Objective one

Although for the x-direction a mirrored crease pattern is used, most of the found data confirm the projection method as can be seen in table G.13 and G.14. The results which differ from the expected result will be discussed separately.

- **Crease C: x^--direction** The H_0 is rejected in contradiction with the hypothesis. The first thing to notice is that the set of measurements into the x^--direction has a relative high variance. The plot of the raw data does not indicate any unfolding. For unfolding you would expect a clear peak and/or a combination of several saw teeth inside the raw data plot. There is no indication of any of that. But there is a relative large spread of noise inside the graph compared with other creases. Random noise around an equilibrium line does indicate free movement. The above average height of the equilibrium line

	Creases							
	A		B		C		D	
	$\bar{f}$	$Var(\bar{f})$	$\bar{f}$	$Var(\bar{f})$	$\bar{f}$	$Var(\bar{f})$	$\bar{f}$	$Var(\bar{f})$
x^+	0.5782	0.0198	1.6562	0.0479	0.3792	0.0182	1.8886	0.0311
x^-	0.3686	0.1553	0.4304	0.1072	0.3304	0.1088	1.5206	0.4266
y^+	0.3798	0.0185	0.6596	0.0206	0.6832	0.0422	7.8528	4.3037
y^-	0.0238	0.0137	-0.0460	0.0116	0.0465	0.1419	0.3750	0.0355

Table G.11: Table created with the function of formula G.1. The clean measurement is subtracted from the average of the creases. The creases A, B, C, D are included.

	Creases			
	F		G	
	$\bar{f}$	$Var(\bar{f})$	$\bar{f}$	$Var(\bar{f})$
x^+	0.2279	0.0136	0.5172	0.0328
x^-	0.3328	0.1026	0.4256	0.1071
y^+	0.5963	0.0212	0.2756	0.0560
y^-	0.2134	0.0047	-0.0616	0.0107

Table G.12: Table created with the function of formula G.1. The clean measurement is subtracted from the average of the creases. The creases F, G are included.

	Creases								
	A			B			C		
	T	n	$Rejected$	T	n	$Rejected$	T	n	$Rejected$
x^+	29.2020	5	Yes	34.5762	5	yes	20.8352	5	yes
x^-	2.3735	5	No	4.0149	5	yes	3.0368	5	yes (!)
y^+	20.5297	5	yes	32.0194	5	yes	16.1896	4	yes
y^-	1.7372	5	No	-3.9655	4	No	0.3277	6	No

Table G.13: The rejection of null hypothesis is shown in the table for crease A,B,C. The boolean which represent the rejection is accompanied by the test statistic (T) and the number of measurements. If contrary rejected or not with the hypothesis then the result is indicated by a (!).

	Creases								
	D			F			G		
	T	n	$Rejected$	T	n	$Rejected$	T	n	$Rejected$
x^+	60.7267	4	yes	16.7574	4	yes	15.7683	5	yes
x^-	3.5645	4	yes	3.2437	5	yes (!)	3.9739	5	yes (!)
y^+	1.8247	6	No (!)	28.1274	6	yes	4.9214	5	yes
y^-	10.5634	5	Yes (!)	45.4043	5	yes (!)	-5.7570	5	no

Table G.14: The rejection of null hypothesis is shown in the table for crease D,F,G. The boolean which represent rejection is accompanied by the test statistic (T) and the number of measurements. If contrary rejected or not with the hypothesis then the result is indicated by a (!).

may be due to the fact that the setup was connected too tightly to the sensor, but it is necessary to avoid friction in the perpendicular direction of the measurement. Due the lack of backlash in this direction there could have been additional friction inside the measurement resulting in a contradiction with the hypothesis. This argument is reinforced by the fact that this measurement was made on a different day and the experiment had to be rebuilt.

- **Crease D: y^+-direction** The H_0 is not rejected but it should has been. Although the null hypothesis is near the threshold of the rejection. This set of measurements is not rejected due the large variance of 4.3 within the measurement. The Variance is ten times higher then the next set of measurements in line. Although the mean of the y^+-direction of crease D would tend to reject the $H_0 = 0$ with a mean value of 7.85. The variance is large due the use of a second template to prevent deformation of the paper anywhere other then the foldline. Due the relative thickness of the template the origami object is placed into the $\mathbb{R}^3$ instead of the $\mathbb{R}^2$. The creases are not sharp but have a curve resulting in a high variance.

- **Crease D: y^--direction** The H_0 is rejected in contradiction with the hypothesis. However the H_0 should have been rejected, so the hypothesis is wrong. This problem will be tackled by the introduction of virtual creases. As will be explained later on.

- **Crease F: x^--direction** The H_0 is rejected in contradiction with the hypothesis. This set of measurements has the same argumentation as the x^--direction of crease C. This measurement was caught up later on a different day therefore the experiment had to be rebuilt. Note that the test statistic T value is near the decision turning point. If an higher certainty (lower p-value) was chosen then the hypothesis H_0 would not have been rejected.

- **Crease F: y^--direction** The H_0 is rejected in contradiction with the hypothesis. However the H_0 should have been rejected, so the hypothesis is wrong. This problem will be tackled by the introduction of virtual creases. As will be explained later on.

- **Crease G: x^--direction** The H_0 is rejected in contradiction with the hypothesis. Note that the H_0 just above the threshold has been rejected. The raw plot shows a lot of noise and shows no unfolding behavior. but shows in the middle around $-2000\,\mu$m and $-5000\,\mu$m noise on a higher equilibrium line. The mathematical model expect that the sheets should move freely. The mathematical model do not take into account that the sheets interact with each other on a physical level. For example friction between the sheets. This phenomena probably explains the absence of unfolding in the raw graph but for a while an higher equilibrium line. Taking the sheet interaction into account the hypothesis H_0 would not have been rejected and therefore the sheet would have a free movement.

G.7.2. Objective two

No conclusion can be made about objective two. For example crease B, the constraint of x^+, x^- and y^+ should be proportional equal. Although the measurements of y^+ and x^--direction are near each other they still to different. The same is true for the measurement into the x^+-direction for which can be said it is significantly larger then the y^+ and x^--direction. Therefore I tend to reject objective two. Additional research should be done to include or exclude any conclusions about the ratio.

G.7.3. Discussion: introduction of "virtual" creases

The the null hypothesis ($H_0 : \mu = 0$) of the y^--direction from crease D and the y^--direction of crease F are rejected in contradiction with the hypothesis. After studying both crease patterns only one conclusion can be made. These specific hypotheses were wrong. So what happened?

Figure G.18 is a projected representation of the D crease pattern. It consist of three folds from opposite folding. At the level of the creases the prediction from the projection method is correct. Crease E_1 and E_2 result into a constrain into right direction and crease E_2 has a resulting constraint into the left direction.

However, the interaction between crease E_1 and E_3 is not taken into account. The outer pink sheet of crease E_1 and the inner blue sheet of E_3 are from different creases, but behave as they are from the same crease. Although this crease does not exist is has a constraint. Therefore "virtual" creases are introduced.

If two creases are enclosed by each other, a third "virtual" crease exist. The "virtual" crease has the opposite direction of the the outer crease, in this case E_3. The virtual crease can be defined by projecting either E_1 on E_3 or E_3 on E_1, the smallest value seems to be the true value. For the moment the virtual crease seems to be true only for opposite folding. New thought experiments should be done to validate this statement.

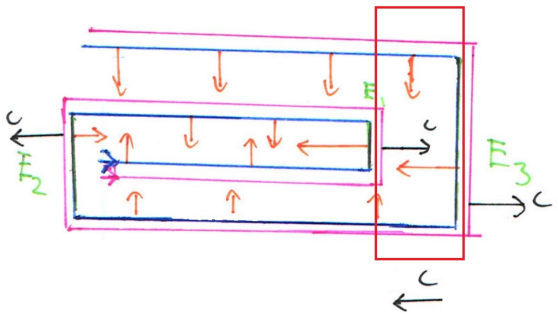

Figure G.18: A combination of the which ladder and opposite folding. The normal vector and constraint vectors are shown. The red box shows the location of the virtual crease.

	Creases						
Direction	A	B	C	D	E	F	G
x^+	no	yes	no	yes	yes	no	no
x^-	yes	yes	yes	yes	yes	yes	yes
y^+	yes	yes	yes	yes	yes	yes	yes
y^-	no	no	no	no	yes	no	no

Table G.15: The expected constraints in the directions x^+, x^-, y^+, y^- for each crease pattern. If the crease pattern is constraint then a "yes" is shown or else a "no". This table refers to objective one.

G.8. Conclusion

The first objective is confirmed with the rectified hypothesis with the use of virtual creases. The second objective could not be validated, additional research should be done.

Objective one determines if a sheet is constraint including the direction. Objective two validates the proportion of the constraints.

The remaining deviations from objective one can be explained due friction inside the experimental setup, friction between the sheets or due the use of a second template. Beside the virtual creases no other weird behavior occurred which can not be explained. If the experiment is repeated, it would be advised to perform more measurements on the crease patterns. Also a next experiment should involve the physical behavior and interaction of paper with paper. To have a more clear result, certainly with an higher amount of creases.

Note: The constraints induced by virtual creases are in the article renamed to secondary creases.

H

Optimization

For certain situations resistance against different stresses is required. A lot of fold combinations can be made by varying the distance between a fold and its angle. The question arises; "What is the optimal crease pattern for a given situation?". This chapter will dive into the optimization of the folded strips.

H.1. Optimization flowchart

For a given situation an optimal crease pattern needs to be found. For engineering purposes there is no need to have an unique solution, a range of best solutions will also satisfy. For a crease pattern within a bounded strip, the problem emerges that the number of creases is variable inside the optimization problem, in other words the number of variables is variable. The total number of variables is limited due the length of the strip, therefore the number of variables is finite. In order to handle different amount of variables the optimization is discretized into the number of creases, as can be seen in Fig.H.1. For each amount of creases an optimal crease pattern needs to be determined. This process is repeated for each subset of folding (stages). From the section B.3.1 is known that the the subset $\mathcal{H}$ is folded first, followed by $\mathcal{V}^1$. Just like Fig.H.1 indicates, more subsets can be added to the optimisation problem in order to have creases which intersect crossing creases etc.. However, this report is restricted to subset of $\mathcal{H}$ and $\mathcal{V}^1$.

H.2. Optimization Algorithm

The input for the intended algorithm depends on the subset and the number of creases. A crease of subset $\mathcal{H}$ can be defined with three variables, 1) the location on the y-axis ($x_1^{\mathcal{H}}$), 2) the angle between the incoming and outgoing strip ($x_2^{\mathcal{H}}$), 3) and the direction of the folding ($x_3^{\mathcal{H}}$), see section B.4, D.3. A crease of subset $\mathcal{V}$ is defined with four variables, 1) the location on the y-axis ($x_1^{\mathcal{V}}$), 2)the location on the x-axis, either left or right ($x_2^{\mathcal{V}}$), 3) the angle of the crease ($x_3^{\mathcal{V}}$), 4) and the direction of the folding ($x_4^{\mathcal{V}}$) As discussed in the previous section the number of variables of the total optimisation is equal to a multiplication of three or four.

The folding can either be $\lambda = -1$ or $+1$ for both subsets. While originating from the right or left side of the strip, $x_{pos} = -\frac{D}{2}$ or $\frac{D}{2}$. All other variables are continue within there domain.
The constraints of the optimization are non-linear ($g(x)$), see section H.4. Therefore the optimization problem is a multi-objective binary mixed-integer nonlinear problem (MOMINP). The constraints are not easy to differentiate, accordingly the problem seems to be non-convex. A genetic algorithm can be used to solve these types of problems. For a genetic algorithm the "convergence to the global optimum cannot be guaranteed, but will yield "good" solutions on average" [42]. The optimization problem is defined in Eqn.H.1 within the the set of feasible solutions $\mathcal{G}$. Feasible solutions space is defined as $\mathcal{G}^{\mathcal{H}} : \left\{0 \leq x_1 \leq L, \quad 0 \leq x_2 \leq \frac{pi}{2}, \quad x_3 = \pm 1\right\}$ and $\mathcal{G}^{\mathcal{V}} : \left\{0 \leq x_1 \leq L, \quad x_2 = \pm 1, \quad 0 \leq x_3 \leq \frac{pi}{2}, \quad x_4 = \pm 1\right\}$. With L as the total length of the strip. Note that the feasible solution space of higher subsets are the same as for $\mathcal{G}^{\mathcal{V}}$.
The optimization problem is formulated in Eqn. (H.1) with the total objective function (d_p) and the constraints represented by $g(X)$ inside the feasible space $\mathcal{G}$.

$$\begin{aligned} &\min_x -d_p(x) \\ &\text{s.t.} \quad g(x) \leq 0 \\ &\qquad x \in \mathcal{G} \end{aligned} \tag{H.1}$$

H.3. Objective of the optimization

The constraint of the creases are projected to an orthogonal subset. In total there are five objectives ($F(x)$), constraints of the x^+, x^-, y^+, y^- direction and the number of stacked faces, see sections D.2, E.1.1,

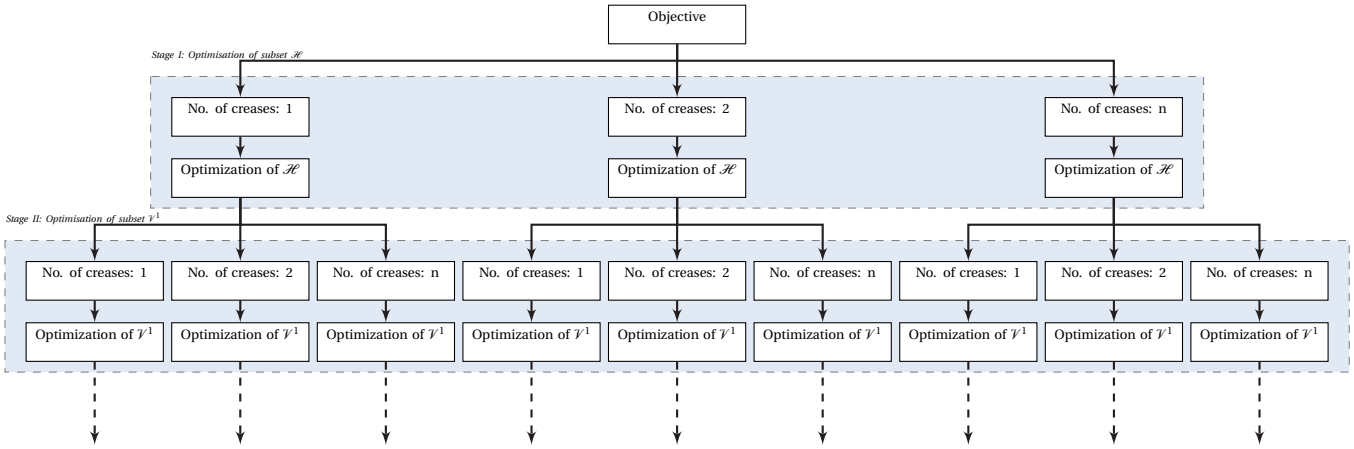

Figure H.1: Optimization flowchart. In order to find an optimal crease pattern an optimization is used. The optimization program has a number of stages which is equal to the number of folding sets going from $\mathscr{H}$ to $\mathscr{V}^n$. Each stage involves a discretization after which it will find an optimum crease pattern.

F.

$$F(x) = \begin{bmatrix} f_1(x), & f_2(x), & f_3(x), & f_4(x), & f_5(x) \end{bmatrix} \quad \text{[43]} \tag{H.2}$$

with: $f_1(x) = |x^+|, \quad f_2(x) = |x^-|,$
$f_3(x) = |y^+|, \quad f_4(x) = |y^-|, \quad f_5(x) = L$

Depending on the situation, a designer wants to have an optimal set of creases. For instance a desired resistance, due a set of creases, evenly spread into all directions or a certain ratio between the objectives. The individual desired objective will be represented with z_i. The designer could also place a certain emphasis on individual objectives with the use of weights, w_i. To give preference to the different objectives, the Weighted Metric Method [44] and the Global Criterion Method [43] are combined as is often done in Compromise Programming [43]. The total objective function (d_p) is shown in Eqn.H.3, with p as "individual relative deviations can be raised to any power ($p = 1,2,\ldots\infty$)" [43].

$$d_p(x) = \left(\sum_{i=1}^{5} w_i \left| \frac{F_i(x) - z_i}{z_i} \right|^p \right)^{1/p} \quad \text{[43], [44]} \tag{H.3}$$

$$\text{with:} \quad 0 < w_i < 1, \quad \sum_{i=1}^{5} w_i = 1, \quad p = 1,2,\ldots\infty \tag{H.4}$$

For the Pareto optimization the following objective is used:

$$d_p(x) = w_i \left| \frac{F_i(x) - z_i}{z_i} \right| \quad \text{[43], [44]} \tag{H.5}$$

$$\text{with:} \quad 0 \le w_i \le 1, \quad \sum_{i=1}^{5} w_i = 1, \quad p = 1,2,\ldots\infty \tag{H.6}$$

H.4. Constrains of the optimization

The optimized system is bounded by the axioms of origami. With the use of these axioms the folded ($\mathscr{F}$) and unfolded state ($\mathscr{F}^{-1}$) of a crease pattern can be related [14]. The main goal of constraining strips is to join two kirigami sheets that are located on the x,z-plane. The strips are therefore not allowed to penetrate the x,y-plane. This is realised by constraining all the vertices to the first and second quadrant in folded state ($\mathscr{F}$), see Eqn.H.7. Also the individual creases (E) within a subset are not allowed to intersect, see Eqn. (H.8).

$$g_1(x): \qquad V \ge \begin{bmatrix} -\infty \\ 0 \end{bmatrix} \quad \text{with} \quad V \in \mathscr{F} \tag{H.7}$$

$$g_2(x): \qquad E_i \not\subset E_j \quad \text{with} \quad E \in \mathscr{F}^{-1}, \mathscr{F} \tag{H.8}$$

A constraint is imposed on opposite folding, Eqn. (H.9). A crease (E_k) which is part of opposite folding must be placed outside the already laid ($\prec$) faces (F_i).

$$g_3(x): \qquad \left(\bigcup_{i=0}^{n} F_i \right) \not\subset E_k \qquad \text{for} \quad \begin{cases} F_i \prec E_k \\ E_k \in \mathscr{F} \\ \lambda_{k-1} = \lambda_k \end{cases} \tag{H.9}$$

The following constraints apply on the algorithm. Additional constraints for the algorithm are shown in Eqn. (H.10). Equation (H.10) defines that the order of folding operations happens from the bottom of the strip into the upwards direction. In addition, Eqn. (H.11) prevents numerical error within the algorithm by setting a minimal distance between the vertices of

an arbitrary distance.

$$g_4(x): \qquad V_{i,A,y} < V_{j,A,y} \quad \text{for} \quad i < j \quad \text{and} \quad V \in \mathscr{F}^{-1} \tag{H.10}$$

$$g_5(x): \qquad \text{if} \quad V_i \neq V_j \quad \Rightarrow \quad ||V_i - V_j|| > 7 \cdot 10^{-1} \tag{H.11}$$

The total nonlinear constraints of the optimization problem can be formulated as followed $g(x) = \{g_1(x), g_2(x), g_3(x), g_4(x), g_5(x)\}$ for the subsets $\mathscr{X} = \mathscr{H}, \mathscr{V}^1, \mathscr{V}^2, \ldots$

I

Optimization algorithm

The chapter I is the implementation of chapter H. Where chapter H is mainly mathematical, this chapter is practical. It discusses the structure of the code and how the constraints and objectives of the optimization are achieved. Also the advantages and drawbacks will be discussed.

I.1. How to run the code

The code is written for Matlab R2020b and is not suitable for earlier versions. Earlier versions of Matlab lack the Matlab function "*sgtitle()*" used for the layout of the graphs.

The code can be executed by running the file "*main_file_version_3*". The file "*main_file_version_3*" contains all the parameters that a user wishes to modify. The required (called) functions to run the algorithm are stored into the folder "Functions_Optimization". Depending on the subset each crease has either three (subset $\mathscr{H}$) or four (subset $\mathscr{V}$) variables. In advance to the execution of the code the user needs to determine the number of creases per subset, the dimensions of the strip (L,D), initial direction of the strip (*init_direction*). An desired solution can be found by tweaking the weight factors (Z_H, Z_V) and the objective values (w).
The parameters of the file "*main_file_version_3*" should be reasonable. For example, 30 creases on a strip with a length of 2 is not reasonable, but three is. In order to prevent issue's due numerical problems, the algorithm is constrained in such away that all creases within a subset will have a minimal distance of at least "0.07" to each other. Therefore only a finite number of creases are allowed.

I.2. Optimization algorithm

The up-following sections involves the implementation of the optimization.

I.2.1. Genetic Algorithm

The system is optimized with a genetic algorithm represented by the Matlab function "*ga()*". Due the nature the genetic algorithm all constraints of the mixed-integer system, including the linear constraints, must be defined with non-linear functions. The constraints can be found in the function "*nonlcon_func*" and " *nonlcon_func_subset_V*". From the genetic algorithm the parameters "*PopulationSize*" and the number of "*Generations*" can be changed. This has influence on the processing time and the acquired solution. For a genetic algorithm the "convergence to the global optimum cannot be guaranteed, but will yield "good" solutions on average" [42]. Therefore a sufficient number of generations and a decent size of the population is advised. In order to have a feasible solution the constraint tolerance is set to zero.

Fig.I.1 and I.3 show a live plot of the function "*ga()*" on two different moments within the optimization. Fig.I.1 has not yet found a feasible solution. This can be recognized if the black line ("best solution") touches the horizontal axis. Fig.I.3 has found a feasible solution, the black line is detached from the x axis. After a certain amount of time or generations an optimal solution is found. If no feasible solution has been found the parameters of the optimization algorithm can be altered, the number of crease needs to be reduced or the length of the strip needs to be extended.
A reduction in the average distance (Fig. I.1) indicates that the differences of individuals within a generation is reduced, in other words the algorithm tends to go to an optimal solution.

I.2.2. Genetic Algorithm multi-objective - Pareto front

The Pareto optimization is executed with a multi-objective genetic algorithm represented by the matlab function "*gamultiobj()*". Unfortunately the Matlab function is not able to handle mixed-integer

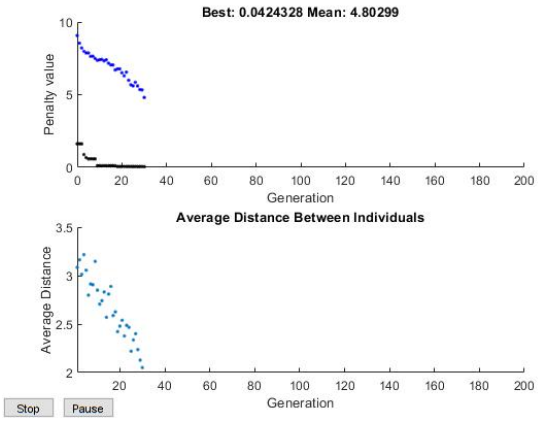

Figure I.1: A screenshot of the live plot from the genetic algorithm of the Matlab function *ga()*. The first plot shows the penalty function and the second plot the average distance of the individuals within a generation. The present screenshot has not yet found a feasible solution.

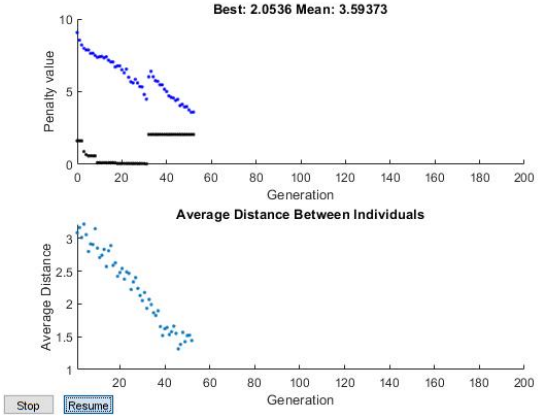

Figure I.2: A screenshot of the live plot from the genetic algorithm of the Matlab function *ga()*. The first plot shows the penalty function and the second plot the average distance of the individuals within a generation. The present screenshot has found a feasible solution but not yet an optimal.

optimization problems. The MathWorks Support Team presented a solution by redefining the functions "CreationFcn", "MutationFcn", "CrossoverFcn" [45]. With these adapted functions the optimization algorithm is able to handle integer variables. The downside of the presented functions is that all integer variables for each individual are same value. But within a subset the creases need to have an independent integer value for $\lambda = \pm 1$ and in addition for subset $\mathcal{V}$ $x_{pos} = \pm 1$. Therefore I updated the functions "CreationFcn", "MutationFcn", "CrossoverFcn" with an additional randomisation in such a way that also the integers variables within an individual are independent. This makes the Matlab function suitable for the problem with a crease pattern, the creases are allowed to have its own random integers (λ, x_{pos}).

While creating a Pareto front, the optimization shows a live plot of its status. The live plot shows the gained Pareto front. The live plot also includes how the individuals relate to each other, the total spread within a generation, the distance of the individuals to each other and the fitness of each individual. Also the score of the objective functions of the individuals can be found within the live plot.

I.3. Computation time

The computation time will increase rapidly with an higher number of creases within a subset or by a large populations size. Therefore, keep the number of creases of each subset below five. The default setting for the number of the population size is set to be *10 min(max(10 nvars,40),100)* and will scale up with the number of variables ($nvars$). The computation of the Pareto plots will have a population size of *20 min(max(10 nvars,40),100)*. The number of generations is by default set to be 200 or 400 and may be changed in order to restrain the maximum number of generations. If the maximum number of generations is relatively low a feasible solution can not be guaranteed and an exit-flag of zero will be returned. It is not advised to change the *Functiontolerance*, "The algorithm stops if the average relative change in the best fitness function value over MaxStallGenerations is less than or equal to FunctionTolerance" [46]. The default setting of the *Functiontolerance* by matlab is set to 10^{-6} for the single objective genetic algorithm and 10^{-4} for the multi-objective genetic algorithm. After testing the optimisation algorithm it seems that the genetic algorithm can remain for a longer period near a found solution without having a significant change in the solution space. Therefore the *Functiontolerance* is changed to $\cdot 10^{-5}$ for the single genetic algorithm of subset $\mathcal{H}$ and $\cdot 10^{-3}$ for subset $\mathcal{V}$.

I.4. Exit-flags

The exit flags of the genetic algorithm are shown in table I.1 [17]. In principle negative flags should be avoided, rerun the code if a negative flag occurs. In case of a exit-flag zero, the populationsize and/or the number of generations should be increased. A solution is found if a exit-flag of one is returned. If errors keep occurring check if there is a reasonable amount of creases within the length of the strip.

I.4.1. Structure of the algorithm

Each subset is handled in sequence from $\mathcal{H}$ to $\mathcal{V}^1$ as is motioned in section H.1. Although Fig.H.1 suggest an unlimited number of subsets, the algorithm only allows folding in subset $\mathcal{H}$ and $\mathcal{V}^1$. For both subsets,

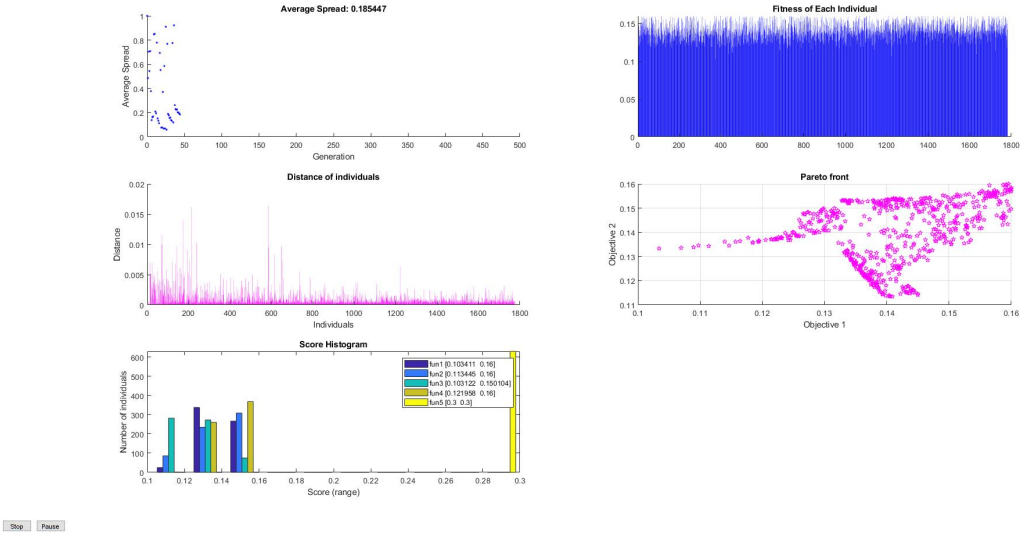

Figure I.3: A screenshot of the live plot from the multi-objective genetic algorithm of the Matlab function *gamultiobj()*. The first plot shows the average spread of the individuals within a generation. The second plot shows the distance of all individuals. The third plot shows the score range. The fourth plot the fitness of each individual. The final plot, the most important plot, the Pareto front of the objectives.

Exit-Flag	**Meaning**
1	"The subproblem is solved using a tolerance less than FunctionTolerance, and the constraint violation is less than ConstraintTolerance"
3	"Value of the fitness function did not change in MaxStallGenerations generations and the constraint violation is less than ConstraintTolerance."
4	"Magnitude of step smaller than machine precision and the constraint violation is less than ConstraintTolerance."
5	"Minimum fitness limit FitnessLimit reached and the constraint violation is less than ConstraintTolerance."
0	"Maximum number of generations MaxGenerations exceeded."
-1	"Optimization terminated by an output function or plot function."
-2	"No feasible point found."
-4	"Stall time limit MaxStallTime exceeded."
-5	"Time limit MaxTime exceeded."

Table I.1: Possible exit flags of the genetic algorihm. Source: [17]

the optimal crease pattern is calculated first after which a Pareto front is calculated. The calculation of the Pareto front is optional, and is used to compare the found solution with solutions in general.

I.5. Recomposition of the faces

The algorithm calculates the folded state of each subset by mapping the creases from unfolded state to the folded state. A different option would be defining the faces (polygon) in unfolded state and map the faces to folded state. With the the projection method in mind, which depends solely on the creases, the choice has been made to use the approach to calculate the folded state by mapping the creases and not the faces. Despite it did seem as be a good idea it was undoable to determine the exact number of stacked sheets, although an approximation can be made see also section **??**. Also the constraint which prevent the intersection of the sheet due opposite folding was not liable enough. Therefore the faces are recomposed from the creases in folded state. The recomposition is done for subset $\mathscr{H}$ and subset $\mathscr{V}$.

I.5.1. Recomposition of faces subset $\mathscr{H}$

The recomposition of subset $\mathscr{H}$ is straight forward. By mapping from the unfolded state to the folded state all indices of the variables are persevered. The polygons which represent the faces can simply be created with the given set of creases. Each face is enclosed by the consecutive creases. Note that the crease within a subset are not allowed to intersect.

I.5.2. Recomposition of faces subset $\mathscr{V}$

The recomposition of subset $\mathscr{V}$ is less straight forward. The fact that creases are not allowed to cross each other is used to recompose subset $\mathscr{V}$. The entire strip is divided in segments defined by the raw edges and the creases of subset $\mathscr{H}$. Two example segments are shown in Fig.I.4. A crease of subset $\mathscr{V}$ can only cross a single crease of subset $\mathscr{H}$ once. Secondly the crease can only originate from the rawedge, or go from one crease of $\mathscr{H}$ tot another crease of $\mathscr{H}$. In combination with the fact that creases from the same subset are not allowed to cross, a segment can be divided in faces having either three, four, five or six vertices.

Figure I.4 shows a crease pattern in unfolded state, it facilitates the interpretation of the different faces. A triangular face is enclosed by a raw edge a crease from subset $\mathscr{H}$ and a crease from subset $\mathscr{V}$ and can therefore only be located in the corners of

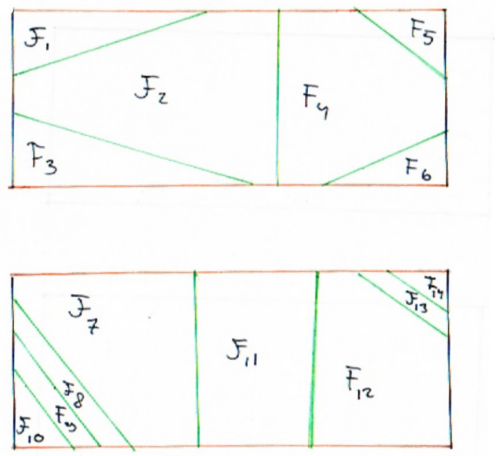

Figure I.4: Two randomly created segments from a crease pattern in unfolded state. The orange creases represent $\mathscr{H}$ and the green lines represent the creases of subset $\mathscr{V}$. Triangular faces are F_1, F_3, F_5, F_6, F_10, F_14. Rectangular faces are F_8, F_9, F_11, F_13. Pentagonal faces are F_7, F_12. Hexagonal faces are F_2, F_4.

the segment. Fun fact there is a maximum of four triangular faces within a segment. A rectangular face is easily to distinguish, it is surrounded by two creases from subset $\mathscr{H}$ and two creases from subset $\mathscr{V}$. A rectangular face only occurs in the middle of the segment or is located next to a triangular face. However the upcoming guideline separate these two types rectangular faces. The pentagonal and the hexagonal faces are less common, and can only occur in the presence of a triangular face. Notice that a pentagonal and the hexagonal faces only occur on the left or right side of the segment. As the Fig. I.4 indicates a pentagonal face only occurs if it is next to either two rectangular faces or one triangular face and one rectangular face. In other cases an hexagonal face will occur.

The procedure to determine the faces is as followed for each segment. First find all the triangular faces. Secondly find all the rectangular faces adjacent to the triangular faces. Thirdly, find all pentagonal and hexagonal faces. Finally, the remaining faces will be rectangular. Note that mapping the creases from folded to unfolded state will alter their location, but the shape of the face is preserved due the folding axioms (section B.1.1) also the indices of the vertices are preserved. Therefore the presented recomposition of the faces in unfolded state also works for the folded state and is used in the algorihm.

I.5.3. Recategorization towards the subset $\mathscr{V}$

The previous sections discusses; how to find all the faces from a crease pattern. It is realized from the

point of view of subset $\mathscr{H}$. However, in order to define the constraint for opposite folding of subset $\mathscr{V}$ or to determine the number of stacked sheets, all faces should be reorganized towards the point of view of subset $\mathscr{V}$. This new structure will include two fields "*bottom*" and "*top*" for each crease of subset $\mathscr{V}$. The field "*bottom*" is comprised from all faces which are laid before the present crease, so the faces from the base upwards till the present crease. The field "*top*" includes only the adjacent faces of the crease of subset $\mathscr{V}$ which are not yet part of the field "*bottom*". In this way all the faces are recategorized from subset $\mathscr{H}$ to subset $\mathscr{V}$ and can be used for determining the constraint of opposite folding and the objective of the stacked sheets.

I.5.4. Drawback of counting stacked faces

Section F includes a definition of stacking (definition **??**). Doing so by counting the number of stacked faces. The algorithm makes a close approximation of the exact number of sheets with the following method; A matrix is created to hold on the faces which are stacked on top of each other. From this matrix the total number of staked faces can be determined.
Fig.I.1 indicates that there is a drawback of the used approach. The correct maximum stacked number faces is equal to eight if only one sheet is used. With the approach mentioned above the found number of stacked faces will be nine. The top faces of the third crease from subset $\mathscr{V}$ does overlap with the first face (see the red circle in Fig.I.1), but this overlapping has no added value in the sense of constraining sheets. However the algorithm will count these kind overlapping leading to a small deviation of the correct value in some cases.

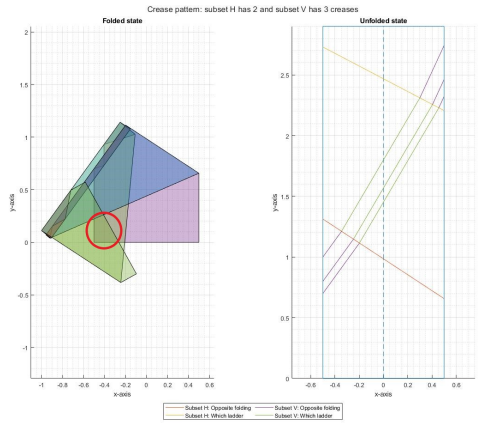

Plot I.1: Folded and unfolded state from a random crease pattern. Subset $\mathscr{H}$ has two creases and subset $\mathscr{V}$ has three creases. The red circle indicates an area for which the faces are counted where they should not be counted.

J

Implementation of the optimization

A folding pattern has been optimized as an example. The algorithm is a live script the input (code) and the output (data and graphs) are displayed within the same file, *main_file_version_3*". This appendix includes the entire file.

Main script - Draft Version 3.2

Sibren Allard - Student Number: 4330846

TU Delft - 01-04-2021

Supervisors: Prof.dr.ir. J.L. Herder && dr.ir F. Broeren

This algorithm does an optimization for a crease pattern consisting of subset H and subset V. The user can enter objective values and weight factors. Likewise the number of creases per subset. The parameters of the genetic algorithm can also be tweaked within this file.

```
clear all;
close all;
```

Inital values

May be adjusted

Properties: Strip

The properties of the strip can be defined by its width (Scalar number) and its length (L, scalar number). Both are dimensionless numbers it is to the user to enter suitable numbers which corresponds with the situation. The variable S (scalar number) indicates the number of sheets to be joint, default value is two. The initial direction ([x;y]) is equal to the direction of the strip from the base. The default initial direction is aligned with the y-axis, which is defined with an orthogonal base with the format ([[x1;y1], [x2;y2]]).

```
L = 3;                                  %   Scalar number
D = 1;                                  %   Scalar number
S = 2;                                  %   Scalar number
init_direction = [0;1];                 %   Vector, [x;y]
Orthogonal_base = [[1;0],[0;1]];        %   Matrix, [[x1;y1],[x1;y1]]
```

Properties: Crease Pattern

The crease pattern consist of 2 subsets of creases, namely subset H and subset V. Subset H is the first subset to be laid, and subset V will be laid on top of subset H. For each subset the number of creases can be determined, via nr_creases_H and nr_creases_V both a scalar number . To increase the computation timedo not make the number of creases of subset v higher then three of four.

```
nr_creases_H = 3;                          % Scalar Number
nr_creases_V = 3;                          % Scalar Number, for fast computation
                                           % not higher then 4.
```

Do not edit the following two of lines code. The number of variables is depends on the number of creases.

```
nvars_H = 3*nr_creases_H;   % The number of variables of subset H
nvars_V = 4*nr_creases_V;   % The number of variables of subset V
```

Properties: Desired solution

The desired result can objective can be passed on to the algorithm with Z. Z has the format [x^+, x^-, y^+, y^- , L], with L as the number of stacked sheets. The algorithm will try to find an optimal solution near this desired goal objective. Often an exact result can not be reached. Therefore it is important to give weight factors to individual objective functions, w. The sum of w must be equal to one. Also the weighted sum parameter can be changed, see for more information the report.

Note that the objective of subset H and V are seperated. With an objective to far out of reached the argorithm can find a solution out of balance. Therefore there is an option to set the objective to the next level.

```
Z_H = [4;4;4;4;4];                          % [x^+, x^-, y^+, y^- , L]
Z_V = [4;4;4;4;5];                          % [x^+, x^-, y^+, y^- , L]
w = [4/25,4/25,4/25,4/25,9/25];           % size(1,5),   sum(w) =1
p = 8;                                    % Scalar Number
```

Properties: Genetic algorithm

A genetic algorithm is used to optimize the crease pattern. The genetic algorithm is based on the evolution. There is a population size of possible inputs, PopulationSize scalar number. The user can set a maximum number of generation, generations scalar number. "The algorithm stops when the average relative change in the fitness function value over MaxStallGenerations is less than Function tolerance" [matlab.com]

Single Optimization

The single optimization uses the matlabfunction "ga()" to find a good solution for both subsets. The parameters can be set below.

Subset H

```
PopulationSize_H = 10*min(max(10*nvars_H,40),100)  % Scalar Number
```

```
PopulationSize_H = 900
```

```
generations_H = 300;                                % Scalar Number
Functiontolerance_H = 1*1e-5;                       % Scalar Number
MaxStallGenerations_H = 20;                         % Scalar Number
```

The number of attempts:

```
trial_H = 1;                                                % Scalar Number
```

Subset V

```
PopulationSize_V = 10*min(max(10*nvars_V,40),100)   % Scalar Number
```

```
PopulationSize_V = 1000
```

```
generations_V = 100;                                        % Scalar Number
Functiontolerance_V = 1e-3;                                 % Scalar Number
MaxStallGenerations_V = 20;                                 % Scalar Number
```

The number of attempts:

```
trial_V = 1;                                                % Scalar Number
```

Pareto Optimization

The found solutions may be compared with the solution space in general. Therefore a pareto plot can be made. The Matlab function “gamultiobj()” is used, with a custom made “CreationFCN”, “MutationFcn” and “CrossoverFcn”. The parameters can be set below.

Subset H

```
PopulationSize_pareto_H = 10*min(max(10*nvars_H,40),100)   % Scalar Number
```

```
PopulationSize_pareto_H = 900
```

```
generations_pareto_H = 500;                                  % Scalar Number
```

Subset V

```
PopulationSize_pareto_V = 8*min(max(10*nvars_V,40),100)   % Scalar Number
```

```
PopulationSize_pareto_V = 800
```

```
generations_pareto_V = 500;                                  % Scalar Number
```

Code Execution

Do not change - Only comment if desired

The needed functions are stored in the map "Functions_Optimization". This map needs to be added to the path so that the functions can be found.

```
addpath(append(pwd,'\Functions_Optimization'))
```

The recomposition of the faces of subset V does create warnings if the constraints are violated. The warning with the id "..." occurs if the algorithm tries to create a face with duplicate vertices. The constraint of opposite-folding needs a set of faces. Before a negative feedback to ga() is returned. This warning is turned off.

Optimization Subset H

The following functions will determine an optimal crease pattern for subset H. The pareto optimization may be turned off.

Single optimization:

```
[x_H,fval_single,exitflag_H,output_H,population_H, scores_H, options_H]...
    = single_optimization_subset_H(L, D, S, init_direction, Orthogonal_base, ...
        nr_creases_H, Z_H, w, p, PopulationSize_H, generations_H, ...
        Functiontolerance_H, MaxStallGenerations_H, trial_H);
```

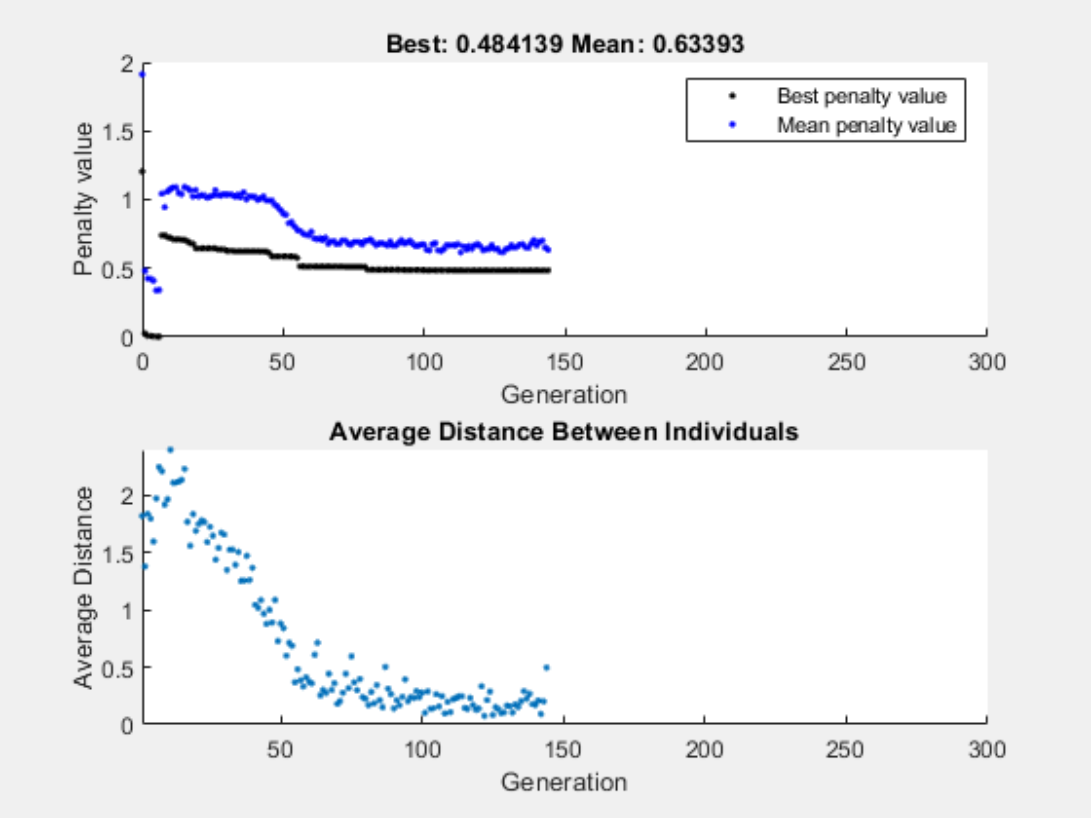


```
Optimization terminated: average change in the penalty fitness value less than options.FunctionTolerance
and constraint violation is less than options.ConstraintTolerance.
```

The used options for the genetic algorithm

```
options_H
```

```
options_H =
  ga options:

   Set properties:
            ConstraintTolerance: 0
```

```
            FunctionTolerance: 1.0000e-05
        InitialPopulationRange: [2×9 double]
                MaxGenerations: 300
           MaxStallGenerations: 20
                      PlotFcn: {'gaplotbestf'  'gaplotdistance'}
              PopulationSize: 900
                 UseParallel: 1
              UseVectorized: 0

  Default properties:
                  CreationFcn: @gacreationuniform
                CrossoverFcn: @crossoverscattered
            CrossoverFraction: 0.8000
                      Display: 'final'
                 EliteCount: '0.05*PopulationSize'
                FitnessLimit: -Inf
            FitnessScalingFcn: @fitscalingrank
                    HybridFcn: []
          InitialPopulationMatrix: []
              InitialScoresMatrix: []
                MaxStallTime: Inf
                     MaxTime: Inf
                 MutationFcn: {@mutationgaussian  [1]  [1]}
   NonlinearConstraintAlgorithm: 'auglag'
                   OutputFcn: []
              PopulationType: 'doubleVector'
                SelectionFcn: @selectionstochunif
```

The found solution:

```
x_H
```

```
x_H = 1×9
    0.7069    0.3874    0.5463    0.8758    1.0715    1.2006         0    1.0000 ···
```

The found crease pattern is plotted below:

```
plot_patterns(x_H,nr_creases_H,D,init_direction,L)
```

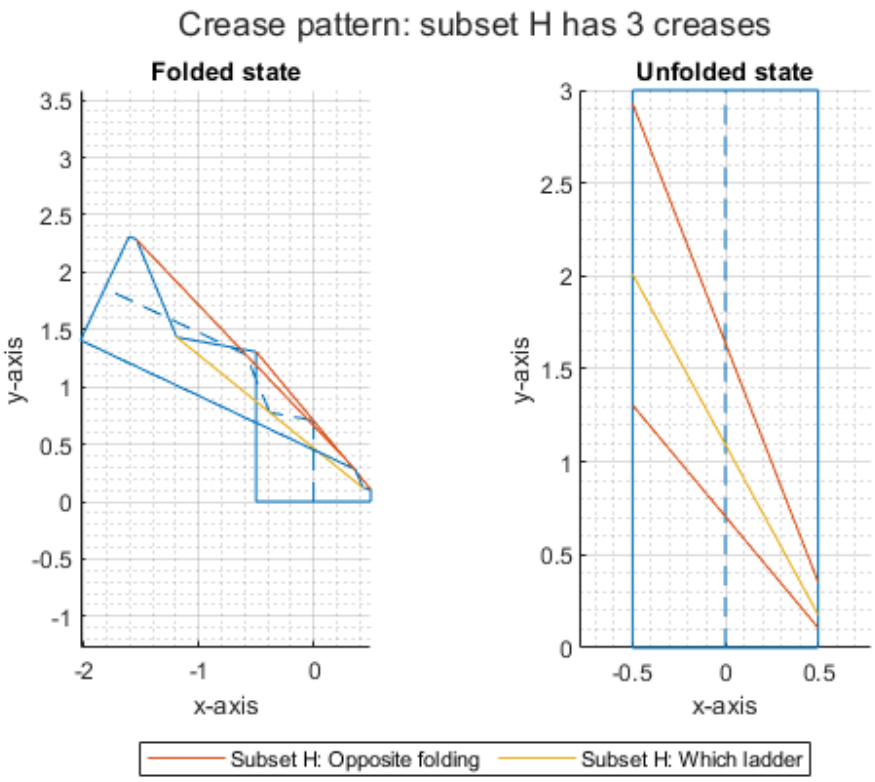

The resulting constraint:

```
Constraint_H = optimization_objective_H(x_H,D,Orthogonal_base,init_direction,S,L)
```

```
Constraint_H = 5×1
   -2.5126
   -2.0003
   -2.6238
   -1.9074
   -2.0000
```

```
optimization_objective_H(x_H,D,Orthogonal_base,init_direction,S,L)
```

```
ans = 5×1
   -2.5126
   -2.0003
   -2.6238
   -1.9074
   -2.0000
```

Pareto optimization:

To reduce the computation time comment the following 3 lines. The Pareto plots hav difficulties with a higher number of creases, therefore the maximum is set to four.

```
if nr_creases_H < 4
    [x_H_pareto,fval_H_pareto,exitflag_H_pareto,output_H_pareto,population_H_pareto,...
        scores_H_pareto, options_H_pareto] = pareto_optimization_subset_H(x_H, L, D,...
```

```
        S, init_direction, Orthogonal_base, nr_creases_H, Z_H, w,...
        generations_pareto_H, PopulationSize_pareto_H);
```

The used options for the Pareto optimization

```
    options_H_pareto
```

The found Pareto plot is shown below:

```
    plot_pareto_subset_H(x_H, x_H_pareto,D,Orthogonal_base,init_direction,S,...
        L,nr_creases_H);
end
```

```
Optimization terminated: average change in the spread of Pareto solutions less than options.FunctionTolerance.
```

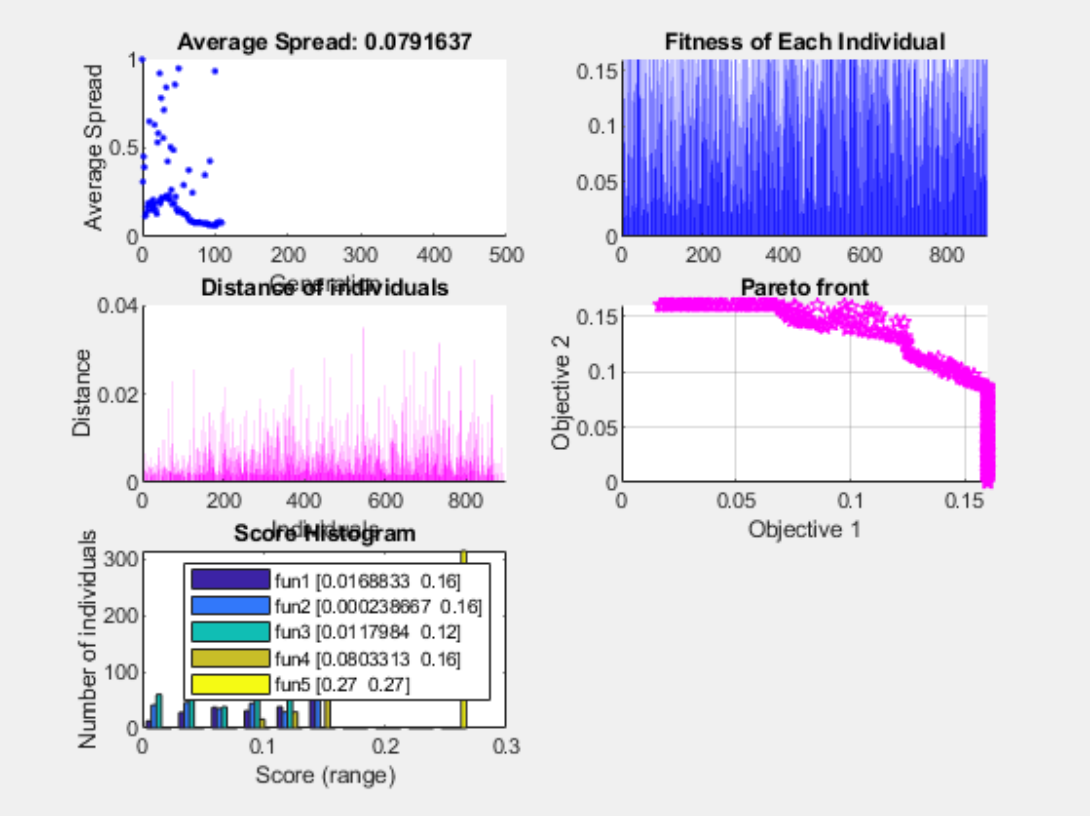


```
options_H_pareto = struct with fields:
          PopulationType: []
            PopInitRange: [2×9 double]
          PopulationSize: 900
              EliteCount: []
       CrossoverFraction: []
          ParetoFraction: 0.3500
     MigrationDirection: []
      MigrationInterval: []
      MigrationFraction: []
            Generations: 500
              TimeLimit: []
           FitnessLimit: []
          StallGenLimit: []
              StallTest: []
         StallTimeLimit: []
```

```
            TolFun: []
            TolCon: []
  InitialPopulation: []
      InitialScores: []
 NonlinConAlgorithm: []
     InitialPenalty: []
      PenaltyFactor: []
       PlotInterval: []
       CreationFcn: @int_pop
  FitnessScalingFcn: []
      SelectionFcn: []
      CrossoverFcn: @int_crossoverarithmetic
       MutationFcn: @int_mutation
 DistanceMeasureFcn: []
          HybridFcn: []
            Display: []
           PlotFcns: {'gaplotspread'  'gaplotscores'  'gaplotparetodistance'  'gaplotpareto'  'gaplotscorediversity'}
         OutputFcns: []
         Vectorized: []
       UseParallel: 1
ConstraintTolerance: 0
```

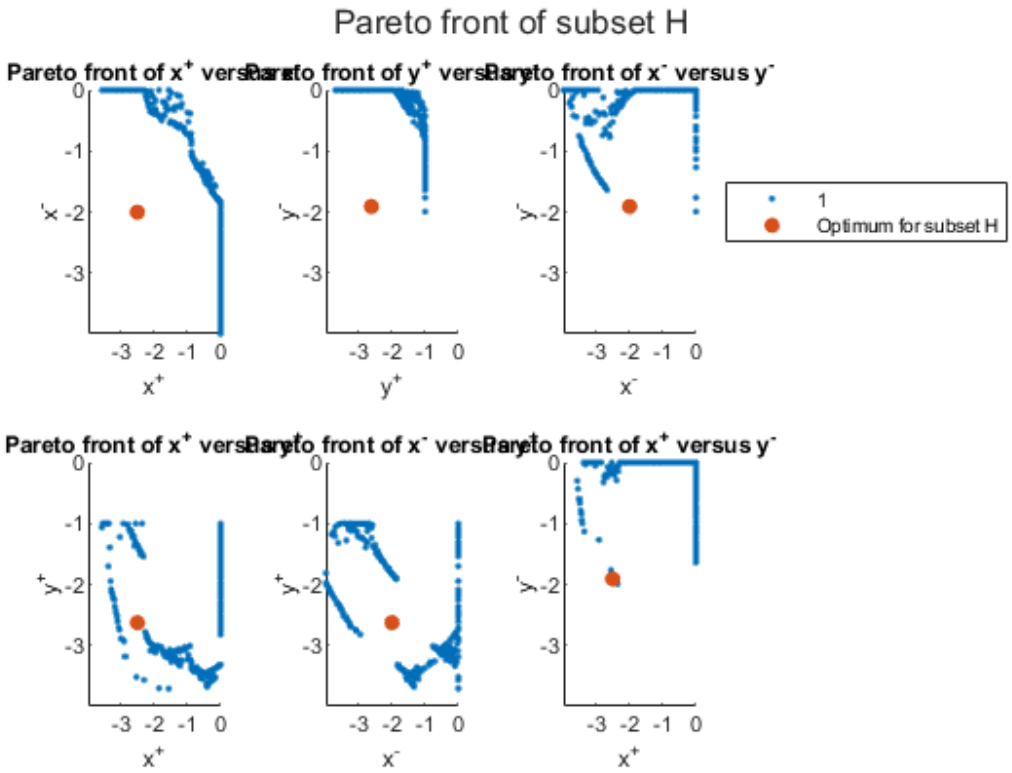

Optimization Subset V

The following functions will determine an optimal crease pattern for subset V. The Pareto plots have difficulties with a higher number of creases, therefore the maximum is set to four.

Single optimization:

```
if exitflag_H > 0
```

```
    [x_V,fval_V,exitflag_V,output_V,population_V,scores_V, options_V] ...
     = single_optimization_subset_V(x_H, L, D, S, init_direction, Orthogonal_base, ...
         nr_creases_V, Z_V, w, p, PopulationSize_V, generations_V, Functiontolerance_V,...
         MaxStallGenerations_V, trial_V);
```

The used options for the genetic algorithm

```
options_V
```

The found solution:

```
x_V
```

The found crease pattern is plotted below:

```
plot_patterns_V(x_H,x_V,D,L,init_direction)
end
```

```
range = 1×2
    1.8000    2.4000
range = 1×2
    2.4000    3.0000
```

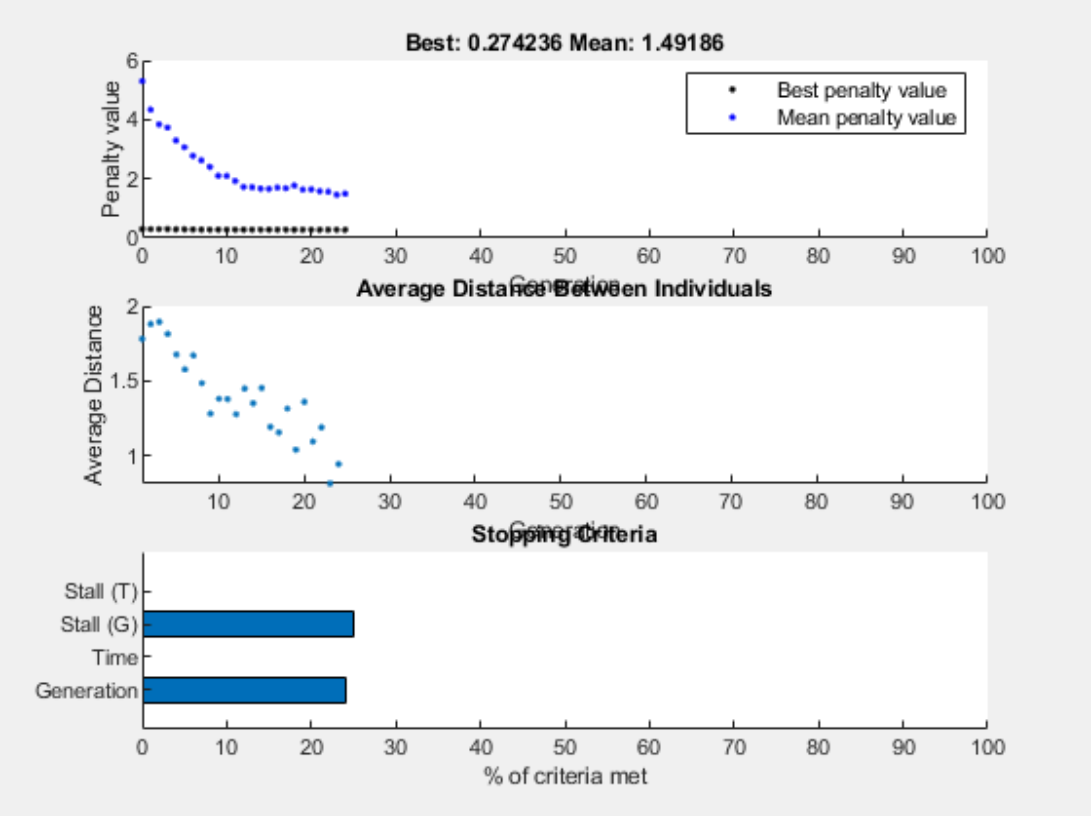


```
Optimization terminated: average change in the penalty fitness value less than options.FunctionTolerance
and constraint violation is less than options.ConstraintTolerance.
options_V =
  ga options:

   Set properties:
            ConstraintTolerance: 0
```

```
              FunctionTolerance: 1.0000e-03
          InitialPopulationRange: [2×12 double]
                  MaxGenerations: 100
             MaxStallGenerations: 20
                        PlotFcn: {'gaplotbestf'  'gaplotdistance'  'gaplotstopping'}
                 PopulationSize: 1000
                    UseParallel: 1
                  UseVectorized: 0

    Default properties:
                     CreationFcn: @gacreationuniform
                   CrossoverFcn: @crossoverscattered
               CrossoverFraction: 0.8000
                         Display: 'final'
                     EliteCount: '0.05*PopulationSize'
                   FitnessLimit: -Inf
               FitnessScalingFcn: @fitscalingrank
                       HybridFcn: []
          InitialPopulationMatrix: []
              InitialScoresMatrix: []
                     MaxStallTime: Inf
                          MaxTime: Inf
                    MutationFcn: {@mutationgaussian  [1]  [1]}
     NonlinearConstraintAlgorithm: 'auglag'
                       OutputFcn: []
                  PopulationType: 'doubleVector'
                    SelectionFcn: @selectionstochunif
x_V = 1×12
    1.5881    1.6820    2.5008         0         0         0    1.2220    1.1309 ···
```

The resulting constraint:

```
Constraint_V = optimization_objective_V(x_V, x_H, D, L, init_direction, Orthogonal_base, S)
```

```
Constraint_V = 5×1
   -2.8898
   -2.9285
   -2.7760
   -2.8247
   -6.0000
```

Pareto optimization:

To reduce the computation time comment the following 3 lines.

```
if nr_creases_V< 4
    [x_V_pareto,fval_V_pareto,exitflag_V_pareto,output_V_pareto,population_V_pareto,...
        scores_V_pareto, options_V_pareto] = pareto_optimization_subset_V(x_H, x_V,...
        L, D, S, init_direction, Orthogonal_base, nr_creases_V, Z_V, w,...
        generations_pareto_V, PopulationSize_pareto_V);
```

The used options for the Pareto optimization

```
    options_V_pareto
```

The found Pareto plot is shown below:

```
    plot_pareto_subset_V(x_H, x_V, x_V_pareto,D,Orthogonal_base,init_direction,S, ...
        L,nr_creases_V)
end
```

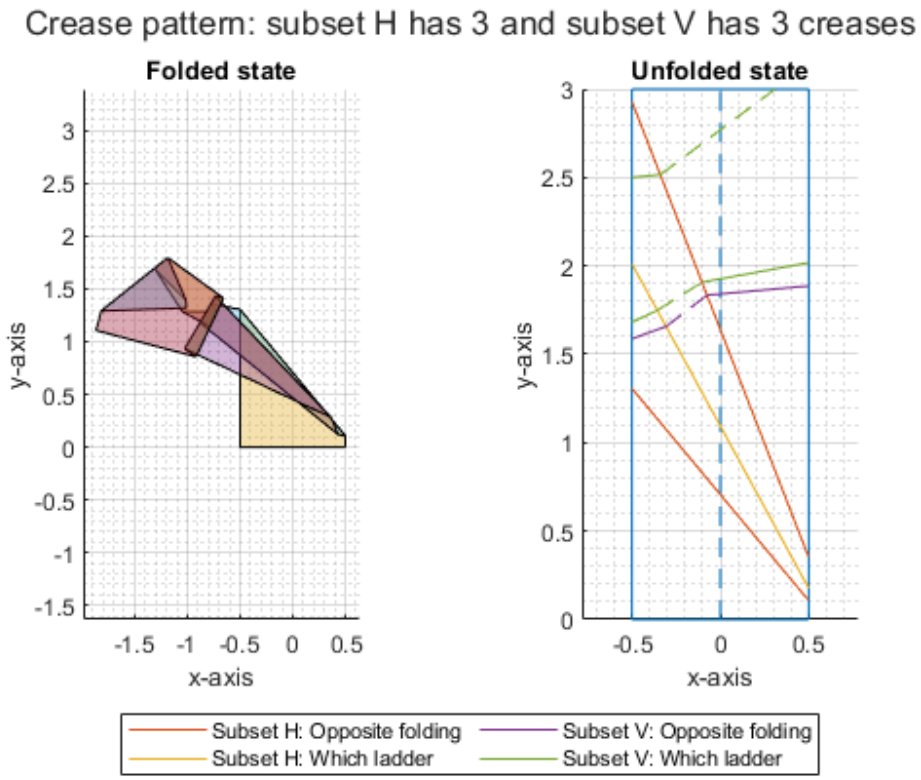


```
Optimization terminated: average change in the spread of Pareto solutions less than options.FunctionTolerance.
```

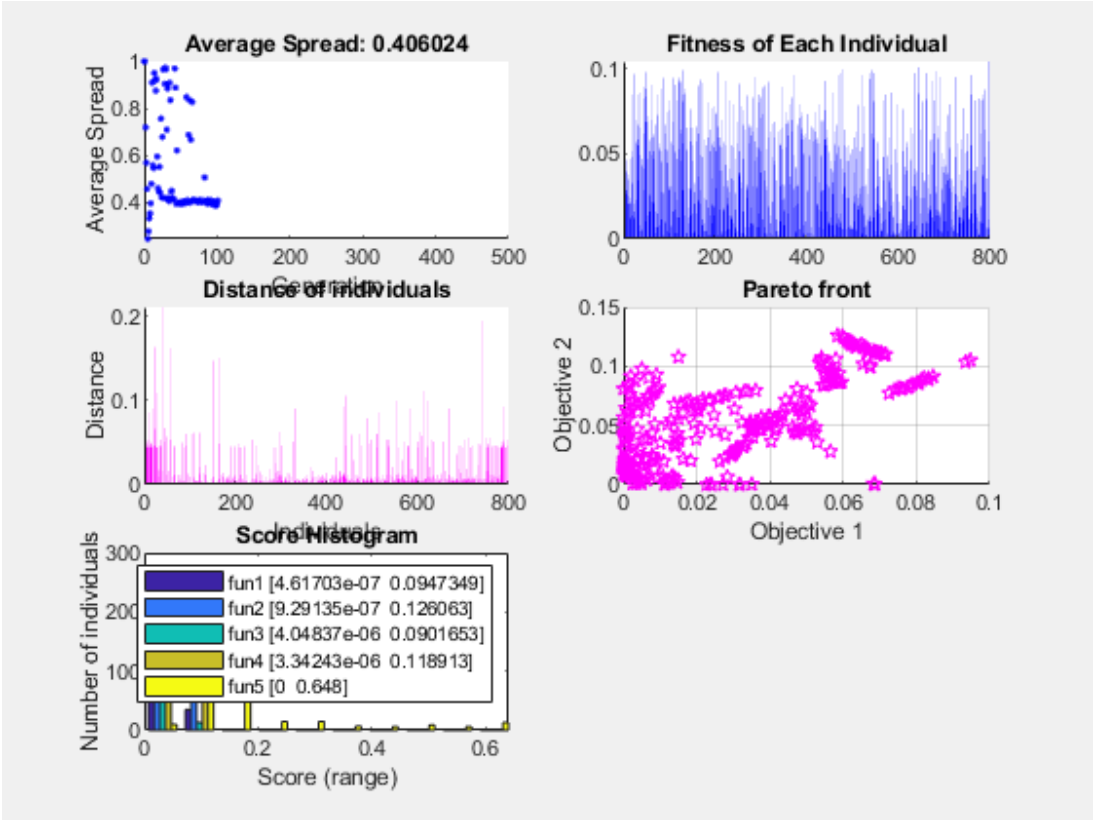


```
options_V_pareto = struct with fields:
         PopulationType: []
           PopInitRange: [2×12 double]
         PopulationSize: 800
            EliteCount: []
      CrossoverFraction: []
         ParetoFraction: 0.3500
     MigrationDirection: []
      MigrationInterval: []
      MigrationFraction: []
            Generations: 500
              TimeLimit: []
           FitnessLimit: []
          StallGenLimit: []
              StallTest: []
          StallTimeLimit: []
                 TolFun: []
                 TolCon: []
      InitialPopulation: []
          InitialScores: []
     NonlinConAlgorithm: []
          InitialPenalty: []
           PenaltyFactor: []
            PlotInterval: []
            CreationFcn: @int_pop
      FitnessScalingFcn: []
           SelectionFcn: []
           CrossoverFcn: @int_crossoverarithmetic
            MutationFcn: @int_mutation
     DistanceMeasureFcn: []
             HybridFcn: []
               Display: []
              PlotFcns: {'gaplotspread'  'gaplotscores'  'gaplotparetodistance'  'gaplotpareto'  'gaplotscorediversi
            OutputFcns: []
            Vectorized: []
```

```
        UseParallel: 1
ConstraintTolerance: 0
```

K

Joining two kirigami sheets

With an optimal crease pattern found, the Kirigami sheets can be joined. Recap, the discretized flaps will be folded into each other. Strips from both sheets are paired with each other in order to make a joint. Every crease placed on one of the strips is also placed on the other. In such a way that the sheets are able to constrain each other.

For illustration a crease pattern is optimized. The crease pattern will consist of six creases evenly divided over subset $\mathscr{H}$ and $\mathscr{V}$ with an objective of $\mathbf{C} : \{x^+, x^-, y^+, y^-\} = \{4,4,4,4\}$. All directions are set to be evenly important but the stacked layers are slightly more important, leading to the following weight factors $w = \{\frac{4}{25}, \frac{4}{25}, \frac{4}{25}, \frac{4}{25}, \frac{9}{25}\}$. The strip has the following dimension; a length of 3 and a width of 1.
The crease pattern of subset $\mathscr{H}$ is optimized first. Figure K.1 represents the crease pattern of subset $\mathscr{H}$ in folded and unfolded state. The orange crease lines are part of opposite folding and the yellow crease lines are part of the Jacobs ladder.
Figure K.2 represents the crease pattern of subset $\mathscr{V}$ in folded and unfolded state. The crease lines of subset $\mathscr{H}$ are shown in orange and yellow while the crease lines of subset $\mathscr{V}$ are shown in green and purple.

The crease patterns are embedded on the discretized flaps. The crease patterns of the pink and blue sheet are mirrored to each other, in order to have a fold on the same location, see Fig. K.1. Figure K.2 is half way the folding operation. And Fig. K.3 is the resulting folded state of the kirigami sheets. To have a clear image the sheets are placed on top of each other. Note that the the first opposite fold is folded upwards in such a way the sheets are pointing to each other.
Figure K.4 and K.5 are the representation of the actual object, both sheets lay in the same plane. Figure K.4 is an isometric view of the joined Kirigami object and Fig. K.5 has several side views and a front view.

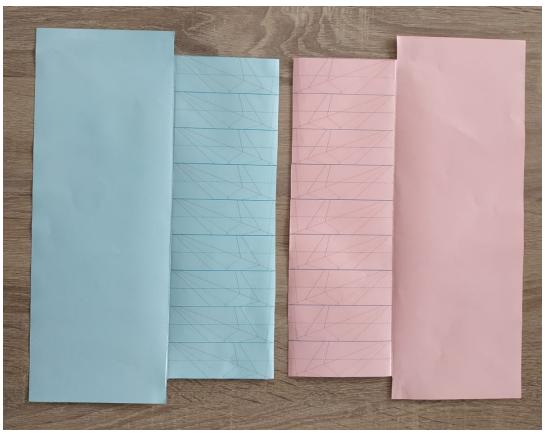

Figure K.1: Two kirigami sheets, not folded into each other. Both sheets have discretized flaps with a crease pattern embedden in them.

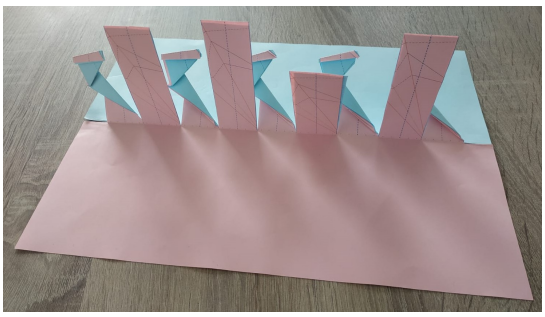

Figure K.2: Two kirigami sheets, partially folded into each other. Strips from both sheets are paired with each other.

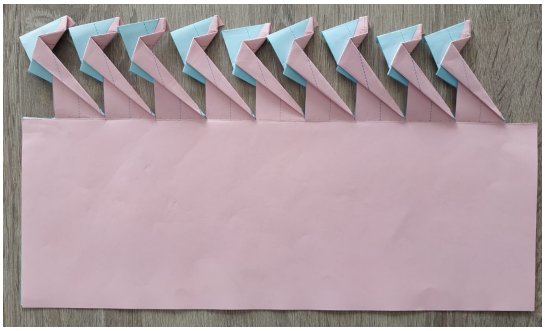

Figure K.3: Two kirigami sheets, folded into each other. The sheets are on top of each other for illustration purposes.

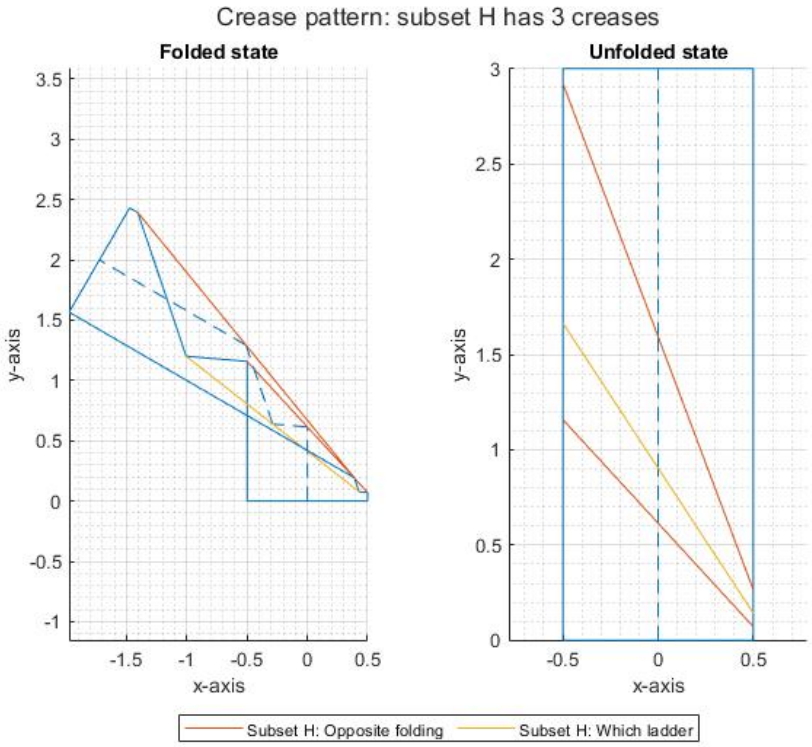

Plot K.1: Two kirigami sheets, not folded into each other. Crease pattern $\mathscr{H}$. A x-ray view of a possible solution from the optimization algorithm which has as objective $\mathbf{C}: \{4,4,4,4,4\}$.

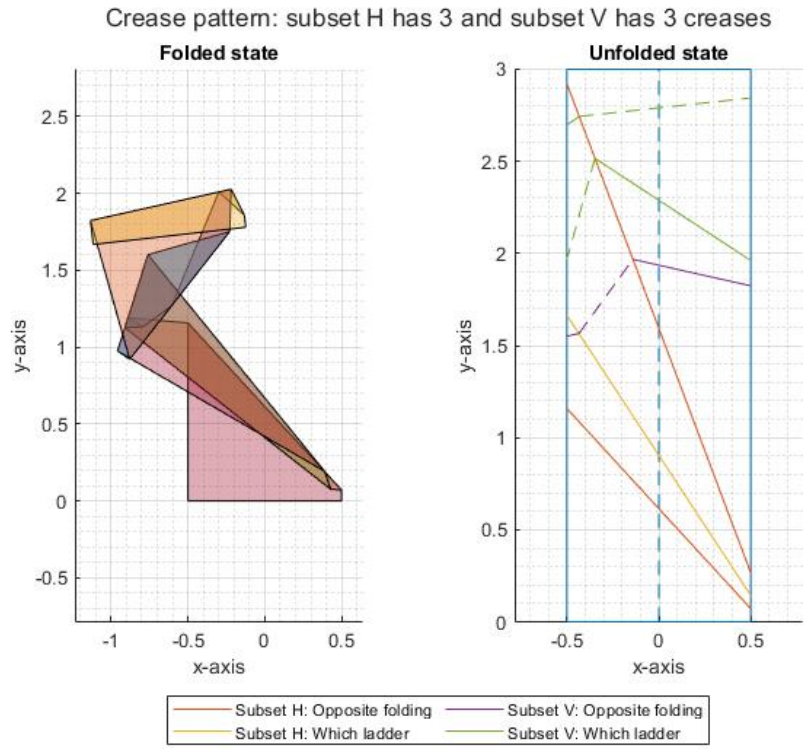

Plot K.2: Crease pattern $\mathscr{H}$ and $\mathscr{V}$. A x-ray view of a possible solution from the optimization algorithm which has as objective $\mathbf{C}$: $\{4,4,4,4,4\}$. The true primary constraint is found to be $C^{\mathscr{V}} = \begin{bmatrix} -2.9741 & -2.7615 & -2.9535 & -2.8230 & -6.0000 \end{bmatrix}$. Both subsets have three creases. The mountain valley assignment can be distinguished by a dashed and straight line.

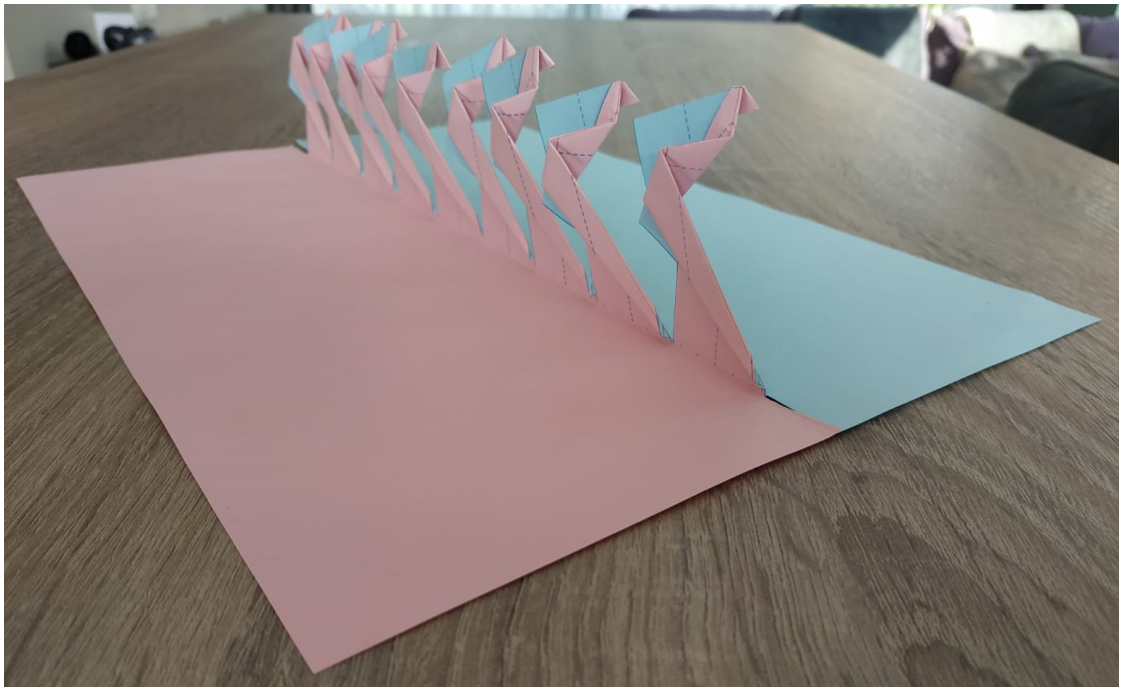

Figure K.4: Isometric view of the joined Kirigami sheets. Two sheets are joined with nine strips.

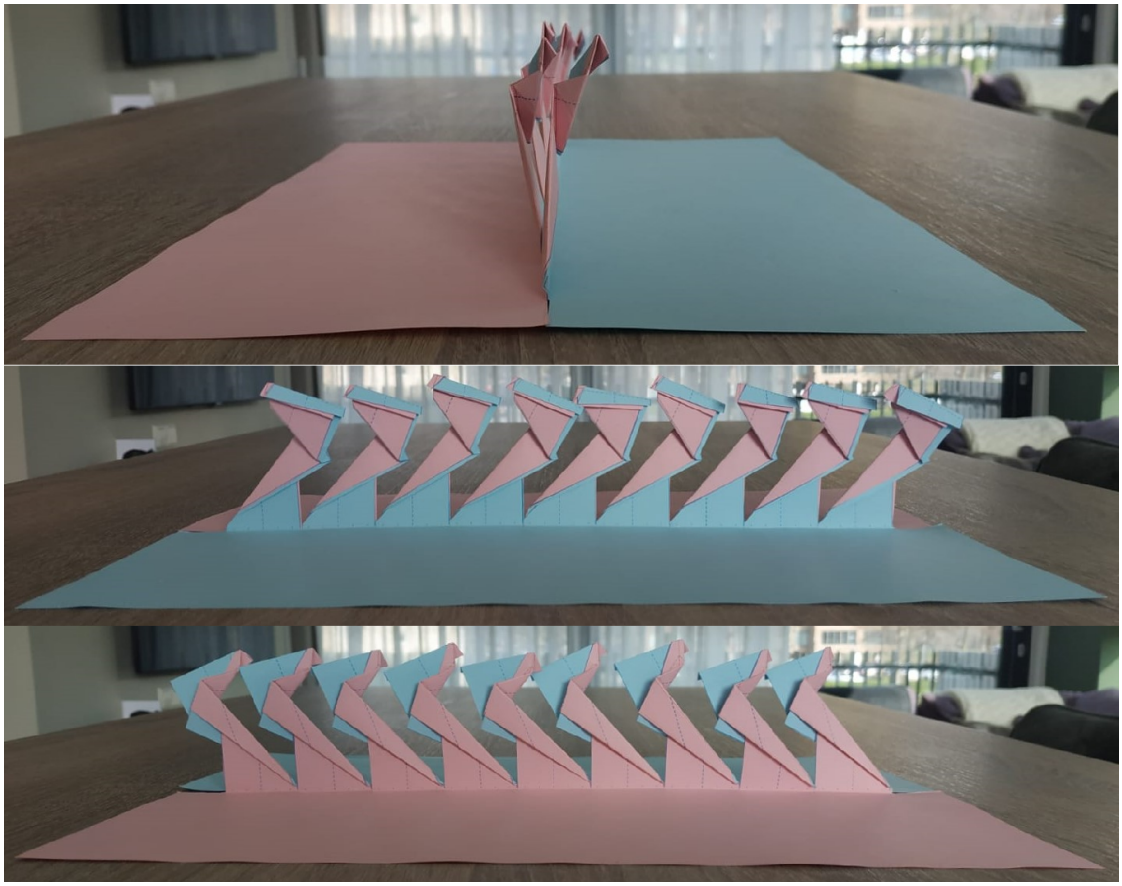

Figure K.5: Front and side views of the joined Kirigami sheets. These sheets are joined with nine strips. Top figure; front view, second figure: side view one, third figure: side view two.